TECHNISCHE UNIVERSITÄT MÜNCHEN

Lehrstuhl für Entwicklungsgenetik

Genetic modeling of a neurodegenerative polyglutamine disorder in zebrafish and analysis of polyglutamine aggregate dynamics

Changsheng Liu

Vollständiger Abdruck der von der Fakultät Wissenschaftszentrum Weihenstephan für Ernährung, Landnutzung und Umwelt der Technischen Universität München zur Erlangung des akademischen Grades eines

Doktors der Naturwissenschaften

genehmigte Dissertation.

Vorsitzender: Univ.-Prof. Dr. A. Gierl

Prüfer der Dissertation:

1. Univ.-Prof. Dr. W. Wurst
2. Univ.-Prof. Dr. R. W. Köster
(Technische Universität Braunschweig)

Die Dissertation wurde am 27.09.2012 bei der Technischen Universität München eingereicht und durch die Fakultät Wissenschaftszentrum Weihenstephan für Ernährung, Landnutzung und Umwelt am 18.10.2012 angenommen.

Ⅰ Abstract

Polyglutamine (polyQ) diseases are a family of nine neurodegenerative disorders caused by an unstable CAG expansion in the respective genes. The polyQ expansion causes pathogenic protein misfolding and conformational rearrangements, resulting in protein aggregation followed by neurodegeneration.

Spinocerebellar ataxia type 3 (SCA-3) is caused by a polyQ expansion in the Protein Ataxin-3 (Atx-3) and this disease characterized by neurodegeneration in specific neurons in the spinal cord and the cerebellum, which causes a progressive loss of movement coordination in patients.

Atx-3 is highly conserved among vertebrates. With degenerating neurons being accessible for in vivo imaging analysis and many other advantages, zebrafish is quite suitable to model this polyQ diesease. The zebrafish homologue *atx-3* gene was cloned from cDNA. *atx-3* is ubiquitously expressed during zebrafish embryogenesis as shown by *in situ* mRNA hybridization. In adult brain sections, pronounced *atx-3* expression was detected in Purkinje neurons of the cerebellum. The nuclear translocation behavior of the zebrafish protein Atx-3 is similar to its human homologue upon oxidative stress. Zebrafish Atx-3 has a tendency to form nuclear aggregates.

A zebrafish SCA-3 disease model was generated by stable overexpression of the human pathogenic C-terminal Atx-3 polyQ fragment in cerebellar Purkinje cells resulting in Atx-3 polyQ aggregation. Zebrafish larvae expressing Atx-3 polyQ showed significantly reduced periods of long distance movements compared to larvae overexpressing wild type Atx-3 from humans, suggesting locomotive difficulties. SCA-3 larvae showed eye movement impairments, displaying a phenotypical characteristic for cerebellar dysfunction in SCA-3 patients. Therefore, the established zebrafish SCA-3 model can provide important insights into the mechanisms of SCA-3 pathogenesis and disease progression, and can be especially valuable for drug development regarding polyQ diseases.

Another polyQ disease Spinocerebellar Ataxia type 1 (SCA-1) is caused by polyQ expansion in the nuclear protein Ataxin-1 (Atx-1). In order to unravel the molecular mechanisms underlying polyQ protein aggregation in neurons affected by SCA-1, the dynamics of Atx-1 aggregation were analyzed. Time lapse microscopy revealed the growth and dynamics of Atx-1 polyQ aggregates in the nucleus. The growth of aggregates can occur either from the direct

recruitment of newly synthesized protein, or from fusion of two aggregates, both in zebrafish cell culture and in cerebellar Purkinje cells of zebrafish larvae.

The fusion of Atx-1 polyQ aggregates was enhanced by Actin depolymerization, whereas the overexpression of nuclear but not cytoplasmic Actin increased the number of Atx-1 polyQ aggregates and altered their morphology. Hence, it was concluded that nuclear Actin is involved in Atx-1 aggregation dynamics, substantiated by the colocalization of both proteins and colocalization of Atx-1 polyQ aggregates with the Actin depolymerizing factor Cofilin-1. Thus, these findings can lay a foundation to understand the molecular mechanisms of SCA-1 and other polyQ diseases.

Ⅱ Zusammenfassung

Polyglutamin (polyQ)-Erkrankungen sind eine Gruppe von neun neurodegenerativen Krankheiten, die durch eine instabile Expansion des Codons CAG in den entsprechenden Genen verursacht werden. Die polyQ-Expansion in den zugehörigen Proteinen führt zu Proteinfehlfaltungen and Konformationsänderungen, was wiederum in Proteinaggregation und schließlich Neurodegeneration resultiert.

Spinocerebelläre Ataxie Typ 3 (SCA-3) basiert auf einer polyQ-Expansion im Gen *ataxin-3* (Atx-3) und führt zu neuronaler Degeneration im Rückenmark und im Kleinhirn, was zu einem progressiven Verlust der Bewegungsfähigkeit der betroffenen Patienten führt.

Atx-3 ist in Vertebraten hoch konserviert. So war es möglich, ein SCA-3-Krankheitsmodell in Zebrafisch zu etablieren. Hier lassen sich Neuronen besonders gut *in vivo* mikroskopieren, so dass Zebrafisch einen sehr guten Modellorganismus für polyQ-Erkrankungen darstellt. Das Zebrafisch-Homolog atx-3 wurde aus cDNA kloniert. Atx-3 wird ubiquitär während der Zebrafisch-Embryogenese exprimiert, was durch *in situ* mRNA-Hybridisierungen gezeigt werden konnte. In Schnitten des adulten Hirns wurde vermehrte atx-3-Expression in den Purkinje-Zellen des Cerebellums festgestellt. Wie das humane Homolog wird das Zebrafisch-Protein Atx-3 bei oxidativem Stress in den Zellukern transportiert. Zebrafisch Atx-3 tendiert dazu, nukleäre Aggragate zu bilden.

Im Zebrafisch-SCA-3-Krankheitsmodell wird das humane pathogene C-terminale Atx-3-polyQ-Fragment stabil in cerebellären Purkinje-Zellen überexprimiert, was zu einer Aggregation von Atx-3-polyQ führt. Zebrafisch-Larven, die Atx-3-polyQ exprimieren, zeigen signifikant verkürzte Perioden von Bewegung über lange Distanzen im Vergleich zu Larven, die Atx-3-Wildtyp exprimieren. SCA-3-Larven zeigen Einschränkungen bei der Augenbewegung, ein typischer Phänotyp bei Funktionsstörungen des Kleinhirns wie er auch schon bei SCA-3-Patienten beobachtet wurde. Aufgrunddessen kann das etablierte SCA-3-Modell wertvolle Einblicke in die Entstehung und den Verlauf dieser Erkrankung liefern und auch nützlich für Entwicklung von Therapiemöglichkeiten für polyQ-Erkrankungen sein.

Eine weitere polyQ-Erkrankung ist die Spinocerebelläre Ataxie Typ 1 (SCA-1). SCA-1 wird durch eine polyQ-Expansion im nuklären Protein Ataxin-1 (Atx-1) verursacht. Um die molekularen Mechanismen zu entschlüsseln, die der polyQ-Proteinaggregation in SCA-1-betroffenen Neuronen zu Grunde liegen, wurde die Dynamik der Atx-1-Aggregation untersucht. Zeitraffer-Aufnahmen zeigten das Wachstum und die Dynamik von Atx-1-polyQ-Aggregaten im Zellkern. Das Wachstum der Aggregate resultiert entweder aus der direkten

Aufnahme von neu synthetisiertem Protein oder der Fusion von zwei Aggregaten. Beide Mechanismen konnten in Zebrafisch-Zellkultur und in cerebellären Purkinje-Zellen von intakten Zebrafisch-Larven beobachtet werden.

Die Fusion von Atx-1-polyQ-Aggregaten wurde durch Aktin-Depolymerisierung verstärkt, wohingegen die Überexpression von nukleärem, aber nicht zytoplasmatischem Aktin die Anzahl von polyQ-Aggregaten erhöhte und sich außerdem auf die Morphologie der Aggregate auswirkte. Daraus wurde geschlossen, dass nukleäres Aktin an der Dynamik von Atx-1-Aggregaten beteiligt ist, untermauert durch die Ko-lokalisierung von beiden Proteinen und der Ko-lokalisierung von Atx-1-polyQ-Aggregaten mit dem Aktin-depolymerisierenden Faktor Cofilin-1. Diese grundlegenden Resultate können dazu beitragen, die molekularen Mechanismen von SCA-1 und anderen polyQ-Erkrankungen besser zu verstehen

Ⅲ Acknowledgements

I owe a huge debt of gratitude to many people for their long-lasting support and encouragement which was invaluable for my doctoral study. I gratefully acknowledged some of them in the following paragraphs. However, I am aware of the fact that all the words below cannot express all the gratitude and respect to them.

First and foremost I thank my supervisor, Prof. Dr. Reinhard Köster, for taking me into his lab, for the scientific discussion, advice and continuous support which is always so greatly appreciated. Particularly, I never forget that he saved me out of danger when I was nearly drowning in Isar River that year. Otherwise I cannot write these words at the moment. I always keep the gratefulness to him. It also reminds me to be calm and careful in rivers.
Many sincere thanks to my thesis committee members: Prof. Dr. Reinhard Köster, Prof. Dr. Wolfgang Wurst; Prof. Dr. Chichung Lie and Dr. Ingo Burtscher. They kept me focused and directed, and supported me whole heartedly.

I am immensely grateful to my good friends and colleagues throughout the years. Among them, Dr. Kazuhiko Namikawa had many valuable ideas and suggestions on my project and experiments. Dr. Niklas Senghaas gave me a lot of guidance in cell culture and other experiments, especially many tricks using microscopes and softwares. Dr. Thomas Weber and Dr. Hideaki Matsui introduced me to the secrets of zebrafish behavioral tests. Dr. Jennifer Hocking helped me a lot with English writing. Dr. Wiebke Sassen carefully edited my abstract and translated it into German. Dr. Martin Distel let me know how to balance the life between work and family. Enrico Kühn, Anna-Lena Kerner and Rosemarie Söllner offered me a lot of guidance in experiments. In addition, they helped me a lot in dealing with calling and writing in German, solved many problems for the living in Germany.
I want to thank Petra Hammerl, Timo Fritsch, Sylvie Böhme, Anni Sedlmeir and Vera Banjac, who did excellent work in the fish facilities. They took care of the fish very well, provided me the most important specimen in my work. I gratefully acknowledge my other colleagues: Eva Saxinger, Angela Traudt and Christiane Lach. They provided me excellent technical supports.

Many thanks to Prof. Dr. Martin Korte who offered generously access to the excellent facilities in Braunschweig in 2011. Thanks a lot to Dr. Martin Rothkegel for the valuable discussion and suggestion on my project, and also for the reagents and technical supports. Many sincere thanks to the following people for all the technical guidance and friendly

treatment when I used the cell culture and confocal microscope in Korte's lab: Dr. Marta Zagrebelsky-Holz, Dr. Martin Rothkegel, Dr. Kristin Michaelsen-Preusse, Yves Kellner, Qin Li, Anita Remus, Stefanie Schweinhuber, Sabine Zessin and many more. I sincerely thank Claudia Frädrich, who offered me a lot of kindly help when I used the instruments in the institute of Microbiology in Braunschweig.

I thank Dr. Daniela Vogt-Weisenhorn, Elisabeth Güll and Angelika Landgraf at the Helmholtz Zentrum München, and Ursula Behrendt at the TU Braunschweig for all the administrative work, nice supports and helps to me.

It is quite lucky to work in such nice and supportive environment to do science, both in Helmholtz Zentrum München and Technical University Braunschweig. I thank all the people who created it. I enjoyed the days to work with you.

I also want to say thanks a lot to all the fishes sacrificed in my experiments. Without them I cannot obtain the findings in this thesis.

I am deeply grateful to Barbara Schenberger and Kathrin Huter. Barbara helped me to find an apartment in quite short time after I arrived in Germany, thus my family can reunite in Germany. Kathrin offered me a lot help when I moved to Braunschweig. Particular, I thank her for getting a kindergarten place for my son, which we liked very much. All these helped to focus on my research.

I sincerely acknowledge my former colleagues and good friends in Shanghai. Thanks a lot for the scientific training, encouragement and supports. I never forget their help and guidance, and most importantly, the passion to pursue science. Thanks a lot to all my previous mentors. Without you, I cannot be myself today.

I would like to express my gratitude to all the Chinese friends in Munich and Braunschweig. I really appreciate all the helps they offered to me and my family. I could never overstate my love for my close relatives, thanks to their encouragement and best wishes for my carrier and life.

I am particularly indebted to my parents. Every tiny success I obtained is due to their long year's hard working and support, due to their education and never-ending encouragement.

Last, but by no means least, very special thanks to my dearly beloved family.

Ⅳ Table of Contents

1 Introduction

1.1 General introduction of polyglutamine disease

Polyglutamine (polyQ) diseases are an inherited neurodegenerative disease family including several spinocerebellar ataxias (SCA-1, 2, 3, 6, 7 and 17), Huntington disease (HD), dentatorubral-pallidoluysian atrophy (DRPLA) and spinal bulbar muscular atrophy (SBMA). These diseases are caused by triple nucleotide CAG repeat expansion encoding polyglutamine (polyQ) stretches in several unrelated causative genes, whereas a normal repeat number has no pathological consequence (Hanako et al., 1996; Paulson et al., 1997; Aislinn et al., 2007). When the CAG repeats in the respective causative genes are above a critical threshold, which varies in different disease, they lead to neuronal loss and a degenerative phenotype. The number of the CAG repeats and the disease onset are negatively correlated, which means the longer polyQ repeat, the earlier the onset of the disease will occur and the more severe the symptoms will be, indicating the important contribution of the expanded polyQ repeats to the pathogenesis. Fig.1-1 shows the 9 kinds of polyQ diseases identified at present, and the causative proteins with the pathogenic polyQ ranges and its native functions (Williams and Paulson 2008).

This polyQ expansion causes protein misfolding and conformational rearrangements, which result in proteins aggregate formation in the degenerative neurons of specifically affected brain regions (John et al., 1998; Jieya et al., 2007). The common mechanisms of neuronal cell death in polyQ diseases is very complicated as many pathological events caused by the presence of polyQ proteins can lead to cell death, for example, the activation of cell death pathways, mitochondrial dysfunction, transcriptional dysregulation, impairment of the ubiquitin-proteasome system (UPS) and autophagy malfunction, axonal transport defects, or unfolded protein response. Other pathogenic consequences such as excitotoxicity, metabolic stress, or accumulation of free radicals may induce cell death by further enhancing the mitochondrial dysfunction (Peter et al., 2009).

Disease	Protein name	Protein size, polyQ position and disease repeat range	Protein function
SBMA	Androgen receptor		Testosterone-activated steroid receptor
HD	Huntingtin		Possible scaffolding protein linked to diverse cellular pathways
DRPLA	Atrophin-1		Possible transcriptional corepressor
SCA1	Ataxin-1		Transcriptional corepressor involved in transcription regulation, cell specification and synaptic activity
SCA2	Ataxin-2		Component of RNA processing and translational regulation pathways
SCA3	Ataxin-3		Deubiquitinating enzyme involved in protein quality control
SCA6	P/Q-type calcium-channel subunit α1A		Voltage-sensitive calcium-channel subunit
SCA7	Ataxin-7		Component of histone acetyltransferase complex (TFTC/STAGA) and transcriptional regulation pathways
SCA17	TATA-box-binding protein		Component of core transcriptional complex TFIID

Fig. 1-1. Polyglutamine disease proteins and their functions. The nine known polyQ diseases are listed along with their causative proteins. The protein's relative size compared to other polyQ disease proteins is represented by the length of the schematic protein, which their putative functions are listed on the right. Gold bars represent the relative location of the polyQ repeat in each protein, and gold arrows indicate the range of repeat lengths associated with pathogenic conditions. Whereas CAG/polyQ repeat length is generally stable in an individual (with modest somatic mosaicism), repeat length often changes size in successive generations of a family (Williams and Paulson 2008).

Although the different polyQ disorders have several common clinical characteristics and possible common pathological mechanisms, the respective disease proteins share no homology outside the polyQ sequence, neither structurally and functionally similarity (Zoghbi and Orr, 2000; Gatchel and Zoghbi, 2005). The different neurodegenerative processes and clinical characteristics of each polyQ disease could be explained by the polyQ expansion in different causative proteins, and their different expression in the different diseases. In all these diseases, the context of the expanded repeat and the abundance, subcellular localization and

interactions of the proteins and mRNAs constitute the factors responsible for disease-specific phenotypes (Gatchel and Zoghbi, 2005). Therefore, it is necessary to study different polyQ diseases for investigating the particular mechanisms and develop effective therapies for each disease, where as a comparision of different polyQ disease will reveal common altrics within this diseases family. In this thesis, the polyQ proteins causing SCA-3 and SCA-1 are studied in particular.

1.2 SCA-3 symptoms and pathogenesis

1.2.1 General introduction of SCA-3

Spinocerebellar Ataxia type 3 (SCA-3, also termed Machado-Joseph disease, MJD), is an autosomal, dominantly inherited neurodegenerative disorder (Kawaguchi et al., 1994). SCA-3, at first described in the people of Portuguese Azorean (Coutinho and Andrade, 1978, Rosenberg, 1992 and Sudarsky and Coutinho, 1995), is the most prevalent spinocerebellar ataxia in many countries worldwide, including Germany, China, Brazil and Portugal etc. (Coutinho et al., 2010). It is caused by the abnormal polyQ expansion in the Ataxin-3 (Atx-3) protein, which could induce neurotoxicity in cerebellar dentate neurons, basal ganglia, the brain stem and the spinal cord (Hanako et al., 1996; Paulson et al., 1997; Jieya et al., 2007).
In wild type Atx-3, the length of polyQ stretches ranges between 12 and 44, while in SCA-3 patients the length is increased between 45 and 87 Qs. Although there is an overlap (around 45-51 repeats) between the healthy and disease groups (Van Alfen et al., 2001; Maciel et al., 2001; Riess et al., 2008).
The pathological hallmark of SCA-3 is the presence of nuclear aggregates formed by the polyQ expanded Atx-3 in the human patients' brain. Though the causative protein Atx-3 is ubiquitously expressed throughout the whole brain, the SCA-3 neurodegeneration profile selectively involves neuronal loss in specific brain regions (Paulson et al., 1997; Schmidt et al., 1998), including the cerebellar dentate nucleus, pallidum, substantia nigra, thalamus, subthalamic, red, and pontine nuclei, cranial nerve nuclei and the anterior horn and Clarke's column of the spinal cord (Woods and Schaumburg, 1972; Romanul et al., 1977). Cerebellar Purkinje cell is also a neuronal population affected in SCA-3 disease. It was reported that the Purkinje cells were mildly degenerated in many cases (Landau et al., 2000; Muñoz et al., 2002). In many SCA3 autopsy samples, it was observed that less than 25% Purkinje cell was lost (Durr et al., 1996; Schols et al., 2004).

Previous studies have suggested the neurodegeneration in SCA-3 patients at late stages may be more widespread, including the visual, auditory, vestibular, somatosensory, ingestion-related, dopaminergic and cholinergic systems (Coutinho and Andrade, 1978, , Kanda et al., 1989, Rosenberg, 1992, and Sudarsky and Coutinho, 1995; Durr et al., 1996; Rub et al., 2008; Riess et al., 2008; Deller et al., 2008; Alves et al., 2008; Shimizu et al., 2010).

Clinically, SCA-3 has several characteristic symptoms, including the progressive cerebellar ataxia, which involve obvious gait imbalance, actions tremor, and other general neuromuscular complications like dystonia, speech difficulty (dysarthria), muscle tone (spasticity), rigidity, postural instability and proprioceptive loss, visual nystagmus, double vision and speech disorders (dysarthria), dysphagia, amyotrophy, corticospinal and autonomic nervous system dysfunctions and neuropathy. Many patients also develop oculomotor dysfunction (ophthalmoparesis), bulging and staring eyes. Ophthalmoparesis is the most distinctive characteristic, being very rare in non-SCA-3 patients (Rosenberg, 1992; Sudarsky and Coutinho, 1995; Soong et al., 1997; Riess et al., 2008; Coutinho et al., 2010).

Currently, there is no effective therapy available to cure or delay the disease onset of SCA-3. For a better understanding the pathogenesis mechanisms of SCA-3, one of the basic questions is to first clarify the native functions of the causative protein Atx-3.

1.2.2 Structure and functions of Atx-3

Atx-3 is widely distributed among many species, including plants, fungi, nematodes and vertebrates. In mice and humans, Atx-3 displays a ubiquitous expression among different tissues and cell types, and it is widely expressed throughout the whole brain. In neurons, Atx-3 is predominantly a cytoplasmic protein, while in various cell types; Atx-3 is present in both the cytoplasm and the nucleus (Paulson et al., 1997; Schmidt et al., 1998; Trottier et al., 1998; Ichikawa et al., 2001; Costa et al., 2004;).

Revealed by structure investigations, Atx-3 is composed of a globular N-terminal domain termed Josephin domain (JD, amino acid residues 1-182 in the human protein), followed by a flexible C-terminal tail (Masino et al., 2003). The Josephin domain contains highly conserved amino acids, and it displays ubiquitin (Ub) protease activity, while the C-terminal tail contains two (or three, (Harris et al., 2010).) Ub-interacting motifs (UIMs) and a polyQ sequence of variable size. (Burnett et al., 2003;Albrecht et al., 2004; Nicastro et al., 2005). Resulting from alternative splicing, different isoforms of human Atx-3 have been reported. With the heaviest molecular weight being about 42 kDa (Goto et al., 1997; Trottier et al., 1998; Ichikawa et al.,

2001). 40-43 kDa isoforms can be observed in normal human beings, yet the functions of these different isoforms are not well known.

Involvement in protein quality control system

The Ub protease activity in the N-terminal JD of Atx-3, (with the meaning that Atx-3 has the ability to cleave isopeptide bonds between Ub monomers), is responsible for the turnover of short-lived or damaged proteins (Doss-Pepe et al., 2003). Through the UIMs in its C-terminus, Atx-3 can bind polyUb chains, interacting with both K48 and K63-linked chains in a UIM-dependent manner (Burnett et al., 2003, Donaldson et al., 2003; Chai et al., 2004). Furthermore, it was proposed that Atx-3 participates in the regulation of aggresome formation, and in the degradation of proteins sent from the endoplasmic reticulum (Wang et al., 2006). Taken together, these investigations suggest that Atx-3 normally functions in protein quality control pathways in the cell.

Involvement in transcription regulation

Previous studies reported that Atx-3 is also involved in transcriptional regulation. Atx-3 can interact with two transcriptional repressors – Histone deacetylase 3 (HDAC3) and nuclear receptor co-repressor (NCor) (Evert et al., 2006), and with three transcriptional activators: cAMP response element-binding protein (CREB)-binding protein (CBP), p300 and p300/CBP-associated factor (PCAF) (Li et al., 2002); and Histones (Li et al., 2002, Evert et al., 2003 and Rodrigues et al., 2007). These interactions are dependent on the C-terminal polyQ containing domain of Atx-3.

1.2.3 Mechanisms of SCA-3 Pathogenesis

Considering its severity and lack of therapy at present, it is critical to understand the pathogenesis mediated by Atx-3polyQ for developing effective medical approaches to mitigate the severe symptoms of the patients worldwide.

Proteolytic cleavage of Atx-3

Several investigations proposed that the proteolytic cleavage of Atx-3 contributes to its pathogenesis, and the C-terminal fragment is considered to be crucially important for the aggregation and cytotoxicity of the pathogenic atx-3 polyQ variant. This cleavage results in polyQ expanded C-terminal fragments of Atx-3 with the size of about 36 kDa. Similar

fragments have been detected in the degenerative brain regions in SCA-3 patients, and also in many cell and animal disease models (Yoshizawa et al., 2000; Tarlac and Storey, 2003; Goti et al., 2004; Haacke et al., 2007; Colomer Gould et al., 2007; Jung et al., 2009).
These toxic fragments can perform aggregation, recruit other proteins including normal Atx-3, and seed the formation of intranuclear inclusions (Paulson et al., 1997; David et al., 2005).
It was reported that the truncation of Atx-3 to remove the ubiquitin protease domain, or mutation of the ubiquitin protease activity, dramatically enhances toxicity (Hanako et al., 1996). Furthermore, in studies in transfected cell lines or transgenic mice, the polyQ expanded C-terminal fragments of Atx-3 showed increased toxicity to induce cell death (Ikeda et al., 1996; Paulson et al., 1997; Haacke et al., 2006; Breuer et al., 2010).
Preventing proteolytic cleavage of Atx-3 by mutating its putative cleavage sites reduced formation of the C-terminal fragments of Atx-3, and protein aggregation, as which lead to a reduced the neuronal toxicity in a *Drosophila* model of SCA-3 (Tarlac and Storey, 2003; Jung et al., 2009). The development of Atx-3 protelysis inhibitors appear to be beneficial for preventing SCA-3 pathogenesis (Tarlac and Storey 2003; Shao and Diamond, 2007; Jung et al., 2009).
Atx-3 was reported that it could be cleaved by Caspases (e.g., Caspase-1) and calcium-dependent calpain proteases in cell lines, and this proteolysis can increase the aggregation of polyQ-expanded Atx3 (Berke et al., 2004; Haacke et al., 2007; Jung et al., 2009).
Through an investigation using induced pluripotent stem cell (iPSC)-derived neurons from SCA-3 patients, it was proposed that Calpain but not Caspases performed the proteolysis in an activity dependant manner which initiates Atx-3 to form SDS-insoluble aggregates (Koch et al., 2011). This suggests that neuronal activity contributes to disease progression.

PolyQ protein aggregation

The pathological polyQ tract exerts a toxic gain of function to the host protein, by transiting it to a novel, toxic conformation, altering its normal interaction with other proteins, and subsequently generating ubiquitinated aggregates in neurons (Bevivino and Loll, 2001; Tanaka et al., 2001; Chow et al., 2004; Jana and Nukina, 2004; Muchowski and Wacker, 2005; Nagai et al., 2007; Williams and Paulson, 2008). It was reported that the Atx-3 aggregates contained β-rich fibrillar structures of amyloid, like the amyloid aggregates observed in Alzheimer's and prion diseases (Bevivino and Loll, 2001; Chen et al., 2002; Ellisdon et al., 2006 and 2007). This fundings suggest similarities between different neurodegenerative diseases.

Interestingly, the wild type non-expanded Atx-3 itself also displays a tendency to aggregate, but shows slower kinetics than the pathogenic forms, suggesting the relevance of regions outside the polyQ domain is also contributing to protein aggregation (Chow et al., 2004, Chow et al., 2004; Gales et al., 2005; Masino et al., 2004; Masino et al., 2011).

Nuclear accumulation

Under normal conditions, Atx-3 is a predominantly cytoplasmic protein in neurons, while it becomes accumulated during disease progression but also upon heat shock and oxidative stress in the nucleus of neurons or fibroblasts from patients. It was pointed that the nuclear localization of Atx-3 is required for the manifestation of symptoms in SCA-3, as suggested by the evidence from SCA-3 mouse models, in which pathogenic Atx-3 was forced to express in the nucleus by using nuclear localization signal (Bichelmeier et al., 2007).
The involvement of Atx-3 aggregation in the pathogenesis of SCA-3 may be through various possible ways: (a) dysregulation of transcription, through sequestration of factors/co-factor or repressors involved in transcription (Chai et al., 2002; McCampbell et al., 2000); (b) disturbance of the protein quality control systems of the neurons, via sequestration of proteasome components and molecular chaperones (Paulson et al., 1997; Chai et al., 1999; Warrick et al., 1999; Ferrigno and Silver, 2000; Muchowski et al., 2000; Schmidt et al., 2002;); (c) blocking of axonal transport, resulting from motor protein recruitment and physical blocking (Gunawardena et al., 2003). Hereby the progress in transsciptional dysregulation affected by polyQ expanded Atx-3 was briefly reviewed below.

Transcriptional dysregulation

The transcriptional dysregulation was reported in a transgenic SCA-3 mouse model, even before the symptoms arose. This Atx-3Q79 overexpressing mice exhibited down regulated transcripts related to Histone acetylation, synaptic transmission, intracellular calcium signaling/mobilization or MAP kinase pathways, GABA(A/B) receptor subunit, heat shock proteins and transcription factors regulating neuronal survival and differentiation. This finding was in accordance with the idea that Atx-3 is involved in transcriptional regulation and the polyQ expanded Atx-3 may lead to cerebellar dysfunction and ataxia by dysregulating normal cerebellar transcription (Chou et al., 2008 and 2011).
Besides the nuclear aggregates, axonal aggregates formed by Atx-3polyQ were observed in patients´ brains, in the fiber tracts connecting brain regions known to undergo

neurodegeneration in SCA-3 (Seidel et al., 2010). Similar to nuclear inclusions, these axonal aggregates were co-localized with Ubiquitin and the proteasome and autophagy associated shuttle protein p62, indicating involvement of Atx-3 in the neuronal protein quality control system. Based on the correlation between aggregate containing axons and degenerating neuronal nuclei, it was proposed that these axonal aggregates may interfere with axonal transport and to cause negative consequences for neuronal function and survival, thereby playing a role in neurodegeneration in SCA-3 (Gunawardena et al., 2003; Seidel et al., 2010). The picture in Fig. 1.2 summarizes the toxic mechanisms mediated by polyQ expanded Atx3, derived from the review by Matos et al., (2011).

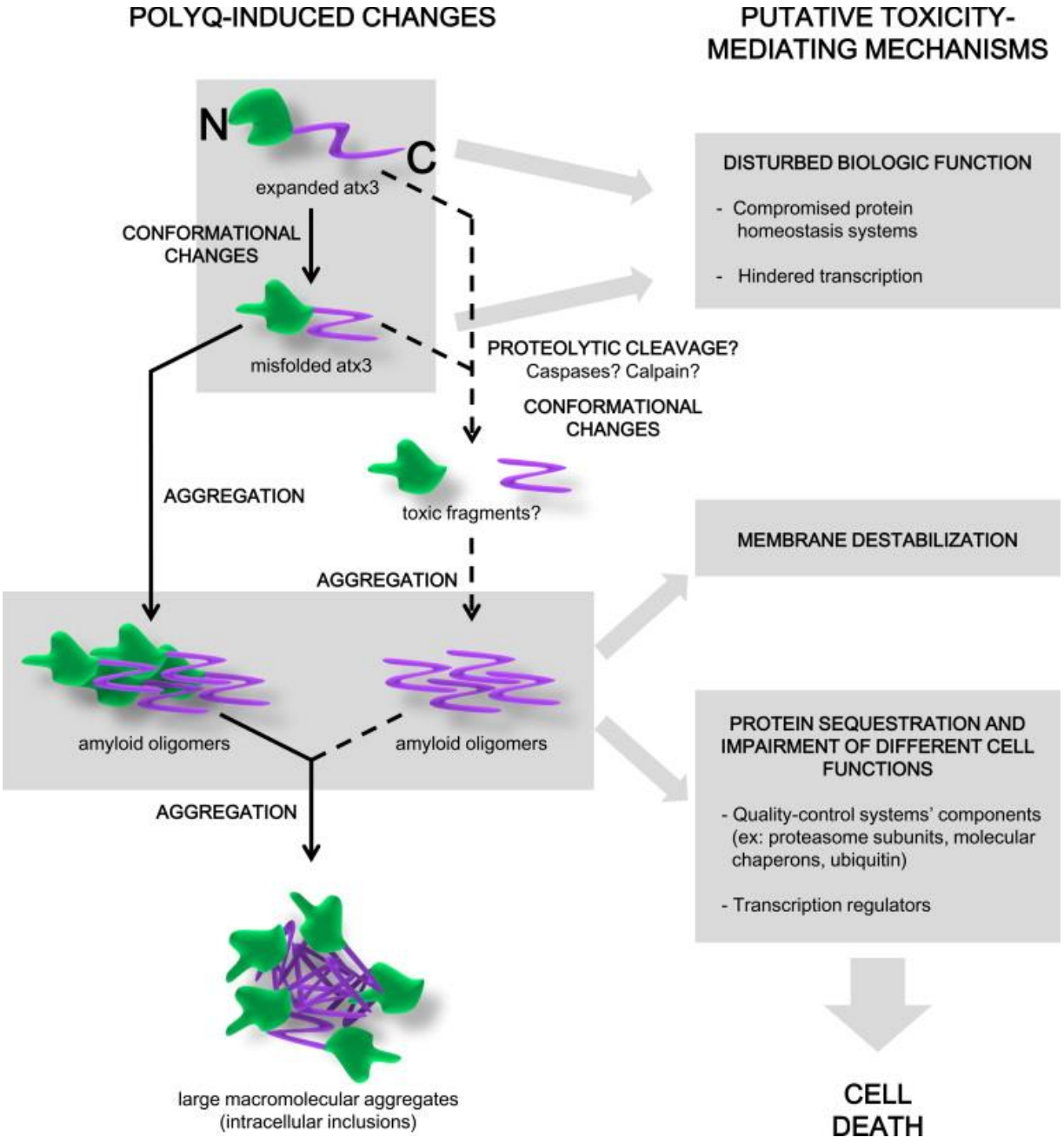

Fig.1-2. Putative mechanisms mediating expanded Atx-3 toxicity. Atx-3 with polyQ expansion induces the pathogenesis of SCA-3. Expanded Atx3 perform aggregation and resulting large macromolecular inclusions. Proteolytic cleavage of Atx-3 and the resulting C-terminal fragments may be an important event contributing to oligomerization, and the subsequent seeding aggregation. The soluble amyloid-like oligomers appearing during the aggregation process may exert deleterious toxicity on the cells, possibly destabilizing the cell membranes and/or recruiting important proteins with consequent disruption of important cellular systems, like transcription, protein homeostasis, etc (Matos et al., 2011).

1.3 The development of SCA-3 disease models

Models for the human neurodegenerative disease SCA-3 in animal systems have provided valuable tools to dissect molecular mechanisms of disease pathology (John et al., 1998), not only deepening our understanding the emergence and progression of SCA-3, but also facilitating the development of therapeutical approaches. At present, transgenic SCA-3 disease models in mouse, rat or fruit fly were generated through expressing human full-length pathogenic Atx-3, or the C-terminal polyQ expanded fragment of this protein (see Fig.1-3).

1.3.1 A brief review of the progress in SCA-3 disease modeling

The first SCA-3 transgenic animal model was generated by Ikeda and his colleagues (Ikeda et al., 1996). The mice expressing the truncated C-terminal Atx-3 domain containing a Q79 stretch in Purkinje cells displayed a degeneration of Purkinje cells, severe atrophy of the cerebellum and behavioral deficits. Cemal et al. (2002) generated the first transgenic mice to express full length pathogenic Atx-3 under the control of its own regulatory elements by using a yeast artificial chromosome (YAC) containing the whole human expanded *ATXN3* gene and its regulatory elements. This model displayed several mild motor and sensory deficits, like wide gait, tremor, and disability to correct body position and reduced weight gain, similar to the SCA-3 patients.

The recent progress on SCA-3 disease modeling was reviewed in detail by Veronica F and Conceição Bettencourt et al. In addition, considering the conversation of the atx-3 homologues between fly and human, *Drosophila* is also an alternative animal for SCA-3 disease modeling. At least the fruit fly models could mimic some pathology features of SCA-3, like the nuclear inclusions and neuronal loss. However, the symptoms severity, disease onset and the formation of nuclear inclusions differs between different models (Warrick et al., 1998; Warrick et al., 2005; Jung et al., 2009). Regarding *Drosophila* models, one of their advantages is that, the pathogenic protein expression could be directed to specific brain

regions and neuronal cell types through the GAL4-UAS system, because there are a plenty of these strains available in the in *Drosophila* research field. In this way, the pathogenic response of specific neuronal cell types in the disease could be investigated. Here, some representative models are listed below, with the promoters driving the atx-3 transgene and the expression cassette.

Ref.	Organism	Promoter	Atx-3 Construct
Ikeda et al., 1996	mouse	L7 (Purkinje cell)	C-terminus Atx-3Q79
Warrick et al., 1998	fruit fly	*elav; gmr*	C-terminus Atx-3Q78
Cemal et al., 2002	mouse	*atx-3*	Full-length Q64/84
Goti et al., 2004	mouse	*prp*	Full-length Atx-3Q71
Warrick et al., 2005	fruit fly	*elav; gmr*	C- terminus Atx-3Q78 Full-length Atx-3Q78
Bichelmeier et al., 2007;	mouse	Portion of *prp*	Atx-3Q70/148
Jana Boy 2009	mouse	*prp+Tet-off*	Full-length Atx-3Q71
Chou 2008	mouse	*prp*	Full-length Atx-3Q79
Alves et al., 2008	rat	lentiviral vector	Full-length Atx-3Q72
Silva-Fernandes A, 2010	mouse	*cmv*	Full-length Atx-3Q94
Jana Boy 2010	mouse	*huntingtin*	Full-length Atx-3Q148

Fig.1-3. Several representative SCA-3 animal models with the regulatory element to drive expression of the respective Atx-3 variant.

Purkinje neuron degeneration was observed when pathogenic Atx-3 was overexpressed either driven by its own promoter (Cemal et al., 2002; Boy et al. 2009) or a brain ubiquitous expression promoter Prp (Goti et al., 2004; Bichelmeier et al., 2007) or by a Purkinje cell promoter L7 (Ikeda et al., 1996), or htt promoter (Boy et al., 2010) in mouse or rat models.
In addition to the SCA-3 modeling in mouse with the truncated form of Atx-3 expression (Ikeda et al., 1996), the similar truncated Atx-3 variant was also targeted to select tissues in fruit fly, where pronounced deleterious effects were observed (Warrick et al., 1998). Based on the previous evidence the toxic C-terminal Atx-3 fragment is proposed to be a suitable pathogenic construct in order to replicate the motor disorders or other pathological characteristics for SCA-3 disease modeling in zebrafish.

1.3.2 Why is SCA-3 modeling needed in zebrafish?

The previously generated mouse and fly models are quite viable, which mimicked many features of SCA-3, like neuronal cell death, nuclear aggregate formation and ataxia symptoms. However, the exact pathogenesis mechanism of SCA-3 is still not well known, neither effective therapies are available. Zebrafish could provide another alternative animal model to understand the pathogenesis of SCA-3 disease, and even facilitate to develop effective medical approaches aiming to mitigate the severe symptoms of the patients.

Zebrafish is a vertebrate, evolutionary conserved to human beings. A plenty of evidence demonstrate that the functional conservation between the causative proteins of human neurodegenerative disease and their zebrafish orthologues. This suggests that the zebrafish may represent a reliable tool to replicate the human neurondegeneration disease. Zebrafish is well accessible for high resolution live imaging and genetic manipulation, cheap to maintain and easily to produce large amounts of offspring in short time. Thus zebrafish produces plenty of methodological opportunities for addressing SCA-3 pathogenic events directly in vivo at cellular resolution. Because of their external development, large number of progeny and aqueous environment, a zebrafish SCA-3 model could also provide high throughput screening, which should facilitate the identification of leading compounds for developing therapies. Due to this reason, zebrafish is quite suitable to generate human disease models, for SCA-3.

One of the polyQ diseases, the Huntington disease has already been modeled in zebrafish via transient expression of the causative Htt protein fused with GFP (Miller et al., 2005). PolyQ protein inclusions containing GFP were observed, and associated with the loss of rod outer segments and rhodopsin expression from the zebrafish retina. The correlation between the severity of the morphological phenotype and the polyQ repeat number was also replicated in this zebrafish HD model. This progress in HD modeling in zebrafish provides some guidelines for generating other polyQ disease models by using zebrafish.

1.4 General introduction to SCA-1 symptoms and pathogenesis

Spinocerebellar ataxia type 1 (SCA1) is a dominantly inherited neurodegenerative disease caused by polyQ expansion in Ataxin-1 (Atx-1). The pathogenic polyQ-expansions (usually between 39–82) in Atx-1 induce neurotoxicity which results in selective loss of Purkinje cells in the cerebellum, atrophy of specific brain stem neurons (Janghoo et al., 2008; Krol et al.,

2008; Joana et al., 2008). Patients suffer from progressive loss of motor coordination, ataxia, dysarthria, oculomotor palsy, amyotrophy, sensory disturbance and problems with swallowing, etc.

Fig.1-4. Schematic representation of the Atx-1 architecture. The positions of the polyQ tract (Q) and of the AXH motif are indicated as well as S776 (Chiara, and Pastore et al., 2009).

Although the exact native function of Atx-1 is still unclear, it has been suggested that Atx-1 is involved in transcriptional regulation, as it can bind to RNA and interact with multiple transcription factors. The large pathogenic polyQ tract alters the native conformation of the protein, subsequently undergoes aggregation in the affected neurons. Previous investigations proposed that polyQ expanded Atx-1, like its wild-type form, can interact with several transcriptional repressor or nuclear proteins and incorporates them into these complexes, for example Capicua (CIC), GFI-1 and TIP60-RORa, which could perturb the native functions of these interactions. Thus the gain of Atx-1 functions may lead to a loss of functions of its binding proteins. In addition, the pathogenesis of SCA-1 may result at least in part also from the loss of normal Atx-1 function.

Besides the formation of an Atx-1-CIC complex which causes a loss of CIC function during SCA-1 pathogenesis, Lim and Zoghbi et al.,2008 showed that polyQ expanded Atx-1 can form another particular large complex with RBM17 (RNA-binding motif protein 17). This complex may have a function in RNA splicing, contributing to a gain-of-function mechanism during SCA-1 pathogenesis. PolyQ expansion in Atx-1 strongly enhances the formation of an Atx-1–RBM17 complex both in cell culture and in the cerebellum of Atx-1 polyQ knock-in mouse. Further, polyQ expansion can alter the proportion of the mutant protein participating in the formation of the two known complexes in vivo, due to a competition with Atx-1. This investigation provides a molecular mechanism to explain how polyQ expansion causes both gain and loss of function to SCA-1 pathology.

PolyQ diseases are generally thought to be caused by protein misfolding and polyQ aggregation, although increasing evidence revealed an involvement of protein domains other than the polyQ tracts in pathogenesis. For example, polyQ expanded Atx-1 does not cause cerebellar degeneration if the nuclear localization signal or the AXH domain is deleted, also a mutation (from Serine to Alanine) that prevents phosphorylation at residue 776 represeats a non-toxic Atx-1 variant. Chen et al. (2003) reported that the protein 14-3-3, a multifunctional regulatory molecule, could interact with Atx-1, stimulates Atx-1 aggregation and increases

steady-state levels of Atx-1, thus aggravates neurodegeneration shown in a SCA-1 fly model. The interaction of Atx-1 and protein 14-3-3 requires Akt phosphorylation at S776 in Atx-1. In this investigation, the evidance that phosphatidylinositol 3-kinase/Akt signaling and 14-3-3 cooperate to modulate the neurotoxicity of Atx-1, provides insight into SCA-1 pathogenesis

1.5 PolyQ protein aggregation, neurotoxicity

1.5.1 PolyQ protein aggregation is a pathological hallmark of polyQ diseases

Aggregation of the polyQ protein in affected neurons is a hallmark of the neurodegenerative polyQ diseases. There is a great body of evidence showing that these polyQ containing protein aggregates are present in degenerating neurons in human patients, and as well as in animal models of these diseases (David et al., 2005; Shao et al., 2007). The proteins involved in polyQ diseases are prone to aggregate and accumulate already in their natural non-expanded from. Previous evidence proved that the expansion of the polyQ sequences facilitates aggregation of the disease protein. Intracellular and/or nuclear inclusions are common feature of polyQ diseases. Growing evidence suggests that the cell nucleus is the main pathogenic subcellular site for SCA-1, -7 and HD, whereas the cytoplasm is considered to be the site for SCA-2 and SCA-6 pathogenesis.

However, it is still under debate whether the aggregates of polyQ protein are pathogenic themselves or they simply reflect the disease process. The fact that they are preferentially observed in susceptible neurons indicates that they likely represent pathological markers of the underlying progressive pathogenesis, but they could also serve some neuroprotective functions.

1.5.2 Where does the neurotoxicity of polyQ protein aggregates come from?

Nuclear and/or cytoplasmic protein aggregates are observed in most polyQ diseases, occurring in different brain regions depending on the disease. Although the exact mechanism of neurotoxicity remains unclear, accumulating evidence suggest that the aggregation of the polyQ disease proteins is closely linked to the disease progression.

Two widely proposed, yet still debated theories of polyQ pathogenesis argue either failures in protein homeostasis and/or a transcriptional dysregulation. Evidence suggesting a failure in protein homeostasis includes the formation of Ubiquitin-positive inclusions in the affected neurons, the recruitment of proteasome components and molecular chaperones to nuclear inclusions, and the ability of molecular chaperones to suppress toxicity in disease models when being overexpressed (Zoghbi et al., 2001). Evidence supporting transcriptional perturbation includes expanded polyQ-induced alteration in gene expression and the surpression of Histone acetyltransferases by polyQ proteins.

Transcription factors and cofactors are important nuclear proteins and can interact with polyQ containing proteins. One remarkable example is the transcriptional coactivator, cAMP response element-binding protein (CREB)-binding protein (CBP), which was found to colocalize with polyQ nuclear aggregates. CBP functions as a coactivator for multiple diverse transcription factors; therefore, its sequestration in polyQ nuclear inclusions could inhibit this important transcriptional component in the disease affected neurons.

Doi et al found that the RNA-binding protein FUS/TLS is the major component of nuclear polyQ aggregates in a cellular model of Huntington´s disease. They also reported that FUS/TLS binds to nuclear inclusions in the brains of SCA-1, 2, 3 and DRPLA patients.

However, it is still controversial whether the misfolded polyQ protein monomers and/or the final inclusions and/or the intermediate oligomers are toxic or whether aggregate is a protective response by the cell. Therefore it is important to understand the molecular mechanisms underlying the polyQ protein aggregation process in relation to the disease progression. Even if polyQ inclusions are not the major toxic species, the aggregation process appears closely linked to pathogenesis. Therefore, it is critical to understand the polyQ aggregation dynamics during neuronal degeneration.

1.5.3 Dynamics of polyQ protein aggregation and its regulation

1.5.3.1 Dynamics of polyQ protein aggregation

Through *in vitro* study, it is accepted that the polyQ aggregation proceeds a nucleated growth polymerization process and results in the accumulation of β-sheet rich fibrillar structures that detected by electron microscopy. For example, the HD causative protein Huntingtin (Htt), has a strong propensity to aggregate into insoluble β -structures, with the aggregation being greatly dependent on the length of the polyQ repeates (Cooper et al., 1998). It has been shown that proteins carrying longer polyQ repeats could perform a faster aggregation and exerts a

more severe toxicity, compared to shorter polyQ variants. Wanker et al showed that the N-terminal peptide of Htt with pathological polyQ tracts (Q51-122), but not the wild type (Q20 and 30), N-terminus could form high molecular weight protein aggregates with a fibrillar or ribbon-like morphology, reminiscent of scrapie prion rods and β-amyloid fibrils in Alzheimer's disease. They also reported that the formation of amyloid-like Htt aggregates in vitro not only depends on polyQ repeat numbers but also critically depends on protein concentration and time of expression. The in vitro aggregation of Htt can be seeded by preformed fibrils. Together, these results suggested that amyloid fibrillogenesis in Huntington's disease is a nucleation-dependent polymerization.

The dynamics of polyQ aggregation is being unraveled, but is still poorly understood (Fig.1.4). It is unclear whether aggregation proceeds via linear addition of single molecules or whether there are oligomeric intermediates. In addition, the stage of polyQ aggregation that causes neurodegeneration remains unclear. Whatever the mechanism, a critical issue for understanding the pathogenesis of polyQ diseases is to elucidate the dynamics of polyQ aggregation.

It is proposed that polyQ protein aggregation is a fast process involving small and invisible structures. Due to the technical difficulties, the detailed process of aggregation is quite hard to monitor and observe. The hypothetical nucleation process during aggregation has been deduced from in vitro studies, and supported by synthetic polyQ peptides studies in Htt and Atx-3, etc. PolyQ protein aggregation is initiated by a polyQ expanded monomer, which is misfolded and it functions as the critical seed for further aggregation. The single polyQ monomer can form oligomers via linear addition of monomers. Subsequently, the intermediate dynamic product continues the nucleation process to form bigger sizes of aggregation products, which are termed of protofibril, fibril, fiber, and are finally visible by microscopy as aggregates being termed inclusions. Another in vitro study showed that the kinetics were characterized by long lag times followed by rapid aggregate growth, with a strong dependence of aggregation lag time on monomer concentration. The hypothetical aggregation process of Htt is depicted by Fig. 1-5 (Legleiter et al., 2010).

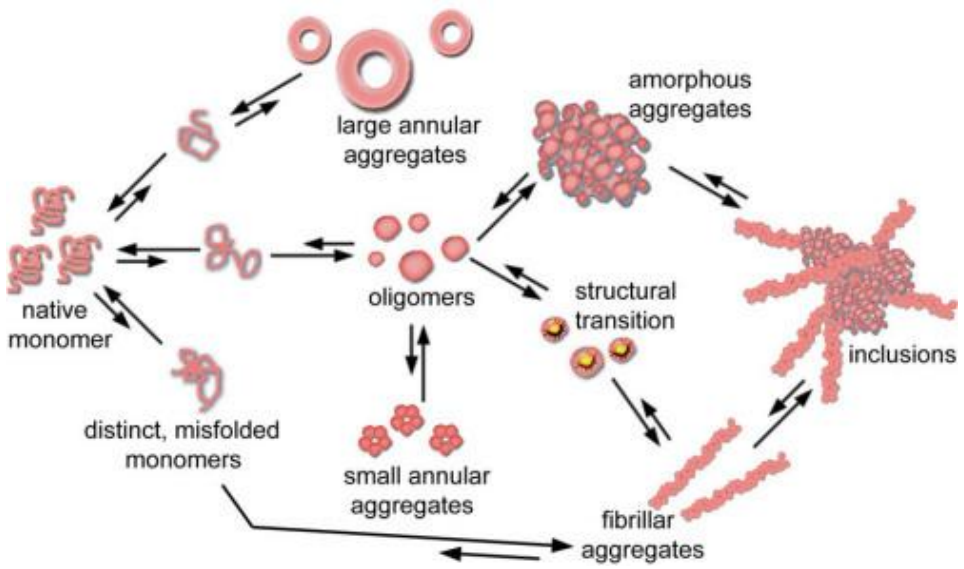

Fig.1-5. Hypothetical model of polyQ-mediated Htt aggregation. Native polyQ monomer undergoes a structural conversion to β-sheet, which further aggregate resulting in the formation of annular aggregates, oligomers, large amorphous aggregates, and fibril intermediates through a linear growth mechanism. In this model, a structural transition occurs within an oligomer to initiate fibril elongation. Subsequently, fibril elongation can be obtained through oligomers and monomers direct accumulation. Many of these higher order aggregates can accumulate together, resulting in the characteristic large inclusions observed in polyQ disease.

Many questions that are relevant for the dynamics of polyQ aggregation and polyQ disease pathogenesis and its progression remain unanswered. For example, how do polyQ aggregates behave in the affected neurons of animal models and patients patients? Are the dynamics of the polyQ protein aggregation process affected by the recruited proteins? Whether the neurotoxicity is regulated by this process? What suggestions can be obtained from the process of polyQ aggregation towards the development of therapies? These answers are quite important for understanding the disease mechanisms and for mitigating the symptoms of patients or even cure them.

1.5.3.2 The neurotoxicity of different aggregation products

The expanded polyQ domain can transit into an abnormal conformation which may exert toxicity in several ways, including: (a) functional alteration of the polyQ protein, for example, by changes of its intermolecular interactions (Gervais et al.,2002; Zeron et al., 2002) (b) the generation of toxic oligomers, which are considered to be the more active aggregation intermediates to recruit and stabilize other proteins (Lajoie et al., 2010; Toshiaki et al., 2008) (c) the generation of toxic polyQ-containing fragments after cleavage of the polyQ protein; for example, the SCA-3 causative protein Atx-3 could be proteolytic cleaved and release the

pathogenic C-terminal fragment (Yoshizawa et al., 2000; Haacke et al., 2007); (d) transcriptional dysregulation, caused the specific transcription factors sequestration after recruited by polyQ aggregation, like in SCA-3, the CBP could be recruited by the aggregates, which was mentioned before (Li et al., 2002); (e) proteotoxic stress as a result of the disruption of the quality control systems of the cells; for example, in HD mice, it was suggested that mutant Htt impairs cargo recognition by autophagosomes, which leads to a failure in protein degradation. Large intracellular aggregates formed by Htt are associated with proteasome impairment (Martinez-Vicente et al., 2010); (f) mitochondrial dysfunction. PolyQ expanded Htt could repress PGC-1α, which regulates mitochondrial function and could bind to mitochondria directly, followed by mitochondrial dysfunction (Cui et al., 2006; Shao and Diamond, 2007).

The neuronal toxicity may be derived from the monomer of the polyQ expanded protein itself or from toxic oligomers and/or other intermediate products. It is crucial to discriminate the neurotoxicity of large macromolecular inclusions versus small aggregates or oligomers. Evidence has shown that the large inclusions are inactive and non-toxicity or even protective (Arrasate et al., 2004). This is consistent with the concept that such inclusions represent an end-stage of the cellular response to the misfolded protein.

1.5.3.3 Pathways involved in polyQ protein aggregation

The effects of the interaction between cellular proteins and the polyQ protein monomers and/or other aggregation products were emphasized. Several pathways have been indentified which could reduce polyQ aggregation and even ameliorate cell death in HD and another polyQ disease SBMA. Shao et al., (2008) reported that the aggregation of polyQ expanded Htt and AR peptides can be reduced by the overexpression of Profilin, a small actin-binding factor, which is a direct target of the ROCK1 isoform and also interacts with Htt. Profilin's G-actin binding activity and its direct interaction with Htt are required to reduce the aggregation, which was proven by the inhibition of the ROCK1-mediated phosphorylation of Profilin at Ser-137. Y-27632, an inhibitor of the Rho-associated kinase ROCK, can also reduce the aggregation of polyQ expanded AR via the inhibition of phosphorylation of Profilin. Knockdown of Profilin blocks the inhibitory effect of Y-27632 and leads to an increase of both AR and Htt aggregation. Co-expression of inactive Cofilin, a member of the actin-depolymerizing factor (ADF) protein family can reduce AR polyQ aggregation (Diamond et al., 2008; Nukina et al., 2009). Deletion of the actin-binding regions in AR and Htt protein renders the polyQ-expanded ARN127 and Htt exon 1 less aggregation-prone, and increases

the SDS-solubility of aggregates (Angeli et al., 2010). Thus, this evidence links Actin to the Htt- and AR polyQ aggregation process at least via the ROCK pathway through direct interaction between them.

1.5.4 Current progress on the study of Ataxin-1 aggregation

Protein misfolding and aggregation are central characteristics of the polyQ neurodegenerative diseases, including SCA-1, but the dynamic properties of polyQ protein aggregation of Atx-1 are poorly understood, which is one of the critical issues for understanding how pathogenesis emerges in SCA-1 compared to Htt or AR. Atx-1 polyQ aggregation has different properties with Atx-3 and Htt in cellular mobility and stabilization with CBP revealed by FRAP (Chai et al., 1998), which suggest the necessity to study the dynamics of Atx-1 aggregation, towards understanding the pathogenesis of SCA-1 in the specific affected neuronal cell types.

It was revealed that the pathogenic large polyQ expansion can accelerate the aggregation dynamics of Atx-1, indicated by the enhanced intracellular kinetics as compared to wild type Atx-1 in HEK293T cells (Krol et al., 2008). To directly study the dynamics of polyQ protein aggregation, the fusion of the polyQ protein with a fluorescent protein provides a very useful tool. The Green fluorescent protein (GFP) fused with Atx-1 can mimic the aggregation behavior and maintain its cellular toxicity, even though Atx-1-GFP toxicity is milder as Atx-1 is fused with another fluorescent protein Ds-Red (Rich and Varadaraj, 2007; Paulson et al., 2002). Through this method, it was proven that the wild type unexpanded Atx-1 can also form aggregates, but in a reversible and soluble form without cellular toxicity, while the aggregates formed by Atx1Q85 fused with GFP are irreversible and insoluble (Rich and Varadaraj, 2007).

Besides the length of polyQ, plenty of data show that the domains outside the polyQ sequences are also the involved in the aggregation process. In the case of Atx-1, it was demonstrated that the AXH domain of Atx-1 participates in protein aggregation. For example, When the AXH domain is deleted from Atx-1, the Atx-1 aggregation is noticeably reduced even though it contains a long polyQ tract. When the AXH domain is replaced with a homologous sequence from the transcription factor HBP1, which has no tendency to aggregate, the aggregation is also decreased. These data provide a direct evidence for the involvement of a domain other than the polyQ stretches in polyQ protein aggregation (Chiara et al., 2005).

The intranuclear dynamics of GFP fused to Atx-1Q84 were examined through fluorescence recovery after photobleaching (FRAP) method and compared with other polyQ proteins. It

was revealed that at least two types of Atx-1 inclusions exist; one type undergoes fast and complete exchange with a nucleoplasmic pool and another type contains varying levels of slow-exchanging Atx-1. Slow-exchanging aggregate contains high ubiquitin levels, but surprisingly low proteasome levels. Proteasomes and CBP exhibit highly dynamics in Atx-1 inclusions, indicating that although interact with Atx-1, they are not irreversibly immobilized (Stenoien et al., 2002; Chai et al., 2002). While, polyQ mutated Htt and Atx-3, could cause CBP to be sequestered in a fully immobilized state, losing its ability to modulate transcription. These phenotypes of Atx-1 are quite different with Atx-3 and Htt, even though they all contain an aggregation prone polyQ domain. These findings may help to explain disease-specific elements of pathogenesis in these neurodegenerative diseases.

Furthermore, the different immobility of CBP caused by Atx-1, Atx-3 and Htt suggest that, the different polyQ proteins may have different unique interaction patterns with the cellular proteins, and their aggregation process may be modulated by different pathways. In the case of Atx-1 aggregation, the formation and fusion of Atx-1 aggregates were observed. While, Atx-1 aggregation process and its modulation mechanisms are needed to be explored, especially in the SCA-1 disease affected Purkinje neurons. Thus, further analysis of aggregation dynamics in polyQ expanded Atx-1 is necessary and important towards the understanding the pathogenesis and progression of SCA-1 disease.

1.5.5 The advantages of using zebrafish in polyQ aggregation study

Too many questions need to be answered in polyQ aggregation process. As in mouse and other animal models available at present, it is quite different to observe the polyQ protein aggregates directly in the affected neurons in live animals, which limits the investigation to monitor the real-time behaviors of polyQ aggregates, and to explore the interactions with other molecules. Without this information, it is hard to understand the toxicity of different polyQ proteins to their specific affected neuronal cell types even though they are ubiquitously expressed in human brains, and therefore limits the effects to the understandings of the mechanisms of disease pathogenesis and progression.

Zebrafish provides a quite useful animal tool to perform further investigation of Atx-1 aggregation process. With the advantages of the accessibility of high resolution imaging in live larvae and its evolutionarily conserved features, zebrafish is hopeful to mimic and monitor the polyQ aggregation and interactions with other molecules in disease affected neurons. When Atx-1 polyQ variant are fused to a fluorescent protein, and expressed in zebrafish neurons, its expression and aggregation could be observed directly through bio-

imaging in live embryos. This could provide direct dynamic information of polyQ protein aggregation. The SCA-1 disease model in zebrafish generated in our lab provides the possibility to further study of Atx-1 polyQ aggregation dynamics.

1.6 The aims of this study

1.6.1 Generation of a zebrafish SCA-3 model

Direct expression of the mutant pathogenic atx-3 gene fused to a fluorescent protein (for example CFP) in zebrafish cerebellum may mimic the key characteristics of SCA-3, causing cerebellar neurons to dysfunction and to degenerate accompanied by SCA-3 aggregate formation. Using such model, could be helpful to decode the unclear pathogenesis mechanisms of SCA-3 in vivo by monitor polyQ protein aggregation in degenerating neurons.
Zebrafish SCA-3 disease model is accessible for high resolution imaging, but the first technical difficulty is the maintaining of the transgenic carriers. Therefore, combinational genetics should be applied in this model. Gal4/UAS technique is suitable for this purpose and it has been established in zebrafish (Distel et al., 2009). Gal4/UAS system has the advantages to express Atx-3 in many different neuronal cell types. At present, several kinds of neuronal enhancers are available. Several UAS driven fluorescent reporter lines can be crossed with cell type specific Gal4 activator lines, to obtain transgenic expression in a tissue specific manner in the resulting offspring. Recently, zebrafish cerebellar Purkinje cell enhancer has been isolated. The genetic tools combined with in vivo imaging techniques promise the possibility for establishing a rapidly progressive SCA-3 disease model, which is accessible for high resolution in vivo live imaging and to address the molecular mechanisms underlying cellular causes of neuronal degeneration in SCA-3.
Finally, pharmaceutical compounds can be used easily and tested in such model, which provides the possibility to carry out high throughput in vivo screening, aiming to identify pre-drug compounds, which is quite difficult in mammalian models.

1.6.2 Analysis of Atx-1 aggregation dynamics

The dynamics of polyQ expanded Atx-1 aggregation need to be further clarified, especially in degenerative neurons by in vivo study. As revealed in previous study, when fused to a fluorescent protein, the pathogenic polyQ expanded Atx-1 variant still maintains its cellular toxicity and the aggregation ability, which could help to monitor the behaviors of polyQ protein aggregates. When such Atx-1polyQ fusion variant is expressed in SCA-1 specific affected cerebellar Purkinje neurons, Atx-1 polyQ aggregation dynamics in living zebrafish larvae could be monitored and analyzed.

Considering that polyQ aggregates share many common structural features, the previous investigations on Htt and AR aggregation provide suggestions for Actin involved mechanisms of Atx-1 aggregation. Whether Actin could affect the Atx-1 aggregation in the cytoplasm or in the nucleus remains unclear. The effects of pharmaceutical depolymerization of F-Actin on the Atx-1 aggregation will be examined. The effects of different subcellular localized Actin on the Atx-1 polyQ aggregation will be clarified through co-expression. Furthermore, the colocalization of Actin and Atx-1 polyQ aggregates will be investigated, which could suggest the possible interaction between them.

Profilins and Cofilins are key modulators of Actin polymerization. Profilins maintain the pool of free G-Actin and promote Actin polymerization through interaction with F-Actin forming complexes; Cofilins serve as F-Actin severing and depolymerizing factors leading to the disassembly and local branching of the Actin network. Profilin has been reported that it could decrease Htt polyQ aggregation depending on a direct binding with Htt. Interestingly, A recent yeast-two-hybrid revealed a direct interaction of Atx-1 and Cofilin1(Lim et al., 2006). Whether Cofilin can modulate Atx-1 aggregation is an important question to answer. To uncover such a link between Atx-1 aggregation and Actin and its modulators would not only provide a major step towards understanding the regulation mechanisms of Atx-1 polyQ aggregation but also in the Purkinje cells degeneration mechanisms during the progression of SCA-1 disease.

2 Materials and Methods

2.1 Equipment and Reagents

2.1.1 Equipment

Name	Description and Manufacturer
Centrifuges	Kendro Evolution (Kendro Laboratory Products, München, Germany); Tabletop Centrifuge 5415D and 5415R (Eppendorf, Hamburg, Germany)
Benchtop thermostats	Thermomixer, 5463/Comfort (Eppendorf, Hamburg, Germany)
Binokular	Stemi SV11 (Zeiss, Jena, Germany)
Confocal laser scanning microscopes	Zeiss LSM510 equipped with Argon laser (451, 477, 488, 514nm) and Helium-Neon lasers (561, 594, 633nm), Zeiss LSM510 Meta equipped with Argon laser (451, 477, 488, 514nm) and Helium-Neon lasers (543, 633nm) (Zeiss, Jena, Germany) Olmpus FV1000 equipped with Argon laser, and DPSS Laser 559nm
Developing machine for radiographs	Curix60 (AGFA, Köln, Germany)
Electrophoresis power supplies	Electron EC105 (Thermo Fisher Scientific, Rockford, IL, USA); Power Pac 3000 (BioRad, München, Germany)
Fluorescent Stereomicroscope	MZ 16FA equipped with filters for UV, GFP, FITC/Cy-3, YFP, Rhodamine and Texas Red (Leica, Wetzlar, Germany)
Gel documentation	(Herolab, Wiesloch, Germany) (Intas, Göttingen, Germany)
Gel electrophoresis chambers	(Shelton Scientific (Sigma-Aldrich Chemie GmbH), Deisenhofen, Germany); (Amersham/BD

	Biosciences, München, Germany); (PEQLAB Biotechnologie GMBH, Erlangen, Germany)
Microinjection needle puller	(Narishige, Tokyo, Japan)
Microinjector	FemtoJet Express (Eppendorf, Hamburg, Germany)
Microscope camera	Axiocam HRc digital camera (Zeiss, Jena, Germany)
Objectives	Plan-NeoFluar 5x/NA0.15 Plan-NeoFluar 10x/NA0.3 Plan-NeoFluar 20x/NA0.5 Plan-NeoFluar 40x/NA0.75 DIC C-Apochromat 40x/NA1.20 water immersion Plan-Apochromat 63x/NA1.4 DIC C-Apochromat 63x/NA1.20 water immersion Plan-NeoFluar 100x/NA1.3 Ph3 (Zeiss, Jena, Germany)
PCR machine	PTC 100, MJ Research Inc. (Waltham, MA, USA)
Photometer	Biophotometer (Eppendorf, Hamburg, Germany)
Rotator	(LabInco BV, Breda, Netherlands)
Thermo Incubators	(Memmert, Schwabach, Germany)
Upright compound microscope	Axioplan 2 (Zeiss, Munich, Germany)
XCell II blot module	(Invitrogen GmbH, Karlsruhe, Germany)

2.1.2 Suppliers of chemicals and consumables

Standard chemicals were purchased from Sigma (Munich, Germany), Merck (Darmstadt, Germany), Roche (Mannheim, Germany), Promega (Mannheim, Germany). Enzymes and polymerases were ordered from New England Biolabs (NEB, Frankfurt, Germany), Roche (Mannheim, Germany), Invitrogen (Karlsruhe, Germany), MBI Fermentas (St. Leon-Rot, Germany), and Stragene (La Jolla, CA, USA).

Cell culture medium and supplements were obtained from Gibco and Invitrogen (Karlsruhe, Germany). Reagents used for Western blotting were supplied by Invitrogen (Karlsruhe, Germany), BioRad (Munich, Germany.), Amersham (Munich, Germany). Plastic ware was

delivered by Nunc (Langenselbold, Germany), Roth (Karlsruhe, Germany), Greiner Bio-one (Frickenhausen, Germany) and Eppendorf (Hamburg, Germany). Glassware was produced by Schott (Mainz, Germany).

2.1.3 Antiboides

Antibody	Host Species	Antigen	Dilution	Supplier	ID-No.
Rat anti-HA	Rat	HA	1:500	Roche, Mannheim, Germany	1867432
Cy2 Goat anti-Rat	Goat		1:500	Jackson, West Grove, USA	122-226-072
α ZebrinII	Mouse	Aldolase C	1:500	R. Hawkes, University of Calgary, Canada	RKG #15
Alexa Fluor® 488 chicken anti-mouse IgG (H+L)	Chicken	mouse IgG (H+L)	1:200	Jackson, West Grove, USA	A21200
ANTI-FLAG® antibody	rabbit	Flag	1:1000	Sigma, Munich, Germany.	F7425
Donkey anti rat-HRP	Donkey	Rat IgG (H+L)	1:5000	Jackson, West Grove, USA	712-475-153
Anti mCofilin	Rabbit	Mouse Cofilin	1:200	Sigma, Munich, Germany.	C-8736
Cy2-Anti rabbit	Goat	Rabbit IgG (H+L)	1:200	Jackson, West Grove, USA	111-225-003

2.1.4 Kits, Enzymens and Affinity Purification Reagents

Alkaline Phosphatase (1 U/µL)	Roche Diagnostics, Mannheim, Germany
dNTPs	Roche Diagnostics, Mannheim, Germany
DIG RNA-Labelling mix	Roche Diagnostics, Mannheim, Germany
DNaseI (RNase-free, 1 U/µL)	Roche Diagnostics, Mannheim, Germany
FuGENE® HD	Roche Diagnostics, Mannheim, Germany
Gel Extraction kit	Qiagen, Hilden, Germany
GeneClean Turbo kit	Q-BIOgene, Heidelberg, Germany
GeneRuler™ 1kb DNA Ladder	Invitrogen GmbH, Karlsruhe, Germany
Klenow-Fragment (10 U/µL)	Roche Diagnostics, Mannheim, Germany
Message Machine SP6 Kit	Ambion, Darmstadt, Germany
NucleoBond® PC100/500	Macherey & Nagel, Düren, Germany
Pfu Ultra II DNA polymerase	Stratagene, La Jolla, CA, USA
Pronase	Roche Diagnostics, Mannheim, Germany
Proteinase K, 20mg/mL	Roche Diagnostics, Mannheim, Germany
QIAGEN Nucleotide Removal kit	Qiagen, Hilden, Germany
QIAquick PCR Purification kit	Qiagen, Hilden, Germany
QIA shredder	Qiagen, Hilden, Germany
Restriction endonucleases	MBI Fermentas, St. Leon-Rot, Germany; New England Biolabs, Frankfurt, Germany; Roche Diagnostics, Mannheim, Germany
Rnasin RNase Inhibitor (40 U/ µL)	Promega, Mannheim, Germany
RNeasy Mini Kit	Qiagen, Hilden, Germany
SP6 RNA-Polymerase (20 U/µL)	MBI Fermentas, St. Leon-Rot, Germany
StrataClone Blunt PCR Cloning Kit	Stratagene, La Jolla, CA, USA
T3 RNA-Polymerase (20 U/µL)	MBI Fermentas, St. Leon-Rot, Germany;
	Roche Diagnostics, Mannheim, Germany
T4 DNA-Ligase (5 U/µL)	MBI Fermentas, St. Leon-Rot, Germany
T7 RNA-Polymerase (20 U/µL)	MBI Fermentas, St. Leon-Rot, Germany;

	Roche Diagnostics, Mannheim, Germany

2.1.5 Buffers and medium

Standard buffers were prepared as described by Sambrook and Fritsch (Sambrook 2001). Embryo solutions and standard zebrafish protocols were adapted from M.Westerfield (Westerfield 1955) and Kimmel et al. (Kimmel and Schilling et al.1995).

2.1.5.1. Protein Biochemistry

PBS: 10 mM Na_2HPO_4 2 mM KH_2PO_4 137 mM NaCl 2.7 mM KCl pH 7.4 adjusted with 1 M NaOH	Dry Milk Blocking Buffer: 5% (w/v) Dry milk powder in TBS-Tween
2x HBS (filtered): 280 mM NaCl 1.5 mM $Na2HPO_4$ 50 mM HEPES 1 M NaOH adjusted pH 7.13	2x SDS-Sample Buffer: 125 mM Tris-HCl (pH 6.8) 20% Glycerol (w/v) 4% SDS (w/v) 0.02% Bromphenol blue (w/v) 10% β-Mercaptoethanol (v/v) (add fresh)
SDS-PAGE-Tank Buffer: 25 mM Tris 250 mM Glycine 0.1% SDS (w/v)	TBS-Tween: 20 mM Tris-HCl (pH 7.6) 150 mM NaCl 0.1% Tween20 (v/v)
SF-TAP Wash Buffer: 1x TBS 0.1% NP40.	TEN Buffer: 40 mM Tris-HCl (pH 7.6) 150 mM NaCl 1 mM EDTA
striping solution: 2% SDS	

62.5 mM Tris-HCl pH 6.8 0.08% ß-mercaptoethanol	

2.1.5.2 Embryo raising medium

Danieau-stock Solution 300 %: 58 mM NaCl 0.7 mM KCl 0.4 mM MgSO4 0.6 mM $Ca(NO_3)_2$ 5 mM HEPES (pH 7.2)	Anti-Pigmentation Agent: 0.15 mM 1-phenyl-2-thiourea (PTU) 1x PTU (optional) Dilute 1:10 for working solutions
Anaesthesia: 0.002 g/mL Tricaine in 30 % Danieau	Egg Water 0.3 g/L Instant Ocean Salt Mix/osmosis water

2.1.5.3 Histology

20x SSC: Tris-Acetate 3 M NaCitrate 300 mM pH 7.0 adjusted with NaOH	PTW: 0.1% Tween in PBS (v/v) PTW DMSO: 1% DMSO in PTW (v/v)
NGS Blocking Solution: 10% NGS (Normal Goat Serum) in PTW Fixation Buffer: 4% PFA in PTW (v/v) Glycine: 20 mg Glycine in 1 mL ddH_2O	ISH Staining Buffer: 0.1 M NaCl 0.1 M Tris pH 9.5 50 mM $MgCl_2$ 0.1% Tween

2.1.5.4. E.coli & Cell Culture medium

LB-Medium: 10 g Bacto-Trypton 5 g Yeast Extract 10 g NaCl Water add 1 L in 1 L deionised water pH 7.4	LB-Agar: 10 g Bacto-Trypton 5 g Yeast Extract 10 g NaCl 15 g Agar In 1 L deionised water
Cell Culture Medium (Mammalian Cells): DMEM Dulbecco's Modified Eagle Medium 10% Fetal Bovine Serum (v/v) 1% Penicilin/Streptomycin (v/v) 1% Glutamin/Glutamax (v/v)	Cell Culture Medium (PAC2 Cells): L-15 Leibovitz Medium 10% Fetal Bovine Serum (v/v) 1% Penicilin/Streptomycin (v/v) 1% Glutamin/Glutamax (v/v)

2.1.6 Software for image rendering and analysis

2.1.6.1 Confocal microscope and Fluorescent Stereomicroscope software

Axio Vision Software 4.5SP1 (Zeiss, Jena, Germany)
FV-10 ASW 2.0 (Olympus, Tokyo, Japan)
Leica LAS AF Lite (Leica, Wetzlar, Germany)

2.1.6.2 Imaging rendering and analysis

Adobe Illustrator CS5 (Adobe, San Jose, CA, USA)
Adobe Photoshop CS5 (Adobe, San Jose, CA, USA)
ImageJ 1.37+Macro Time stamper (NIH, Bethesda, MD, USA)
QuickTime Player Pro Version 7.1.6 (Apple, Cupertino, CA, USA)

2.1.7. Bacteria strains and cell culture lines

XL1-Blue E. coli strain is described in Bullock et al.1987.
StrataClone soloPace Competent Cells are described in (Stratagene, La Jolla, CA, USA)

2.1.7.2. Cell culture

HEK 293T cells, a human embryonic kidney cell line (Graham et al., 1977), Hela cells (Puck et al., 1956), a cervical cancer cell line and PAC2 zebrafish Fribroblast Cells (Amsterdam et al., 1999; Senghass and Köster, 2009)

2.1.8 Fish Strains

2.1.8.1 Wild type

The wild type AB strain (ZFIN) was used for analyzing certain mRNA expression patterns, and also for microinjection, to obtain transient expression or to generate transgenic lines.

2.1.8.2 Mutant strains

Fish of the Brass strain (EKK Will Waterlife Resources, Gibbonston, FL, USA), could be considered as wild type zebrafish, with less pigment formed by melanocytes on the body surface. Embryos of this strain are suitable for observing the colorful signal or fluorescent protein. This line was used for analyzing mRNA expression pattern, and also used for microinjection, to obtain transient expression or generate transgenic lines.

2.1.8.3 Transgenic lines

Tg[5×UAS:fyntagRFPT-T2A-HA-atx3Q84]
This transgenic effector line was generated to obtain pathogenic atx3Q84 fragment expression in specific neuronal cell types, when crossed to corresponding activator Gal4 lines. The membrane localized FyntagRFPT was used to observe the morphology of expressing neurons and to monitor their survival state. The HA tag was used to observe the degree of Atx-3Q84 aggregation.

Tg[5×UAS:fyntagRFPT-T2A-HA-atx3Q15]
This transgenic effector line was generated to obtain non-pathogenic atx3Q15 fragment expression in specific neuronal cell types, when crossed to corresponding activator Gal4 lines. The membrane localized FyntagRFPT was used to observe the morphology of expressing

neurons and to monitor their survival state. The HA tag was used to observe the degree of Atx-3Q15 aggregation.

Tg[5×UAS:fynVenus-T2A-atx3Q69-CFP-strep]

This transgenic effector line was generated to obtain pathogenic atx3Q69 fragment expression in specific neuronal cell types, when crossed to corresponding activator Gal4 lines. The membrane localized fynVenus was used to observe the morphology of expressing neuronsand to monitor their survival state. The CFP was used to observe Atx-3Q69 aggregation. The Strep tag could be used for protein isolation and purification.

Tg[5×UAS:fynVenus-T2A-atx3Q15CFP-strep]

This transgenic effector line was generated to obtain non-pathogenic atx3Q15 fragment expression in specific neuronal cell types, when crossed to corresponding activator Gal4 lines. The membrane localized fynVenus was used to observe the morphology of expressing neurons and to monitor their survival state.

Tg[Car8-fynVeuns-T2A-HA-atx3Q99]

This transgenic line was generated to obtain pathogenic HA-atx3Q99 fragment expression specifically in zebrafish Purkinje neurons. The membrane localized fynVenus was used to observe the morphology of expressing neurons and to monitor their survival state.

Tg[Car8-fynVeuns-T2A-HA-atx3Q15]

This transgenic line was generated to obtain non-pathogenic HA-atx3Q15 fragment expression specifically in zebrafish Purkinje neurons. The membrane localized fynVenus was used to observe the morphology of expressing neurons and to monitor their survival state.

Tg[Hb9:KalTA4]

This is a motor neuron activator line, with motor neuron specific expression of Gal4. When crossed to a UAS effector line, the target protein could be expressed in motor neurons.

Tg[5×UAS:FynVenus-T2A –atx1Q75-mseCFP] (Dr.Kazuhiko Namikawa, Köster lab)

This effector line, crossed to a neuronal specific expressing Gal4 line, the activator line, can result Atx1Q75 expression in specific neuronal cell types. The membrane localized Venus can facilitate the observation of neuronal morphology, to indicate the cell´s survival state.

Tg[Her3:KalTA4] （Dr. Andreas Babaryka, Köster lab）

Her3 encodes a zebrafish bHLH protein of the Hairy-E (Spl) family. This activator line can drive expression in the developing mesencephalon /rhombencephalon and the spinal cord, when crossed with an effector UAS line.

2.1.9 Plasmid vectors

#2 pCS2+

pCS2+ is a multipurpose expression vector, useful for high-level transient expression in a wide variety of mammalian cells. It can be used for in vitro transcription, to synthesize RNA probe, which can be used for mRNA expression analysis by in situ hybridization.

It contains a strong enhancer/promoter (simian CMV IE94) followed by a polylinker and the SV40 late polyadenlyation site. An SP6 promoter is present in the 5' untranslated region of the mRNA from the sCMV promoter, allowing in vitro RNA synthesis of sequences cloned into the polylinker. There is a T7 promoter in reverse orientation between the polylinker and the SV40 polyA site for probe synthesis, as well as a second polylinker after the SV40 polyA site, providing several possible sites to linearize the vector for SP6 RNA transcription. The vector backbone is from pBluescript II KS+ and includes the amp resistance gene and an f1 origin for producing single stranded DNA. (Rupp et al., 1994)

#1440 pCS atx1Q82-CFP (Dr. Kazuhiko Namikawa, Köster lab)

It drives ubiquitous expression of human Atx1Q82, fused to Cyan fluorescent protein (CFP) for monitoring Atx1Q82 localization.

#1630 pCS 3×NLS-CFP (Dr. Kazuhiko Namikawa, Köster lab)

It drives nuclear expression of CFP in nucleus.

#1789 pCS lynVenus-T2A-atx1Q82-CFP (Dr. Kazuhiko Namikawa, Köster lab)

It drives ubiquitous expression of human Atx1Q82, to analyze its aggregation, and observe the cell morphology via membrane expressed Venus.

#1878 pBC PrP-MJD15 (obtained from Dr. Thorsten Schmidt)

Prp promoter drives the full length of human wild type non-pathogenic atx3 gene, the polyQ number is 15.

#1879 pBC PrP-MJD77 (obtained from Dr. Thorsten Schmidt)
Prp promoter drives the full length of pathogenic type atx3 gene, the polyQ number is 77.

#2239 pB 14 xUAS-FynVenus-atx1Q82-mseCFP (Dr. Kazuhiko Namikawa, Köster lab)
As an effector plasmid, combined with an activator plasmid, human Atx1Q82 fused with mseCFP can be expressed, membrane localized fynVenus facilitates to obeserve the cellular morphology.

#2256 pCS unctagRFP (Enrico Kühn, Köster lab)
It drives tagRFP expression in the cytoplasm, facilitating to observe the cell morphology.

#2300 pCS atx1Q82-tagRFP
It drives ubiquitous expression of human Atx-1Q82, fused with tagRFP for indicating Atx1Q82 expression. It was cloned from vector: pCSunctagRFPGIpA (#2256), cut by EcoRI and SalI; insert: pCSHatx1Q82tagCFPGI (#1440), cut by EcoRI and SalI. The tag RFP was cloned behind Atx1Q82.

#2634 pCS-T2A-Atx3 C-term
This plasmid carries the fragment of T2A element and the C-terminus of atx3Q77, amplifed from plasmid #1879. The cloning strategy was: 2 times PCR: the 1st PCR: primer #936 and #937, template #1879, the 2ndPCR, primer #782 and #937. SpeI site is in the upstream of T2A-C-atx3Q77. SalI site is behind the atx3Q77.

#2635 pCS-fynVenus-T2A-C-atx3Q77-mseCFP
It was cloned by using the vector: #2168, cut by SpeI and SalI, in order to replace atx1 with C terminal atx3Q77; insert: plasmid # 2634 cut by SpeI and SalI, to get the T2A-C-atx3Q77 fragment. It drives the ubiquitous expression of the C terminal Atx-3Q77 fused with CFP, membrane localized fynVenus facilitates to observe the cell morphology.

#2637 pCS T2A-HA-C terminal atx3Q77

This plasmid carries the fragment of T2A element and C-terminus of atx3Q77, similar plasmid like #2634, but longer. It was cloned after 2 times PCR amplication; The 1st PCR: use primer #1147 and #937, the template is the plasmid #1879. The second PCR: use primer #782 and #937,

#2638 pCS fyntagRFP-T2A-HA-atx3Q84

It was cloned by using the plasmid pcs fyntagRFPT-T2A-NLSCFP; vector cut with speI and XbaI, insert: cut plasmid #2637 with speI and XbaI. It drives the ubiquitous expression of C-terminus of Atx-3Q84, fused with a HA tag.

#2640 pCSfyntagRFPT2A-HA-atx3Q15

It drives the ubiquitous expression of C-terminus non-pathogenic wild type atx3Q15 fragment. This plasmid was cloned in the same strategy with plasmid #2638.

#2641 pB tol500-Car8-fynVenus-T2A-HA-atx3Q99

It drives specific expression of a pathogenic HA-atx3Q99 fragment in zebrafish Purkinje neurons. The membrane localized fynVenus facilitates to observe the cell morphology. This plasmid can be used for generating a transgenic line to model the MJD in zebrafish. This plasmid was cloned from the Vector #2452, cut byEcoRI and XbaI, the fragment T2A-HA-atx3Q84 was isolated from plasmid #2638 cut by SpeI and XbaI, the fragment of fyntagRFP was replaced with Fynverus via cutting with EcoRI and SpeI.

#2643 pB Car8fynVenus-T2A-HA-atx3Q15

It drives specific expression of a non-pathogenic HA-atx3Q15 fragment in zebrafish Purkinje neurons. The membrane localized fynVenus facilitates to observe the cell morphology. This plasmid can be used for generating a transgenic line, as a wild type control of the MJD model in zebrafish. This plasmid was cloned in the same strategy with the plasmid # 2641. The fragment T2A-HA-atx3Q84 was isolated from plasmid #2640.

#2787 pCS-atx1Q82-Venus

It drives ubiquitous expression of human Atx1Q82, fused to a fluorescent protein Venus for monitoring Atx1Q82 localization. This plasmid was cloned from the vector plasmid #1440 after cut with EcoRI and SalI, ligated with the insert fragment of Venus.

#2790 pCS-T2A-cyto actinWT

It carries a fragment of *T2A-cyto actinWT*, a T2A element and a cytoplasm localized wild type actin. This plasmid was cloned from the vector plasmid #2657 after cut with XbaI and SalI, the insert fragment was isolated form #2582.

#2791 pCS-atx1Q82-Venus-T2A-cyto Flag actin WT

It drives ubiquitous expression of Atx1Q82 fused with Venus, and cytoplasm localized wild type Actin. This plasmid was cloned from the vector plasmid #2790 after cut with EcoRI and SpeI, the insert fragment was isolated form #2787.

#2792 pCS-T2A-flag NLS-actinWT

It carries a fragment of *T2A-NLS actinWT*, a T2A element and a nuclear localized wild type actin.This plasmid was cloned from the vector plasmid #2658 after cut with XbaI and SalI, the insert fragment was isolated form #2582.

#2793 pCS-atx1Q82-Venus-T2A-flag NLS-actinWT

It drives ubiquitous expression of Atx1Q82 fused with Venus, and nuclear localized wild type Actin.This plasmid was cloned from the vector plasmid #2792 after cut with EcoRI and SpeI, the insert fragment was isolated form #2787.

#2803 pB-Hb9 :KalTA4

It drives motor neuron specific localized Gal4 expression in zebrafish.
The insert fragment was isolated from plasmid #2715 after cut with NotI.
The vector was obtained from plasmid#2603, after cut with NotI.

#2808 pBC SK-5×UAS-fyntagRFPT-T2A-HA-atx3Q84

It carries 5 times UAS element and membrane localized tagRFPT and a HA fused C terminus of atx3Q84 fragment, which can be used for generating a transgenic MJD model in zebrafish. This plasmid was cloned from the insert fragment *fynTagRFPT-T2A-HA-atx3Q84* was isolated from the plasmid #2638, and the vector of #2488.

#2812 pBC SK-5×UAS-fynTagRFPT-T2A-HA-atx3Q15

It carries 5 times UAS element and membrane localized tagRFPT and a HA fused C terminus of atx3Q15 fragment, which can be used for generating a transgenic control line of MJD

model in zebrafish. This plasmid was cloned from the insert fragment *fynTagRFPT-T2A-HA-atx3Q15* was isolated from the plasmid #2640, and the vector of #2488.

3020 pCS-HA-zf-atx3

It carries a HA tagged zebrafish ataxin-3, which can be used for expressing a wild type zebrafish Atx-3, which could be detected by immunostaining against the HA tag.

This plasmid was cloned from the ligation of vector plasmid #1950 pCS psapHA after cutting with EcoRI/SalI, with the insert fragment, a PCR product amplified from template plasmid #1867, using primer #1432and #1433, and cut with EcoRI/SalI.

#3021 pCS-HA-human atx3

It carries a HA tagged human ataxin-3, which can be used for expressing a wild type human Atx-3, which could be detected by immunostaining against the HA tag.

This plasmid was cloned from the ligation of vector plasmid #1950 pCS psapHA after cutting with EcoRI/SalI, with the insert fragment, a PCR product amplified from template plasmid #1878, using primer #1434 and #1435, and cut with EcoRI/SalI.

2.1.10 Oligonucleotides for cloning and sequencing

No.	Name	Sequence
#704	atax3up1	5'-ATGCGCATGGCGGAGGGAGGAGTGCA-3'
#705	atax3up2	5'-CAGGAGGGCTCTCTGTGCGCGCAGCA-3'
#706	atax3lo	5'-TCACTGGGTGGGTTTGGGCCCGCTGT-3'
#936	T2Ahtax3/ Spe-up	5'-CCACTAGTGAGGGAAGAGGAAGTCTGCTGACCTGCGGA GACGTGGAGGAGAACCCTGGACCTGGCAATTCCACCGAA GCCTACTTTGAAAAACAG-3'
#937	hatx3/Salf us-lo	5'-CCGTCGACACTTTTTTTCCTTCTGTTTTCAAATCATTTCT GAC-3'
#938	Atx3 C-tem-up	5'-CACATGGATGTGAACTCTGTCC-3'
#939	T2A-down	5'-GAAGTCTGCTGACCTGCGGAG-3'

#1059	HA-A3	5'-GCCCATGGCTTACCCTTACGATGTGCCTGACTA CGCCTCAGGTACAAATCTTACTTCA-3'
#1060	SaXbA3C	5'-CCGTCGACTCTAGATTATTTTTTTCCTTCTGTTTTCAA ATCATTTCTGAC-3'
#1136	Sequ atx3polyQ	5'-GAGACGAGAAGCCTACTTTGA-3'
#1145	atx-rt antis	5'-ACAGCGGCTTCTTCTCCATCC-3'
#1147	Z2A-NLS-A3	5'-TGACCTGCGGAGACGTGGAGGAGAACCCT GGACCTGGCAATTCCACCTCAGGTACAAATCTTACTTCA-3'
#1432	zf atx3-S	5'-CCGAATTCGCCGCCACCATGCGCATG GCGGAGGGAG GAG-3'
#1433	zf atx3-AS	5'-CGGTCGACCC CTGGGTGGGTTTGGGCCCG-3'
#1434	human atx3-S	5'-CCGAATTCGCCGCCACCATGGAGTCCATCTTCCACGAG-3'
#1435	human atx3-AS	5'-CGGTCGACCCTTTTTTTCCTTCTGTTTTC-3'

2.2 Experimental Procedures

2.2.1 DNA handling and cloning procedures

2.2.1.1. Plasmid transformation

Transformation is a process of the competent bacterial cells uptake and express exogenous the plasmid DNA. For this purpose, competent bacterial cells which usually kept at -80 °C were thawn on ice. 50 ng-1ug of plasmid DNA was added to 100ul of competent cells, which were kept on ice for 5-30min. The mixture was then heat shocked at 42 °C for 45s to induce bacterial uptake plasmid DNA. After the heat shock, the mixture was kept on ice for 2 min without shaking. 1 ml of Luria Bertani (LB) (without antibiotic) was added to the competent bacterial cells and DNA mixture. Tubes were incubated for 5 min to 1 hour at 37 °C. Then, centrifugation at 8000g was performed for 1 min, 800ul of supernatant were removed for condensing the bacteria. The bacteria pellet was re-suspended with the remaining supernatant and then spread onto a selection plate and incubated overnight at 37$^{\circ C}$ until the suitable size of bacteria colonies appeared.

2.2.1.2. Small scale plasmid preparation from bacteria (Mini Prep)

In order to isolate small scale plasmid DNA for analyzing bacterial clones during molecular cloning, Mini Prep of plasmid DNA was performed from bacteria. 2 ml of liquid bacteria cultures was incubated with selective antibiotics at 37 °C shaking at 200 rpm overnight. Then the bacteria were transferred into a 1.5ml Eppendorf tube. Centrifugation was performed at 13200 rpm, for 1 min to form a bacteria pellet, by removing the supernatant. Buffers from NucleoBond PC100/500 Maxi Prep kit were used for DNA isolation and purification. 200ul RNase containing S1 buffer was added to re-suspend the bacteria pellet. Afterwards, 200ul S2 alkaline lysis buffer was applied and the suspension was incubated for 5 min. 200ul S3 neutralization buffer was added to coagulate denatured proteins and to precipitate the bacterial debris containing large and less supercoiled chromosomal bacterial DNA and proteins. This debris was removed by centrifugation at 13,200 rpm for 10 min. The supernatant was transferred into a new Eppendorf 1.5ml tube. 400 ul Isopropanol was applied to precipitate the plasmid DNA by centrifugation at 13200 rpm, 15min. subsequently, the supernatant was removed. 500ul 70% Ethanol was used to wash the plasmid DNA pellet, followed by centrifugation at 13200 rpm for 15 min. The supernatant was discarded and the DNA pellet was dried in room temperature and re-suspended in 30ul ddH_2O.

2.2.1.3 Large scale plasmid preparation from bacteria (Maxi Prep)

In order to obtain large amount of plasmid DNA, a single bacterial colony containing the target plasmid was cultured in 200ml LB medium, shaking at 200 rpm overnight at 37°C. For obtaining the bacteria pellet, the bacteria culture were centrifuged at 5000 rpm for 10 min at 4°C. NucleoBond® PC100/500 Maxi Prep kit (Macherey&Nagel) was used in all of the following steps. The DNA isolation and purification were performed according to the instructions of the manufacturer. DNA was precipitated by adding isopropanol and centrifugation at 3000 rpm in 4°C for 30 min. The DNA pellet was washed with 70% Ethanol by centrifugation at 13200 rpm 1 min at RT. Subsequently the plasmid was re-suspended in 100-200ul ddH_2O. The DNA concentration was determined by a spectrophotometer and adjusted to 1 ug/ul. Generally, 200-800ug plasmid DNA could be yielded from 200 ml bacterial cultures.

2.2.1.4 DNA or RNA concentration measurement

DNA or RNA concentration can be measured by the maximum absorbance at 260 nm UV light. The Lambert-Beers´law governs the proportional absorbance. At 260 nm UV wavelength, 1 OD corresponds to approximately a concentration of 50ug/ml of pure double-stranded DNA or 40 ug/ml of pure single-stranded RNA. The maximum absorbance of aromatic amino acids in proteins occurs at 280 nm wavelength. Thus, the DNA purity can be estimated by the ratio of A260/A280. A sufficient purity of DNA is given by a ratio between 1.8-2.0, and RNA at 2.0. The concentration was measured in 150ul UV plastic tubes using a BioPhotometer.

2.2.1.5 Restriction endonuclease digestion of plasmid DNA

Restriction endonucleases can cut DNA at specific recognition nucleotide sequences. For analytical purpose, generally 0.5-1 ug DNA was digested with 1-5 units of restriction endonuclease and respective 10×buffer supplied by the manufacturer. The reaction was performed at 37°C for 30 min. For molecular cloning and DNA linearization, 2 ug DNA with 10-30 Units of enzyme were used, and incubated at 37°C for 2 hours. The quality of enzymes digestion was examined by agarose gel electrophoresis using 1-2 ul of the digested reaction mixture.

2.2.1.6 DNA ligation

T4 DNA ligase was used to ligate DNA fragments during constructing a plasmid DNA. The vector and insert DNA were mixed at 1:5 ratio. 1.5 ul 10×buffer and 1.5 ul T4 ligase were added. The total volume was adjusted to 15 ul by adding ddH_2O. The reaction was incubated at room temperature for 30 min. Subsequently the ligation product was transformed into competent bacteria cells.

2.2.1.7 DNA gel electrophoresis

Agarose gel electrophoresis was used to isolate and analyze DNA fragments. When applied to a steady electric field, DNA migrates towards the positive electrode, due to the DNA's negative charge. The migration speed of DNA depends on the size of the DNA fragment. With larger DNA fragments runing slower than smaller ones. Based on this, the different size of DNA fragments can be separated according to their molecular weight. 0.8-1.5% agarose

gels were prepared and castedto in Shelton Scientific and PeQLAB gel chamber systems. 100-200 ng DNA for quantifying its size or 1-10 ug DNA for isolating particular fragments were diluted at 5:1 ratio with 6× loading dye; and the solution was loaded together with a 1kb standard DNA ladder (MBI loading dye from Fermentas) onto the gel. The DNA electrophoresis was performed at a voltage between 100 and 160 V. When the DNA had migrated sufficiently through the gel, the electrophoresis was stopped and the gel was transferred to stain in 1× TAE buffer containing 1 ug/ml Ethidium Bromide (EtBr) for 10 min. EtBr integrates into the DNA resulting in bright fluorescence upon excitation with UV light. The DNA containing gel was visualized by using an ultraviolet light transilluminator and photographed.

2.2.1.8 RNA gel electrophoresis

RNA gel electrophoresis was conducted similarly to DNA gel electrophoresis except these differences: in order to avoid RNA degradation by RNase, the frame, gel chamber and comb were washed carefully with soap, the gel needed to be pre-run for 10 min at 70 V before loading the RNA samples to the wells. 2 ul RNA samples were mixed with 8 ul 5× RNA loading buffer. Before loading onto the gel, the RNA samples were denatured for 10 min at 95 °C to interrupt the secondary structure of the RNA.

2.2.1.9 Extraction of DNA fragments from gels after electrophoresis

After electrophoresis, the EtBr integrated DNA was visualized by UV excitation using an ultraviolet light transilluminator. The DNA fragments of the desired size were cut using a scalpel and the agarose blocks were collected in 2 ml reaction tubes. The extraction of DNA fragments were performed with a Gel Extraction kit, according to the manufacturer´s protocol.

2.2.1.10 DNA purification of PCR products or fragments of restriction digest

By using the QIAquick PCR Purification or Nucleotide Removal kit, the purification of PCR products or digested DNA fragments were performed following the manufacturer´s protocol.

2.2.1.11 Removal of 5´DNA overhang

In blunt end cloning, the removal of 5´DNA overhangs is necessary for the ligation of non-complementary double strand DNA ends created by restriction enzyme digestion. The 5'-DNA overhangs (3' recessed ends) were filled in using the Klenow fragment of the *E.coli*

DNA polymeraseI (Roche). 10x reaction buffer H (Roche), dNTPs at final concentration 200 µM, 2 µL enzyme and purified DNA were mixed (total volume was usually adjusted to 40 µL). The reaction mix was incubated at 37°C for 45 to 60 min. The DNA products was purified for further purpose using the Nucleotide Removal Kit (Qiagen).

2.2.1.12 DNA dephosphorylation

In order to prevent the digested plasmid vector from re-circularization or blunt ended ligation, the DNA was dephosphorylated by using calf intestinal phosphatase (CIP) in 1×reaction buffer, by incubation at 37 °C for 30 min.

2.2.1.13 PCR

A proof reading Polymerase Pfu Ultra (from Stratagene) were used in all the PCR reactions in this work. Plasmid DNA or cDNA isolated from zebrafish by RNA extraction and subsequent RT-PCR was used as template for the PCR reaction and performed as followed:
20 ng DNA template
2 µL 10x PCR buffer
2 µL 2 mM dNTP mix
0.5 µL upper and lower primer (50 pmol/µL)
1 µL DNA-polymerase
Adjust the total volume to 25 µL by adding ddH_2O.

The PCR conditions were set according to the characteristics of the primer and the size of the expected DNA fragment. Generally, template DNA was first denatured at 95°C for 2 min. Annealing temperatures are generally about 5°C below the melting temperature of the primers was determined by experience. 45 s were sufficient for annealing. Elongation was performed at 72°C for 0.5 min/kb fragment length. Usually, 30 cycles were performed. All PCR reactions in this work were performed using a MJ Research Thermocycler PTC-100, and analyzed by gel electrophoresis of an aliquot from the PCR reaction.

2.2.1.14 Purification of RNA

For purification of total RNA extracted from embryos or mRNA transcribed in vitro, the RNeasy Mini Kit was used according to the manufacturer´s guidelines.

2.2.1.15 RNA isolation from zebrafish embryos

An RNeasy Mini Kit was used for total RNA extraction from zebrafish embryos. The RNA extraction was performed according to the protocol from the manufacture. In order to yield a sufficient amount of total RNA, 25 embryos were homogenised in 50 µL RLT buffer (RNeasy Mini Kit) using a syringe or a pestle-homogeniser fitting into Eppendorf reaction tubes. Before transferring the lysates onto QIAshredder columns, 300 µL RLT were added. Potential contaminations from chromosomal DNA were digested by DNaseI (50 µL nucleic acid extract, 6 µL 10x transcription buffer ,2 µL RNAsin, 2 µL DNaseI (RNase free) (Roche, 10 U/µL), incubation at 37°C for 30 min). Subsequently, the RNA was purified using the RNeasy kit. A good quality of the purified RNA was indicated by the integrity of the two major rRNA bands after agarose gel electrophoresis, showing that no degradation had occurred.

2.2.1.16 Preparetion of cDNA

In order to synthesize cDNA from total mRNA extraction products, 5-11 µL RNA template and 1 µL random hexamer primers were mixed and incubated at 70°C for 5 min. At the same time, the reaction mixture were prepared as below:

10 µL 5x Superscript II Buffer,
1 µL RNAsin,
5 µL 2 mM dNTPs,
5 µL 0.1 mM DTT,
Add RNase free water to adjust a total volume to 50 µL.

The reaction solution was mixed with the annealed RNA/primer at 25 °C, and then incubated for 5min. Afterwards, 1 µL SuperScript reverse transcriptase was added and the incubation steps below were applied. The following reactions were performed in a PCR machine.

25°C - 10 min
42°C - 60 min
70°C - 10 min
4°C - ∞

This cDNA product can be kept at -20°C for long term storage or ready for use in further investigation.

2.2.1.17 Cloning of DNA fragments with blunt ends

The blunt cloning kit was used for cloning blunt ended PCR products into a plasmid backbone. The pSC-B vector and bacteria expressing Cre recombinase were provided by the manufacturer. The detailed cloning procedures were performed according to the manufacturer's protocol.

2.2.2 Zebrafish maintenance and manipulation

2.2.2.1 Maintenance of zebrafish

Zebrafish were raised according to standard protocols (Kimmel et al.1995; Westerfield 1995). Zebrafish welfare was carefully considered, according to legal requirements. The zebrafish were cultured in pre-treated water with good quality, which contained suitable Oxygen content, no Chlorine, low content Nitrite and Nitrate, the pH was adjusted to 6.5-7.5, the temperature was kept around 28 °C, and the conductivity of the water was adjusted to 400-700uS.

2.2.3 Methods for genetic manipulation of zebrafish embryos

2.2.3.1 Synthesis of capped mRNA for microinjection into zebrafish embryos

In order to transcribe capped mRNA from pCS2+ plasmids, 10 µg plasmid-DNA were linearized by single enzyme digestion, to obtain a 3´prime to the polyA encoding sequence. The digested products were purified using a Nucleotide Removal kit and dissolved with 35 µL RNase free water provided with the kit.
In order to confirm the entire plasmid DNA was digested, an aliquot of the reaction mixture was applied onto a 1.0% agarose gel for electrophoresis. In vitro transcription of capped mRNA was achieved by using the mMESSAGE mMACHINE® SP6 Kit according to the

manufacturer's protocol. 6 µL of linearized plasmid DNA template, 10 µL 2x NTP/CAP, 2 µL 10x reaction buffer and 2 µL enzyme solution were mixed. The reaction was performed at 37°C for 2-3 h followed by digestion of the template DNA by treating with 1 µL RNase free DNase (Roche) for 15 min at room temperature. The mRNA products was purified using the RNeasy Mini kit and dissolved with 35 µL RNase-free water. The yield of mRNA transcription was analyzed on a 0.8% agarose gel as described before. The mRNA concentration was measured by using a BioPhotometer. Generally, a yield of 6-15 µg mRNA could be synthesized.

2.2.3.2 Cytoplasmic microinjection of nucleic acids

Microinjection of nucleic acids into the embryo cytoplasm at the one cell stage is a universal technique for genetic manipulation of zebrafish embryos. For transient mosaic expression or generation of transgenic fish, plasmid DNA was used that was prepared by maxi preparation and subsequently purified using the GENECLEAN Turbo Kit following the manufacturer's protocol. Plasmid DNA was diluted by water to the desired final concentration of 30-50 ng/µL. Phenol Red was applied into the solution to monitor the injection (1/10 of a 0.5% stock solution). The mixture was filled into a glass capillary that had been pulled to a sharp tipped needle. Injections were performed into the cytoplasm of zygotes using a micromanipulator supported by the use of a binocular. During the injection, embryos were kept in a fixed position in the grooves of 1.5- 2% agarose.
After injection the embryos were transferred into a conventional Petri dish and cultured at 28°C to the desired developmental stages for further studies.

2.2.3.3 Generation and screening of transgenic zebrafish

Embryos injected with expression plasmid DNA as described in chapter 2.2.3.2 were sorted at a suitable development stage for proper fluorescent protein expression. The best F0 founders which showed the correct expression pattern, of a suitable expression level, and neither ectopic nor non-specific expression were maintained until adulthood, to establish the F1 generation, by crossing with the WT fishes.
For embryos injected with a UAS plasmid DNA to generate an effector line or Gal4 plasmid DNA for generating an activator line, all the embryos were raised to adulthood, and then were crossed with a Gal4 or UAS transgenic line respectively to identify positive F0 carriers.

The screening set up was described below: For screening a UAS transgenic line, the F0 adult fishes were crossed with the transgenic line Tg(Her3::Gal4), which drives expression in the developing mesencephalon/rhombencephalon and the spinal cord; for screening a Gal4 transgenic line, the F0 adult fishes were crossed with transgenic line Tg(4X UAS::GFP). The GFP signal could be observed when a positive F0 carrier was crossed. The best F0 carriers were identified based on the same criteria mentioned before. The F1 generation was established by raising transgenic founders to adulthood followed by screening as described.
The F2 and F3 generation were generated like the F1 generation.

2.2.4 Histological Techniques

2.2.4.1 Whole-mount in situ hybridization (ISH)

Generally, most genes are transcribed in a certain specific spatiotemporal pattern. Complementary RNA probes containing UTP nucleotides labeled with an epitope such as digoxygenin or fluorescein could be used to analyze gene expression in whole-mount embryo samples. The antisense RNA probe was hybridized to target mRNA and subsequently detected by antibodies against the respective UTP epitope and coupled to Alkaline phosphatase (AP). This could result in a blue precipitate when the enzyme is incubated in the presence of the substrate NBT/BCIP and therefore, the gene expression pattern could be visualized and photographed.

In vitro transcription of antisense riboprobes

Antisense RNA probes (riboprobes) were synthesized from a linearized plasmid DNA template and conjugated with modified nucleotides using the DIG RNA-labeling mix during *in vitro* transcription, according to the manufacturer's guideline. After that, the DNA template was digested by RNase free DNase. Subsequently, the DIG-labeled RNA probe was purified and collected using the RNeasy Mini kit, following the manufacturer's protocol.The integrity of the RNA probe was verified by RNA gel electrophoresis. The yield of DIG incorporation by dot blots analysis of a serial dilution.

Fixation and storage of zebrafish embryos

Before fixation, the embryos younger than 2 dpf were needed to be dechorionated by using Pronase solution. Subsequently, the dechorionated zebrafish embryos were fixed overnight in

4% PFA/PTW at 4°C. After that, the embryos were dehydrated in 25% 50%, 75% MeOH/PTW, and 100% MeOH 5 min each step and stored in pure MeOH at -20°C for long term use. Prior to ISH, the embryos were rehydrated by washing in 75%, 50%, 25% MeOH/PTW for 5 min each step, and then washed two times with PTW to remove recessive MeOH.

Proteinase K-treatment of embryos

Proteinase K is a proteolytic enzyme , which can be used to treat fixed embryos for a better penetration of RNA probes and antibodies. The embryos were treated in Proteinase K/ PTW (10 µg/mL) solution for the respective incubation time depending on the developmental stage of the embryos as listed below. The digestion was stopped by washing two times with 2 mg/mL Glycine/PTW and subsequent re-fixation in 4% PFA for 20min. To washed out the residual PFA, embryos were incubated with PTW solution for 5 × 5 min.

Developmental stage	Time of proteinase K digest
24 hpf	10 min
36 hpf	20 min
48 hpf	30 min
3 dpf	45 min

Hybridization

After the above treatments, the embryos were transferred to 2 ml RNAase free tubes and pre-hybridized in 1ml of hybridization buffer for 1 h in a water bath at 60°C. The anti-sense RNA probe was diluted in hybridization buffer at the ratio of 1:40-1:200, depending on its quality. The RNA probe was subsequently heated at 95°C for 10 min to disrupt the secondary structures of the RNA. After remove the pre-hybridization buffer, the hot probe was directly transferred onto the embryos. The in situ hybridization was conducted overnight at 60°C in a water bath. The next day, the hybridization solution was discarded, and the embryos were washed two times in 2ml with 50% formamide/2x SSCT, once in 2x SSCT and two times using 0.2x SSCT 45 min each. All the washing steps were performed at 60°C in a water bath.

Antibody detection

After the washing step to remove the recessive RNA probes, blocking was performed to block the unspecific binding sites for anti-DIG Fab-fragments. The embryos were incubated in 10 % NGS in PTW for 1 h on a rotator at room temperature. Afterwards the embryos were incubated in anti-digoxygenin antibody in the NGS solution (diluted at 1:2000 ratio) over night at 4°C. In order to remove the excess antibody, the embryos were washed five times with 5 ml of PTW in a six-well plate for 15 min each time at room temperature on a shaker. Meanwhile, the ISH staining buffer was prepared freshly and filtered by using a 0.22 µm syringe filter. Subsequently, the embryos were equilibrated 5ml ISH staining buffer two times for 5 min each time. And then, 5ml of the BCIP and NBT containing ISH staining solution were added into the 6-well plate. The staining reaction was performed at room temperature. until the blue color appeared. The reaction time depends on the gene expression level and the quality of the RNA probe, and could be ranged from 0.5 h up to overnight. When the solution color became brown during the staining procedure, the staining solution needed to be exchanged. Specialty and intensity of the developing staining were followed by observation under a stereomicroscope from time to time. To stop the colorization reaction, the embryos were washed 3 times for 5 min in PTW. Subsequently, the embryos were transferred into 90% glycerol (v/v) for long term storage and photograph.

2.2.4. 2 Whole mount immunohistochemistry (WIHC) of zebrafish embryos

Fluorescent immunohistochemistry was performed according to the following protocol. After fixation and rehydration, the embryos were incubated in 10% NGS/PTW blocking solution for 1 h at room temperature (RT) in order to block unspecific binding sites. Subsequently, the embryos were incubated overnight at 4 °C with the primary antibody diluted in blocking solution. The following day, for removing the recessive antibody, the embryos were washed 5 times with PTW for 15min each time at RT. And then, the embryos were incubated with the secondary antibody solution 2hr at RT or overnight at 4°C. When the secondary antibodies were conjugated to light sensitive fluorophores such as Cy3, Cy5 or FITC, the incubation needed to be performed in dark. After that, for removing the residual antibody, the embryos were washed at least three times 15 min each in PTW before microscopic observation and image recording.

2.2.5 Nuclear DNA staining

2-(4-Amidinophenyl)-6-indolecarbamidine dihydrochloride (DAPI) is a fluorescent dye which binds strongly to A-T rich regions in DNA. It is well established to label the nuclei of fixed cells. DAPI is excited by ultraviolet light. When bound to double-stranded DNA its absorption maximum is at 358 nm and its emission maximum is at 461 nm. To stain fixed zebrafish embryos, DAPI was added to the medium at a final concentration of 1 µg/µL, followed 30 min incubation at room temperature on a shaker. For facilitating a better penetration of DAPI through the membrane, 0.1% Tween-20 in PBS solution was used to dilute DAPI. The unbound dye was removed by 3 × 5 min washing in PBS.

2.2.6 Biochemical methods

2.2.6.1 Maintenance and transfection of zebrafish PAC2 cells

Zebrafish fibroblast PAC2 cells were used for analyzing the dynamics of Atx1Q82 aggregation. The Pac2 cells were maintained in L-15 Leibovitz Medium, containing 10% Fetal Bovine Serum (v/v) and 1% Penicilin/ Streptomycin (v/v) by using a 10 cm petri dish, and kept in a 28°C incubator, without CO_2 supply (Chu et al. 2008; Rieger et al. 2009; Senghaas and Koster 2009). When the cells were confluent, it was necessary to passage the cells. For this, the medium was removed and the cells were washed once shortly to remove the residual medium. 1 ml Trypsine was added onto the cells and incubated at RT for about 5 min. The cells were detached from the bottom of the plate. To stop the reaction, 4 ml medium was added into the dish. It is not necessary to centrifuge the cell-medium mixture to pellet down the cells and remove the Trypsine. Subsequently, the Pac2 cells were passaged at 1:2 or 1:4 ratio into new dishes. A fast growth of Pac2 cells was dependent on the suitable cell density in dishes. As Pac2 cells do not grow well in lower density, the recommendation of passage ratio is 1:2 - 1:4.

For analyzing the exogenous gene expression, FuGENE HD was used for transfection, due to its good performance in transfection. For the transfection in 1 well of the 24-well cell culture plate, the transfection mixture was prepared as below:

0.5ul plasmid DNA (1ug/ul),

25ul Opti-Mem,

mix the DNA by vortexing shortly,

add 1ul FuGENE

It is important to add the FuGENE last, and to add the reagent directly to the diluted DNA, without touching the sides of the well, for a better formation of transfection complex.
The mixture was mixed well and incubated at RT for 15-30 min. Afterwards, the transfection mixture was transfered to cultured Pac2 cells, with a short gentle shaking. Keep the cells in the incubator 1 to 2 days for observation, treatment or harvesting for the following experiments. The transfection medium can be removed at 6 hours after transfection, replaced with new medium.

2.2.6.2 Maintenance and transfection of mammalian cells

Human embryonic kidney 293T and cervical cancer cell line Hela cells were utilized in this work. 293Tcells were used for protein production because they are easy to maintain, high transfection efficiency and are able to produce large amounts of protein from transfected expression plasmids. The Hela cell line was used for analyzing transfected gene expression and associated phenotypes via high resolution confocal imaging. 293T and Hela cells were maintained, transfected and imaged in the same way. They were maintained at 37°C, with 5% CO_2 in DMEM medium plus 1% PEN/STREP, 1% Glutamin/Glutamax and 10% fetal bovine serum (FBS).
When the cells were confluent, the cells were passaged, by removing the medium. The cells were washed with DPBS solution. 1 ml Trypsine was added onto the cells and they were incubated until they are detached from the dish. For a fast reaction of Trypsin, the dishes could be kept at 37 °C. The reaction of Trysine was stoped by adding fresh medium. The Trypsine can be removed by centrifugation at 1200rpm for 2 min. The cell pellet was re-suspended in fresh medium and the cells were distributed intoseveral new Petri dishes.
293T and Hela cells were transfected using FuGENE HD as described for PAC2 cells. The amount of FuGENE was reduced to 0.5ul.

2.2.6.3 Protein lysate preparation from cultured cells

The transfected cells were harvested at specific time points. Firstly, the cell culture medium was removed and 200ul 2×SDS lysis buffer was added to each well. After incubatation for 1 min, the lysed cells were scratched by pipette tips and collected into a1.5ml tube, and sonicated about 10 seconds, and kept at -80 °C. Before loading onto a SDS-PAGE gel, the protein samples were heated at 95 °C for 5 min.

2.2.7 High resolution microscopy imaging

2.2.7.1 Imaging of cultured cell samples

For fluorescent microscope imaging analysis, cultured cell were seeded and grown on sterilized cover slips or custom made imaging chambers. For fixed samples, the cells were cultured on cover slips first. After fixation and related staining, the cover slips were mounted on imaging slides.

To monitor live Pac2 cells, the cells were grown and kept in a plastic imaging chamber, with a special glass bottom to facilitate the images acquisition. To prepare the optimal cellular conditions, the object stage of the confocal microscope was heated to 28°C, using a self-bulit imaging chamber from card box. To avoid photo bleaching, low dose of laser power was used for screening the suitable object. For the beginning, the focus of microscope imaging was carefully monitored and adjusted if necessary. Suitable laser powers and time intervals of image recording were adjusted to prevent photo bleaching. Subsequently, suitable imaging conditions to prevent photo bleaching, but to record images at high contrast were adjusted.

2.2.7.2 Imaging of zebrafish embryos

In vivo imaging

Living zebrafish embryos were embedded in 1.2% ultra low melting agarose/0.01% tricaine /30% Danieau solution in imaging chambers, with or without a glass bottom, depending on the type of confocal microscope, being either and inverted or upright microscope. After the agarose solidified, the imaging chambers were filled with 30% Danieau solution containing 0.01% tricaine for embryo anesthesia. After imaging, the embryos were released from the agarose by using forceps. For overnight time lapse live imaging, the embryos were incubated at 28 °C by using a custom made heating box around the microscope. Detailed protocols for live zebrafish imaging can be found in Distel et al (Distel and Köster 2007; Fraser and köster 2009).

Imaging of fixed samples

Fixed embryos were embedded similarly as live specimen, but without anesthesia, using PBS instead of 30% Danieau.

2.2.7.3 Processing of images

Confocal images were recorded by using an inverted Zeiss LSM510 or an upright Olympus FV1000 confocal laser scanning microscope. These images were processed with modules of the Axio vision software (Zeiss, Jana Germany) or the FV10-ASW2.0 viewer (Olympus, Tokyo, Japan) for maximum projections, and 3D reconstructions. The obtained image data were exported to TIFF format for further processing with Photoshop CS5, Illustrator CS3 (Adobe, San Jose, America), ImageJ (downloaded from http://rsbweb.nih.gov/ij/) and QuickTime player Pro7.4.5(Apple, Munich, Germany).

3 Results

3.1 Genetic modeling of a SCA-3 disease in zebrafish

3.1.1 Atx-3 is evolutionarily conserved between zebrafish and human

In order to know whether zebrafish contains an ortholog of the human pathogenic gene *atx-3*, the zebrafish genome database was searched. The zebrafish *atx-3* gene is located on the Chromosome 17 - NC_007128.5 in the zebrafish genome, its Gene ID is 394079 (http://www.ncbi.nlm.nih.gov/gene/394079). To confirm its existence experimentally, the zebrafish atx-3 gene was cloned through Reverse Transcription-Polymerase Chain Reaction (RT-PCR).

In order to analyze the degree of similarity that the zebrafish Atx-3 shares with the homolog of the human Atx-3, the amino acid sequences of the Atx-3 proteins were compared by using the Blast tool of the NCBI homepage. The N-terminal Josephin domains in Atx-3 are highly conserved between human, mouse and zebrafish. Compared with human Atx-3, the similarity of the zebrafish and mouse orthologs is 85% and 99% respectively. The similarity of amino acid sequences of the C-terminus of Atx-3 is 52% (zebrafish), and 69% (mouse), respectively. This shows that Atx-3 protein is a well-conserved protein within vertebrates, with highest conservation in the N-terminal Josephin domain.

The primary structure of human Atx-3 was reported before (Masino et al., 2003; Nicastro et al., 2005). Based on the amino acid sequence comparison and prediction, the zebrafish Atx-3 contains similar structures than the human homologue, including the nuclear export sequence (NES) and nuclear localization sequence (NLS) signals, phosphorylation sites, ubiquitin interacting motifs, polyQ sequence and a primary site of ubiquitination (Fig.1). Based on these, it was suggested that not only the sequence but also the function of the zebrafish Atx-3 is evolutionarily conserved between human and zebrafish.

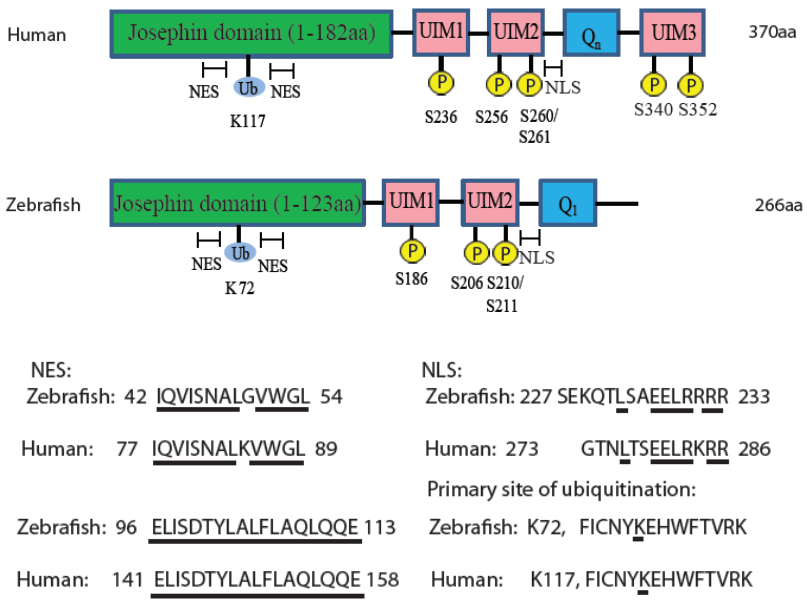

Fig. 1. Comparasion of domain architecture and post-translation modifications of human and zebrafish Atx-3. Human Atx-3 contains an N-terminal the Josephin domain (JD), followed by a flexible C-terminal tail containing tandem ubiquitin (Ub)-interacting motifs (UIM) and a polyQ sequence of variable length. Five serine residues, as phosphorylation sites in the UIMs, and Lysine 117 (K117) as the primary site of ubiquitination were identifed. Two NES in the JD and one NLS linking the second UIM to the polyQ stretches were reported.
Through amino acid sequence comparation, zebrafish Atx-3 has quite similar domain structures and post-translational modification sites, including the N-terminal Josephin domain, two UIMS, two NES, 1 NLS, 3 serine residues as phosphorylation sites and K72 as the possible primary ubiquitination site. Zebrafish Atx-3 has a C-terminal tail, containing only 1 glutamine, at this site of the human pathogenic ployQ stretch, with lower similarities with human Atx-3, compard to the N-terminus. Abbreviation: NLS: nuclear localization signal; NES: nuclear export sequence; UIM: ubiquitin (Ub)-interacting motif.

3.1.2 Expression of atx-3 in the brain of zebrafish larvae

For deciphering the spatial and temporal expression pattern of zebrafish *atx-3* in the brain of zebrafish larvae, RT-PCR and mRNA in situ hybridization was applied. For RT-PCR examination, 25 embryos of different developmental stages each were collected. Subsequently, the total mRNA was isolated and purified from the whole embryos from each time point. The complementary DNA (cDNA) was synthesized by using the total RNA as template. A pair of primers were specifically designed basing on the zebrafish *atx-3* sequence. At last, the zebrafish *atx-3* was amplified by using through PCR and the RT-PCR products were examined via DNA gel electrophoresis and stained with Ethedium Bromide. The zebrafish *atx-3* fragments were documented by using a DNA documentation system. As shown in Fig.2, from 1 to 7dpf, only one specific band at each time point were observed, i.e., the DNA bands of zebrafish *atx-3* could be amplified via RT-PCR, indicating that the *atx-3* was expressed in zebrafish embryos at 1 day post fertilization (dpf) and throughout development until 7 dpf. The cDNA of cytoskeletal Actin was amplified as a control to confirm the quality of the RNA isolated and the experimental system works.

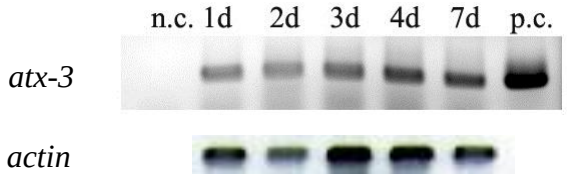

Fig. 2. The zebrafish *atx-3* is expressed in zebrafish embryos from 1-7 (dpf). Zebrafish *atx-3* can be amplified from the reverse-transcriped DNA (cDNA) at respective developmental time point, shown by the bands of RT-PCR products. H_2O as the negative control (nc); the zebrafish *atx-3* plasmid as the positive control (pc).

In order to reveal the detailed tissue specific expression pattern of zebrafish *atx-3*, whole mount mRNA in situ hybridization was performed.

The spatial and temporal expression profiles of whole mount *atx-3 in situ* hybridized embryos are shown in Fig. 3. A ubiquitous hybridization signal of *atx-3* transcripts was detected from 1 to 3dpf. Particularly strong expression was observed in the midbrain at 2dpf. At 3dpf, strong expression was observed around the midbrain-hindbrain boundary (MHB). These findings of a ubiquitous atx-3 expression during embryogenesis are consistent with expression data of the mouse *atx-3* homolog. These results suggest that the *atx-3* may play an important role during embryogenesis.

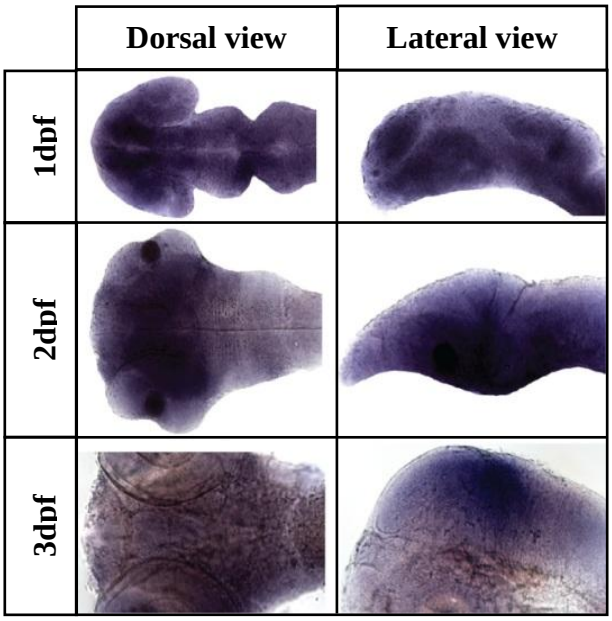

Fig. 3. The ubiquitous expression pattern of *atx-3* mRNA in the brains of zebrafish embryos from1-3dpf. The zebrafish *atx-3* mRNA was detected by mRNA in situ hybridization. From 1 to 3 dpf, the *atx-3* mRNA was expressed in the zebrafish whole brain. The *atx-3* shows strong expression the in midbrain at 2dpf and in the midbrain- hidbrain boundary in the brain of embryos at 3dpf.

3.1.3 Expression of atx-3 in the brain of adult zebrafish

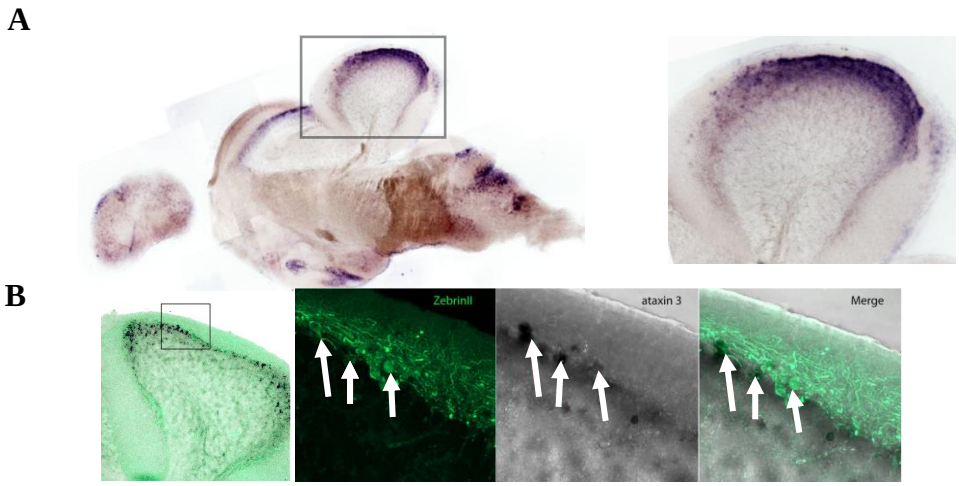

Fig. 4. *atx-3* mRNA expression in adult zebrafish Purkinje cells. A: the *atx-3* mRNA expression, detected by mRNA in situ hybridization on adult brain slices, shows specific expression in certain brain regions, including the Purkinje cell layer of the cerebellum; B. *atx-3* is expressed in Purkinje cells of the adult zebrafish cerebellum, as confirmed by labeling with the Purkinje cell specific antibody ZebrinII (green) and mRNA in situ hybridization (black). The *atx-3* expression was detected first by mRNA in situ hybridization, followed a Purkinje cell specific antibody ZebrinII immunostaining.

For determining where *atx-3* is expressed in the brain of adult zebrafish, the mRNA in situ hybridization was performed on adult brain sections. First, the brain was removed from the shell and fixed with PFA solution, mounted with gelatin, frozen with liquid nitrogen, and cut by using Cryo-Stat, into sections at 15um thickness. Subsequently, the sections were used to perform mRNA in situ hybridization. In contrast to the ubiquitous embryonic expression pattern, *atx-3* is expressed more specifically in the adult brain, where it could be detected in the Purkinje cell layer of the adult zebrafish cerebellum. In addition, *atx-3* mRNA expression was found in cerebellar like networks beneath the optic tectum, in dorsal areas of the hindbrain as well as in ventral diencephalic tissues (Fig.4A).

In the cerebellar Purkinje cell layer Bergman glia, eurydendroid neurons (equivalent of the deep nuclei neurons) and the Purkinje cells themselves can be found. To confirm *atx-3* expression in Purkinje neurons *atx-3* mRNA in situ hybridizations were performed in together with an antibody staining against the Purkinje cell specific ZebrinII protein. *atx-3* expressing cell somata (black) were found to connect to ZebrinII positive (green) dendrites verifying *atx-3* expression in differentiated zebrafish Purkinje neurons (Fig.4 B).

3.1.4 Nuclear accumulation of Atx-3 responding to oxidative stress

Upon oxidative stress human Atx-3 is known to accumulate in the nucleus. To address whether this translocation behavior is conserved by zebrafish Atx-3, first, Hela cells were transfected zebrafish or human wild type Atx-3 expression vector in which the respective *atx-3* cDNA had been fused to an HA tag at the N-terminus. 24hours after transfection, the cells were exposed to 1mM H_2O_2 for 6 hrs. Subsequently, the H_2O_2 treated Hela cells were fixed and stained using a primary antibody against the HA epitope and followed by a secondary antibody conjugated to Cy2. The immunofluorescence data were quantified by counting Cy2 positive cells with fluorescence primarily localized to the cytoplasm (C), nucleus (N) or equal distribution (C/N) between the cellular compartments. Data represent the fraction of total cells counted in each group with a particular localization pattern.

It was proposed that the human Atx-3 is a cytoplasm and nucleus shuttling protein. Like previous reports (Reina et al., 2010), the human Atx-3 accumulation in the nucleus after oxidative stress was observed in Hela cells. After H_2O_2 treatment, the stronger Cy2 signal could be observed in the nucleus (Fig.5A). Quantification of the results showed that, after incubation with H_2O_2 for 6 hours, about 56% of Human and 48% of zebrafish Atx-3 expressing cells showed a the nuclear accumulation of the Atx-3 protein respectively, while only 4% of the human and 2% of zebrafish Atx-3 expressing cells were observed with the Atx-3 accumulation in the nucleus (Fig.5B). Based on these results, it could be concluded that the zebrafish Atx-3 behavior similarly like its human homologue upon the oxidative stress.

A

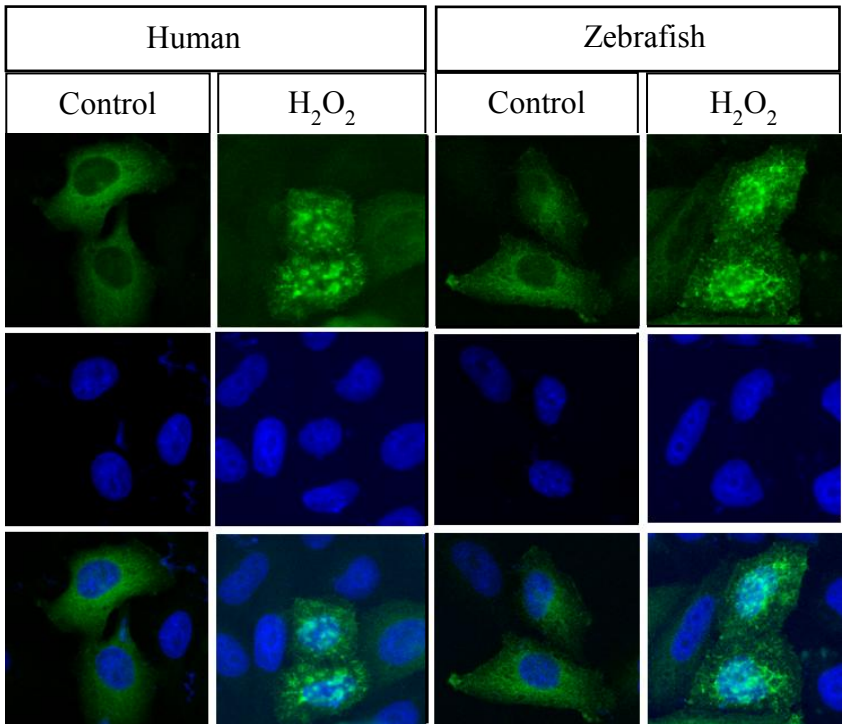

B

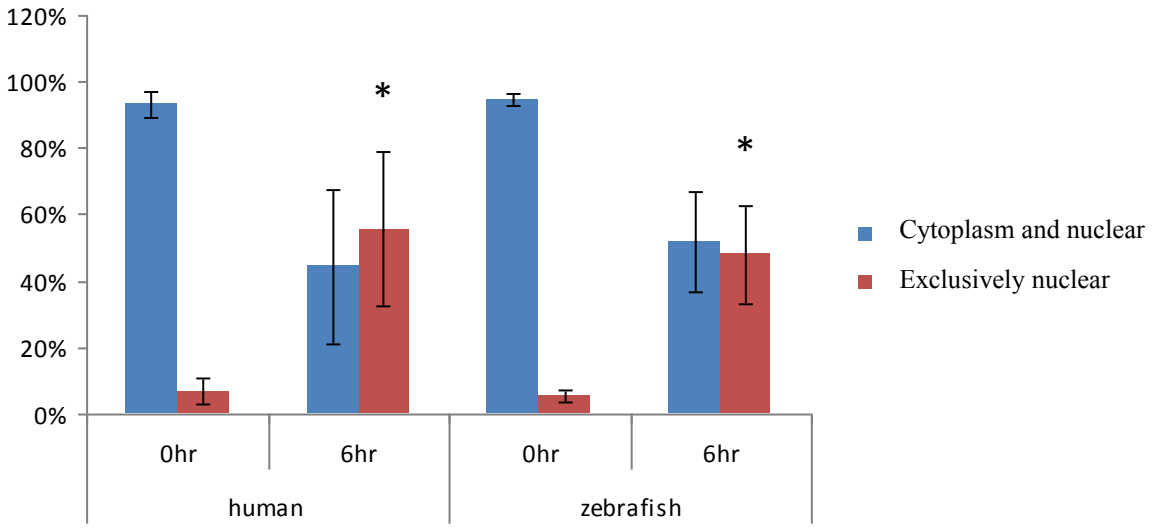

Fig. 5. The zebrafish and human wild type Atx-3 protein accumulates in the nucleus following oxidative stress. Hela cells were transfected zebrafish or human wild type Atx-3 fused to HA tag and exposed to 1mM H_2O_2 for 6hrs. Following treatment, the expression and localization of the HA tagged zebrafish and human Atx-3 were detected via immunostaining against this HA tag. The immunofluorescence data from the secondary antibody conjugated to Cy2 were quantified by counting Cy2, positive cells with a specific localization of Cy2. Transfected cell with fluorescence primarily localized to the nucleus (N), equally distributed to the nucleus and cytoplasm (C/N). Data represent the fraction of total cells counted in each group with a particular localization pattern.

3.1.5 Zebrafish Atx-3 is an aggregation prone protein

Human Atx-3 is an aggregation prone protein due to its specific 3-D structure. To clarify whether also zebrafish Atx-3 could form aggregates, the expression vector (#3020) encoding zebrafish Atx-3 was transfected into Hela cells, which were cultured for 4 days after transfection to reach elevated expression levels of Atx-3. At 1 and 4 days after transfection, the cells were fixed and immunohistochemistry was performed against the HA tag of the respective Atx-3 fusion protein. In addition, a counterstain was applied against chromatin using DAPI. The localization and aggregation state of Atx-3 was indicated by the secondary antibody conjugated Cy2. Short term expression of Atx-3 did not result in aggregate formation. However, 4 days after transfection, in 26% of Hela cells zebrafish Atx-3 was found to aggregate in the nucleus, the human variant formed aggregates could be observed in 45% cells (Fig.6). Thus zebrafish Atx-3 has a tendency to form nuclear aggregates like its human counterpart.

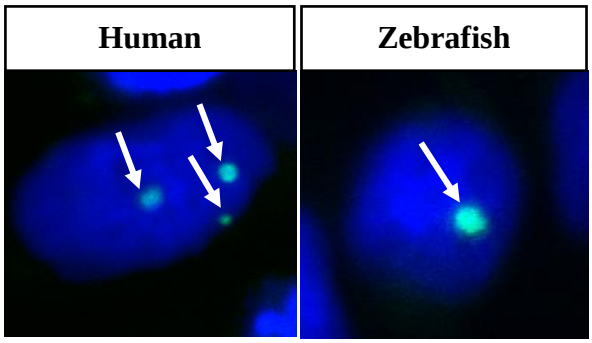

Fig. 6. The zebrafish and human WT Atx-3 can form aggregates, 4days after transfection in Hela cells. The Hela cells were transfected with HA tag fusion of either zebrafish or human WT Atx-3, at 4days after transfection, the expression of Atx3 and aggregation was examined by HA antibody immunostaining.

3.1.6 Strategy and plasmid design for modelling SCA-3 in zebrafish

In order to generate a model for SCA-3 diseasein zebrafish, several plasmids containing the pathogenic human *atx-3* gene were constructed, as shown in (Fig.7). According to previous evidence, the C-terminal of Atx-3 ployQ protein is sufficient to induce neuronal degeneration, inducing early SCA-3 disease onset and increased neuronal toxicity (Ikeda et al., 1996; Warrick et al., 2005). Thus, in the following studies, the C-terminal Atx-3 was used to generate a SCA-3 disease model in zebrafish. First, the C-terminal Atx-3 containing the expanded polyQ stretches, Q69 or Q84 as pathogenic form and Q15 as the wild type non-pathogenic control were cloned into the expression vector pCS2+. Subsequently, two kinds of Atx-3 fusion constructs were constructed.

For direct observation of neuronal morphology, a membrane localized fluorescent protein (FP, fynVenus or fyntag RFPT) was cloned into the constructs. A 2A peptide, T2A from the insect virus *Thosea asigna*, was placed in frame between the 5' fluorescent protein and the C terminal Atx-3 variants. This peptide results in the co-translational 'cleavage' of proteins, leading to expression of multiple cistrons at equimolar levels (Provost, et al., 2007).

Further, the Gal4-UAS system was used for modeling SCA-3 disease in zebrafish (Distel et al., 2009). When a UAS effector line is established, it could be crossed to a neuronal specific Gal4 activator line, to obtain the pathogenic Atx-3 expression in specific neuronal cells, which would be promising to mimic the MJD pathogenesis in zebrafish in specific neuronal cell types. Moreover, in this way, the pathogenic *atx-3* gene could be safely transferred to the next generation, avoiding the possible infertility of zebrafish due to central nervous system dysfunction

First, a UAS effector plasmid carrying a pathogenic *atx-3* or non-pathogenic *atx-3* encoding

cDNA were needed to be constructed as shown in Fig.7.

Fig. 7. The Gal4/UAS strategy for modelling the SCA-3 in zebrafish and the schematic structures of the plasmids for generating stable transgenic activator and effector lines. When the effector UAS transgenic line is crossed with a neuronal specific Gal4 activator line, the membrane localized fluorescent protein (FP) and the C-terminal Atx-3 polyQ will be expressed in the according neuronal cell types. A T2A sequence separating both cDNAs in frame will mediate a cleavage of the peptide. This results in the equal expression amount of the membrane localized fluorescent protein and the C-terminal Atx-3 polyQ.

3.1.7 Cloning of a CFP fused C-terminal Atx-3 polyQ fragment

For direct monitoring of pathogenic Atx-3 expression, localization and aggregation state, the C-terminus of Atx-3 fragment was fused with cyan fluorescent protein (CFP) encoding sequence was cloned. Subsequently, in front of this Atx-3polyQ-CFP fragment, a T2A sequence was constructed as shown in Fig.8.

Fig. 8. The plasmid for generating a stable transgenic line to modelling SCA-3 in zebrafish. The detailed plasmid structure was described in chapter 3.6. The difference is, the C-terminal atx-3 fragment was fused with a fluorescent protein CFP, which was used for the direct monitoring the Atx-3 expression and aggregation state.

3.1.8 Atx-3Q69 fused with CFP does not form aggregation in vitro

Before using the constructs for generating a transgenic line, it was validated whether such CFP fused Atx-3polyQ variant could form aggregates or not. The plasmids were tested in a zebrafish cultured cell line, called Pac2 fibroblasts. First the cells were cultured on cover slips, after 6 hours or overnight, the cells were transfected with these plasmids, together with a Gal4 activator plasmid (#987). At 1 day after transfection, the cells were fixed and the Atx-3polyQ expression and aggregation state was examined by confocal microscope, shown in Fig.9. Neither Atx-3Q69-CFP nor Atx-3Q15-CFP aggregation was observed in Pac2 cells at 1day after transfection (Fig.4). It is possible that Atx-3 fused with CFP at its C-terminus could not form aggregates.

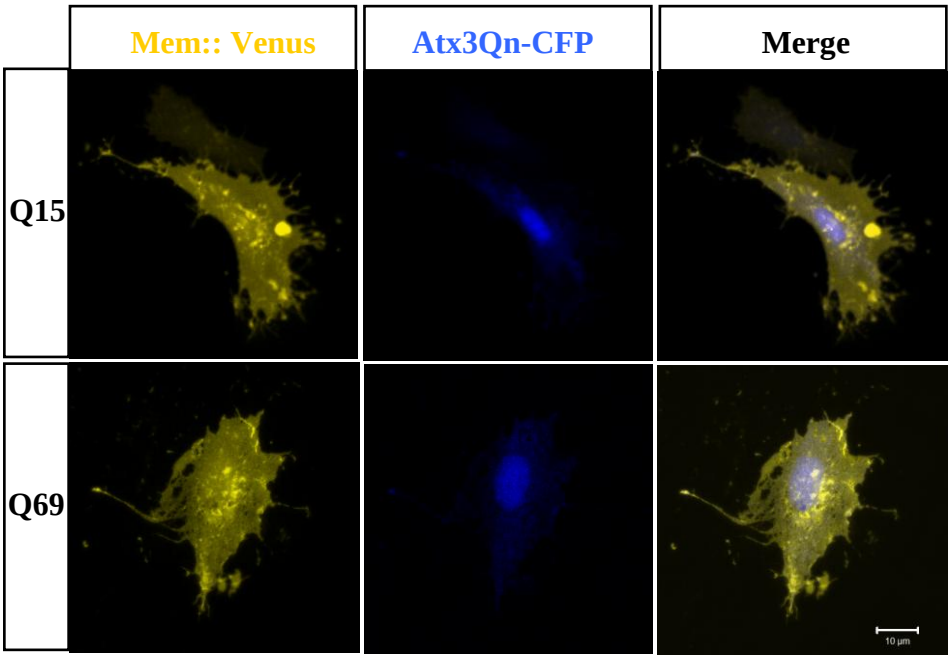

Fig. 9. Atx-3Q69 fused with CFP cannot form aggregates in Pac2 cells at 1 day after transfection. The Pac2 cells were transfected with the plasmids UAS-fynvenus-T2A-C-atx3Q15-mseCFP-strep and Plasmid UAS-fynvenus-T2A-C-atx3Q69-mseCFP-strep, and were fixed at 1day after transfection. The Atx-3Q69-CFP expression and aggregation state was imaged by using confocal microscopy.

3.1.9 CFP fused with the C-terminus of Atx3Q69 does not form aggregates when transiently expressed in zebrafish

Atx-3 aggregates were not discovered, while in the mouse model of SCA-3, neurodegeneration and behavioral defects were indeed observed, we wondered whether the CFP fusion product could induce neuronal cell death in zebrafish. For this purpose, the expression and neuronal toxicity of Atx-3Q69-CFP was examined in a transient expression system in transgenic zebrafish embryos. The plasmids used above were injected into embryos of the Tg (Her3::Gal4) transgenic line at the 1-cell stage, which resulted in expression in cells of the developing mesencephalon/rhombencephalon and the spinal cord (Hans et al., 2004). Expression neurons were imaged at 1dpf by using confocal microscopy (Fig.10)**.**

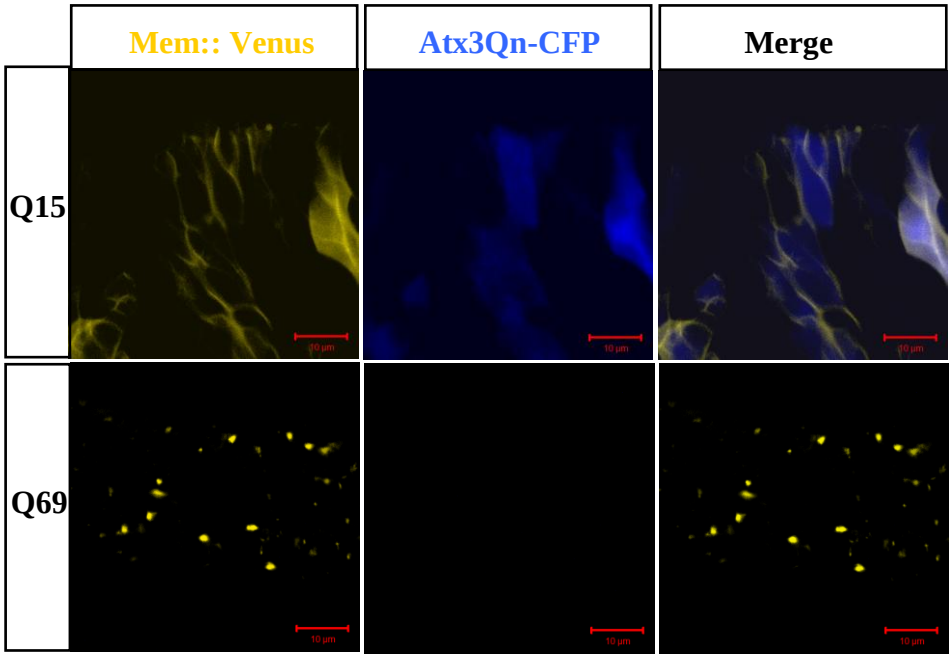

Fig. 10. Transient expression of Membrane localized Venus and Atx-3Q69-CFP in zebrafish brain can cause abnormal neuronal morphology, shown by Venus, but without Atx-3Q69-CFP expression. The plasmid UAS-fynvenus-T2A-C-atx3Q69-mseCFP-strep or the control plasmid UAS-fynvenus-T2A-C-atx3Q15-mseCFP-strep was injected into the embryos of the transgenic fish Tg (Her3::Gal4) strain at one-cell stage. The brains of expressing embryos were imaged by using a confocal microscope. Bar =10um.

When the embryos were injected with the control plasmid UAS-fynvenus-T2A-C-atx3Q15-mseCFP-strep, Atx-3Q15, i.e. CFP expression could be detected. Venus was localized correctly in the membrane. The morphology of the Atx-3Q15 expressing neurons was intact (Fig.10). When the neurons were expressing membrane localized Venus and Atx-3Q69-CFP-strep, CFP, i.e. Atx-3Q69 expression was not detected, while Venus was detected but with incorrect localization, and without cellular morphology (Fig.10). These results suggest that, through transient expression examination, the C-terminal Atx3Q69 fused with CFP-strep was not suitable to analyze pathogenic Atx-3 protein expression and aggregation, not being suitable for modelling MJD in zebrafish.

From these transient expression results, it could be concluded that the C-terminal truncated Atx3Q69 fused with CFP-strep was not suitable to analyze this SCA-3 disease protein expression and aggregation, neither suitable for modelling SCA-3 in zebrafish.

3.1.10 Cloning of a HA tagged C-terminal Atx-3 polyQ fragment

To document problems caused by C-terminal CFP fusion, an N-terminal HA tagged truncated Atx-3Q15/84 fragment was generated, and constructed with a T2A sequence at its N-terminus. This should yield equal expression levels between HA-Atx-3polyQ and the N-terminal membrane localized tagRFPT. This reporter served for the direct observation of neuronal morphology, to monitor the expressing neurons. The schematic structure of the plasmid is shown in Fig.11. The HA-Atx3Q15 plasmid carries a wild type non-pathogenic form of Atx-3; and served as a control.

Fig. 11. Schematic structure of the expression plasmid used for generating a stable transgenic line to model the SCA-3 disease in zebrafish. The detailed plasmid structure is described in chapter 3.6. The difference is that, the C-terminal *atx-3* fragment was fused with a HA tag at the N-terminus, which was used for the monitoring the Atx-3 expression and aggregation state after the immunostaining against the HA tag.

3.1.11 Aggregation of the HA tagged C-terminal Atx-3 polyQ fragment in vitro

In order to know whether the N-terminally HA tagged Atx-3 constructs could form aggregates, the pCS+ expressing plasmids were transfected into a zebrafish fibroblast cell line Pac2 cells. After 2 days, cells were fixed and the HA-Atx-3Q15/82 expression and aggregation was examined by using an anti-HA antibody detected by a Cy2 conjugated secondary antibody. After imaging by confocal microscopy, the aggregates formed by HA-Atx3Q82 (n=3/10) were observed. In contrast, no aggregates were found when the WT control HA-Atx3Q15 (n=12/12) was expressed (Fig.12). This suggests that C-terminal fusion of CFP interferes with proper Atx-3 expression while N-terminally HA tagged fusion protein does not interfere with expression. Therefore it can be used for SCA-3 disease modelling.

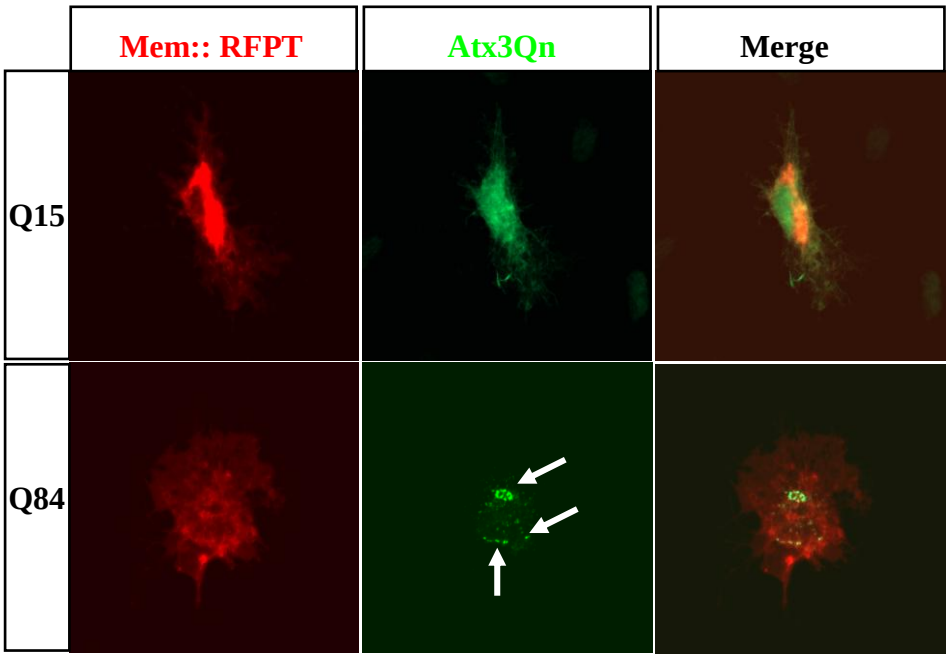

Fig. 12. Truncated Atx-3 polyQ can form aggregates in Pac2 cells when fused to an HA tag at 2days after transfection. FyntagRFP (red) is expressed in the membrane to reveal the cell morphology. HA fused to C-terminus of Atx-3 Q82 can form aggregates, shown by immuno-staining for HA (green), Q15 (WT): cannot form aggregate.

3.1.12 Aggregation of a HA tagged C-terminal Atx3polyQ when transiently expressed in zebrafish

Before the HA tagged C-terminus of Atx-3polyQ could be used to generate a stable transgenic line, it was necessary to clarify proper Atx3polyQ expression and aggregation in a transient expression system.

For this purpose, the constructs UAS-memtagRFPT-T2A-HA-atx-3polyQ were injected into embryos of the transgenic line Tg (Her3::Gal4) at the 1-cell stage, which could drive the expression of Atx-3 polyQ in the developing mesencephalon /rhombencephalon and the spinal cord of injected specimens. At 1dpf, expressing embryos were fixed and stained with an antibody against the HA tag, for detecting the expression and aggregation state of the truncated Atx-3 polyQ variant. The morphology of Atx-3 expressing neurons, and Atx-3 polyQ expression were imaged by using a confocal microscope.

Strong expression of the HA tagged Atx-3Q84 and Atx-3Q15 variant was observed in the central nervous system of the embryos. In addition, aggregates formed by HA tagged Atx-3Q84 were detected, as shown in the Fig.13. The membrane localized tagRFPT in the aggregate containing cells revealed an abnormal cellular morphology, compared with Atx-3Q15 expressing cells. While this HA-Atx-3Q15 was expressed throughout the whole cell, its aggregation was not observed. This showed that specifically the polyQ containing pathogenic

variant results the aggregation in vivo. Thus this variant is suitable for generating a stable transgenic line.

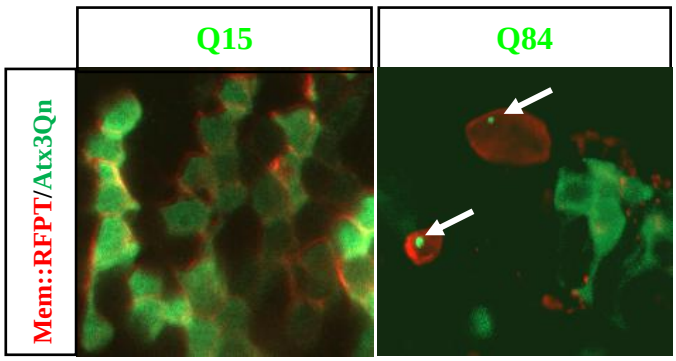

Fig. 13. Atx3Q84 can form aggregates when transiently expressed in embryos of the Tg (Her3::Gal4) strain. Expressing constructs were injected into 1-cell stage embryos of the transgenic line Tg (Her3::Gal4), which drives expression in the developing mesencephalon /rhombencephalon and the spinal cord. Atx-3 expression and aggregation was detected by using a HA antibody and a Cy2 conjugated secondary antibody, abnormal cellular morphology was revealed by the expression of membrane targeted tagRFPT by laser confocal microscopy.

3.1.13 Generation of a stable transgenic zebrafish by using the HA tagged C-terminal Atx3polyQ fragments

In order to model SCA-3 in zebrafish follow the Gal4-UAS strategy mentioned before. For this expression plasmids were cloned into a *Tol2* transposon vector and injected into wild type zebrafish embryos at the 1-cell stage. The injected embryos were raised until adulthood. Subsequently, the adult fish were screened via crossing with Tg (Her3::Gal4) fishes. When the membrane localized tagRFPT fluorescence were observed in the offspring, the parent effector UAS fish was confirmed as a F0 carrier of genome integration. The positive F0 carriers were selected based on a high expression level of the membrane localized tagRFPT. These F0 carriers were crossed with a Purkinje cell specific Gal4 strain, and the embryos were fixed at 9dpf. Subsequently, immunostaining against the HA tag was performed, to confirm the expression and aggregation in case of the HA-Atx-3Q84 construct in Purkinje cells. The best F0 carriers were crossed with wild type fish to produce F1 offspring. Adult fish of the F1 generation were screened in the same way as F0 carriers, subsequently, the F2 and F3 generation were established in the same way.

3.1.14 Aggregation of HA tagged Atx3Q84 in zebrafish Purkinje cells

For evaluating transgene expression in zebrafish Purkinje cells, the stable transgenic lines Tg(UAS-mem::tagRFPT-T2A-HA-atx3Q84/15) were crossed with a Purkinje cell specific activator line Tg (Car8::Gal4) available in our lab. At 4dpf, the offspring was sorted based on

membrane localized tagRFPT under a stereomicroscope. The tagRFPT expressing embryos were raised until 9dpf, fixed with 4% PFA, and subsequently immunostaining against the HA tagwas performed, to detect the expression and aggregation state of Atx-3Q84 and Atx-3Q15 respectively. Atx-3Q84 expression and aggregates were clearly observed in the soma of Purkinje cells at 9 dpf (Fig. 14 B). The expression of Atx-3Q15 was detected in the soma of the Purkinje cells, but without a sign of aggregation (Fig.14 A). These SCA-3 disease characteristics caused pathogenic Q84 pathogene can be mimicked in zebrafish cerebellar Purkinje cells.

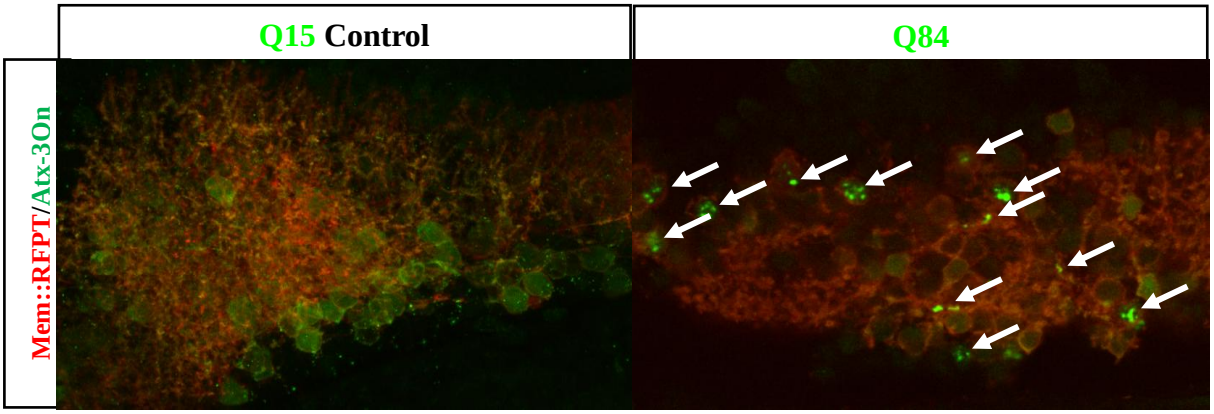

Fig. 14. Atx-3Q84 can undergo aggregation in zebrafish Purkinje cells. Purkinje cells specific expression of Atx-3Q84/15 was obtaind through the cross of carriers of the Tg(PC:: Gal4) and Tg(UAS:mem::tagRFP-T2A-HA-Atx3Q84/15) transgenic strains, and then the offsprings raised until 9dpf. No aggregation were observed when the wild type control Atx-3Q15 was expressed (B) in Purkinje cells. In contrast, clear aggregate is observed with the Atx-3Q84 variant (A). The embryos were subjected to immunostaining against the HA tag and imaged by confocal microscopy.

3.1.15 Swimming defects induced by Atx-3Q84 expression in Purkinje cells

In order to clearify whether the expression and aggregation of the C-terminal Atx-3Q84 fragment in zebrafish Purkinje cells could induce any behavioral defects, stable transgenic embryos of this SCA-3 disease model (Atx-3Q84) were subjected to a comparative behavioral analysis. Freely swimming larvae where monitored over 1 minute and their swimming distance was analyzed by a video tracking system from Viewpoint Inc (Lyon, France). The average swimming distances within one miniute were calculated and compared to embryos expressing the non pathogenic Atx-3Q15 variant. This analysis revealed that larvae expressing the pathogenic variant of Atx-3Q84 were swimming less and showed significantly reduced periods of long distance movements compared to Atx-3 wild type overexpressing specimens suggesting locomotive difficulties in the SCA-3 model larvae (Fig.15).

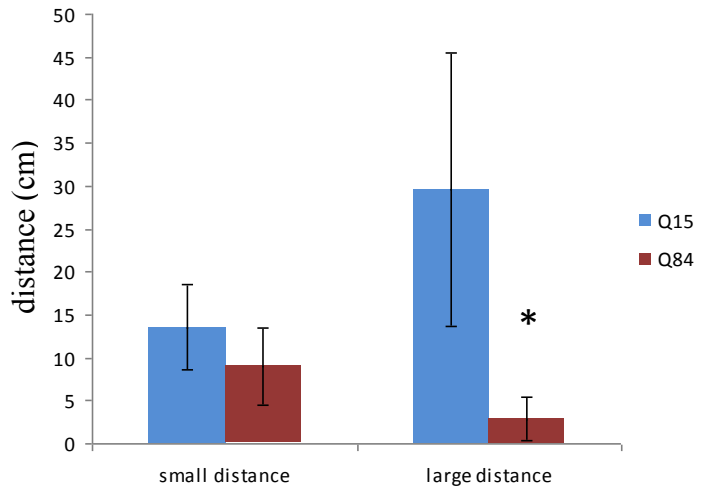

Fig. 15. Zebrafish embryos with Atx-3Q84 expression in Purkinje cells show behavioral defects revealed by their swimming distance within 1min, examined at 9dpf. The embroyos were placed into a culture dish, and monitored druing free swimming over the period of 1 min by the Viewpoint video tracker system. The total swiming distance within 1 min was calculated and compared. Data were obtained form three independent experiments, 5 fishes were examined for each group.

3.1.16 Eye movement defects induced by Atx-3Q84 expression in Purkinje cells

Besides control over swimming, the cerebellum also coordinates the movement of the eyes. In order to unreavel whether the expression of the pathogenic C-terminal Atx-3Q84 fragment in cerebellar Purkinje cells could induce eye movement defects, these SCA-3 larvae were subjected to an assay testing their optokinetic response (OKR). Here larvae follow a regular pattern of moving stripes for which larvae are mounted with their body in low-melting agarose, allowing the eyes to move freely. Larvae expressing the wildtype variant of human Atx-3 (Q15) in cerebellar Purkinje neurons showed regular eye movement (Fig.16). In constrast, pathogenic Atx-3Q84 expressing larvae displayed irregular eye movements and impairment of respondse to the moving stripes continuously. Thus SCA-3 larvae display a phenotypical characteristic for cerebellar dysfunction that are aso observed in SCA-3 patients.

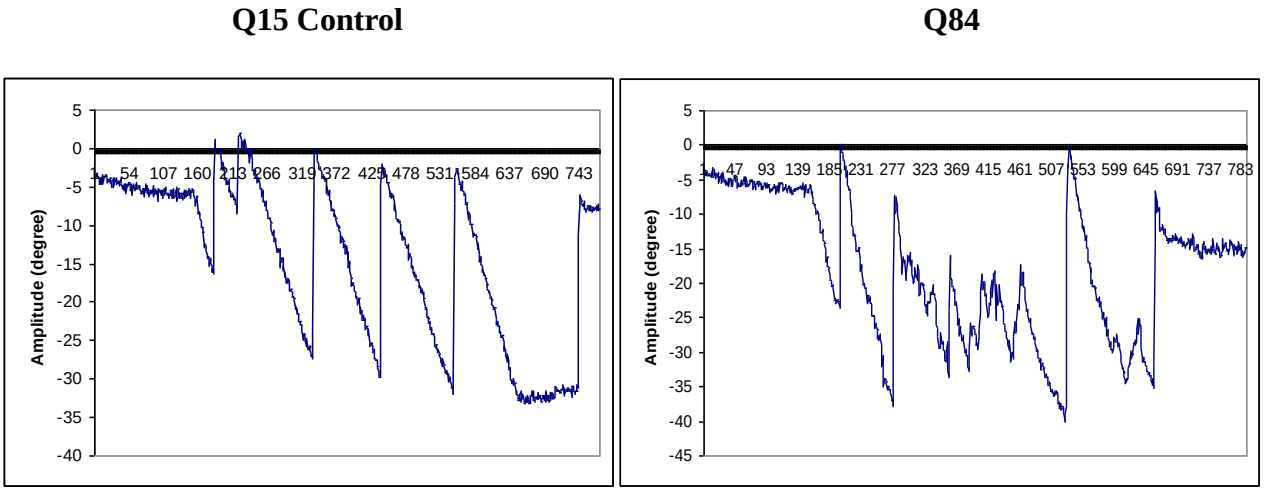

Fig. 16. Eye movement defects caused by Atx3Q84 expression in zebrafish Purkinje cells, examined by optokentic response test. The embryos with Atx3 specific expression in Purkinje cells were embeded in low melting agrose, with free heads but fixed trunks and tails. Then the eye movement in response to moving bars were recorded by a camera and analyzed by using the software ImageJ. The resulting graphs display the angles of eye movements in the embryos.

3.2 Dynamics analysis of Atx-1 polyQ aggregation

3.2.1 Dynamics analysis of Atx-1Q82 aggregation in vitro

The dynamics of Atx1polyQ protein aggregation during neuronal degeneration are largely unknown. We therefore aimed to reveal details of aggregation in a transparent zebrafish model by making use of bio-imaging. First, it was necessary to validate that the human disease protein Atx1polyQ undergoes aggregation in zebrafish in a similar way as in the human cells, and shares similar dynamics or pathogenesis. Therefore, the experiments were first performed in a zebrafish derived cultured cell line Pac2 for comparison with data from human cells. These initial straight-forward studies were followed by an in vivo analysis in living zebrafish.

For overexpressing pathogenic Atx-1Q82 and analyzing its aggregation dynamics in cultured Pac2 cells, a plasmid containing a CMV promoter to drive the expression of Atx-1Q82 fused to CFP (Fig.17 A) was obtained from Dr. K. Namikawa (Köster lab). To observe the cellular morphology, a plasmid containing a CMV promoter to drive the expression of a cytoplasmic localized unctagRFP (Fig.17 B) was obtained from E.Kühn (Köster lab).

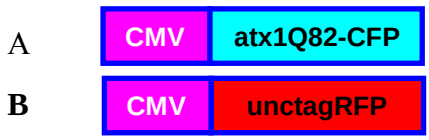

Fig. 17. Diagram of the plasmids, for overexpression and dynamic analysis of human Atx-1 Q82 aggregation in Pac2 cells, and for observing the cellular morphology. A, A CMV promoter driving the expression of pathogenic Atx-1Q82 variant fused to CFP. B, A CMV promoter drives the expression of a cytoplasmic localized unctagRFP.

These two plasmids were co-transfected into the Pac2 fibroblasts. The cells were fixed at one, two and three days after transfection and imaged by using a confocal microscope. Aggregate formation could be observed in the nucleus of Pac2 cells (Fig.18 A). For characterizing the progression of Atx-1Q82 aggregation, the average diameter changes of these aggregates were examined at different time points, and the percentage of cells containing aggregates of different size was quantified.

At 1 day after transfection, the percentage of Pac2 cells containing 1, 2 and 3 aggregates was 4%, 6% and 28%, respectively the rest 62% cells contained more than 4 aggregates. At 2 days after transfection, the percentage of cells containing 1, 2 or 3 aggregates were, 21%, 44% or

25%, and the remaining of the 10% cells contained more than 4 aggregates. At 3 days after transfection, the percentage of cells containing 1, 2 or 3 aggregates were 25%, 37% or 20% respectively, and the remaining of the 18% cells contained more than 4 aggregates. (Fig.18 B) Regarding the average number of aggregates in Pac2 cells, they contained 4.2 aggregates at 1day after transfection. In contrast, at 2 and 3 days after transfection, the average numbers were 2.1 or 2.3 respectively (Fig.18 C). Based on these results, it could be concluded that, the number of Atx1Q82 aggregates decreased over time.

The question of how the size of Atx-1Q82 aggregates could enlarge with the number of aggregates decreased was needed to be answered. The diameters of the aggregates were measured at different time points, and the percentage of cells containing different aggregates sizes and their average of diameter were calculated. At 1 day after transfection, 89% of total expressing cells contained aggregates smaller than 2 μm in diameter. 10% of the cells contained aggregates with diameters between 2 to 4 μm, and only 1% of the cells contained aggregates larger than 4 μm. At 2 days after transfection, the percentage of the cells containing aggregates less than 2 μm, 2 to 4 μm, larger than 4 μm aggregates were 42%, 48% and 10% respectively (Fig.18 D). At 3 days after transfection, the percentage of the cells containing aggregates less than 2 μm, 2 to 4 μm, larger than 4 μm aggregates were 19%, 46% and 35% respectively (Fig.18 D). The average aggregate diameter in all cells was 1.1 μm at 1day after transfection, while at 2 and 3 days after transfection, the average diameter were 2.4 μm or 3.3 μm respectively (Fig.18 E). This showed that the aggregates formed by Atx-1Q82 grow progressively in size in Pac2 cells.

Therefore, through time-lapse imaging, the same individual aggregates were traced during the growth process to investigate size alterations of the aggregates. Individually size of aggregates was measured. Their average diameter was increased from 0.8 μm to 1.4 μm during the imaging period of 12 hours. This shows that aggregates grow by recruiting newly synthesized Atx-1Q82 protein acting as a sink for pathogenic protein.

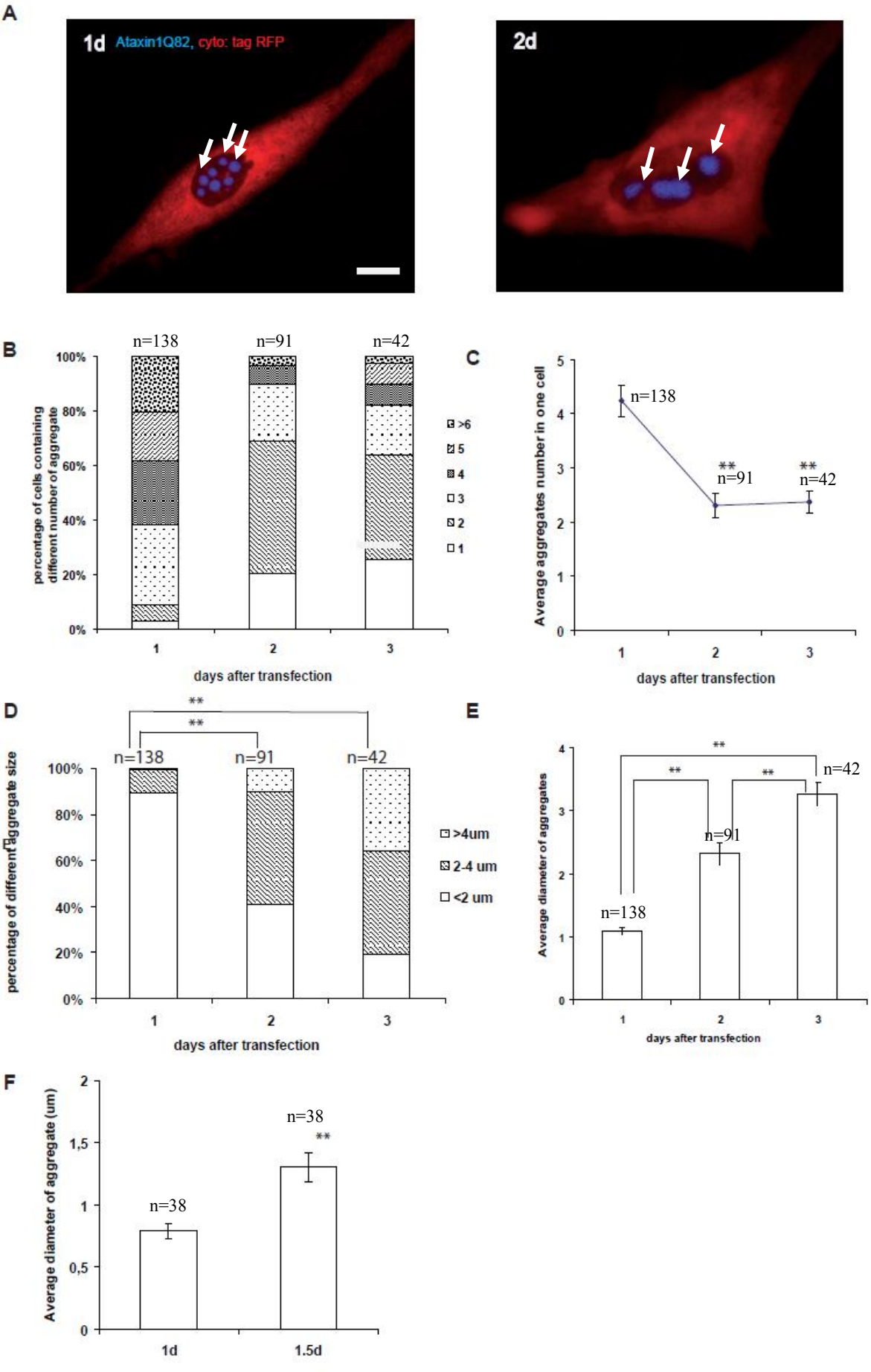
A
1d Ataxin1Q82, cyto: tag RFP
2d
B
n=138
n=91
n=42
100%
80%
60%
40%
20%
0%
percentage of cells containing different number of aggregate
>6
5
4
3
2
1
1
2
3
days after transfection
C
Average aggregates number in one cell
n=138
**
n=91
**
n=42
days after transfection
D
**
**
n=138
n=91
n=42
percentage of different aggregate size
>4um
2-4 um
<2 um
days after transfection
E
**
**
**
n=42
n=91
n=138
Average diameter of aggregates
days after transfection
F
Average diameter of aggregate (um)
n=38
**
n=38
1d
1.5d

Fig. 18. Atx-1Q82 aggregate growth in zebrafish Pac2 fibroblasts. A, Atx-1 Q82 can form aggregates in Pac2 cells (white arrows), scale bar. 5um; B, C, The number of Atx-1Q82 aggregates in single Pac2 cells decreases after transfection percentage distribution of aggregates of the different diameter; E, The average diameter of aggregates increases with time after transfection. The average diameter at 2 and 3 days post transfection is significantly larger than at 1 day post transfection. (T-test, * p <0.01); F, an individual aggregate grow larger from 1 day to 1.5 days, revealed by time lapse imaging.

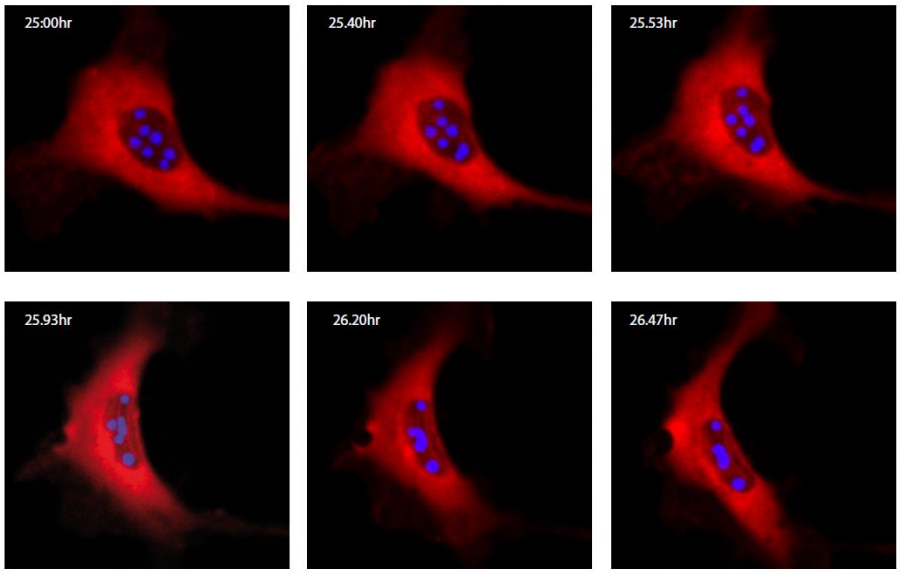

Fig. 19. The Atx-1Q82 aggregates can fuse with each other to form bigger aggregates in Pac2 cells.

For clarifying the reason of the reduction in aggregate number in Pac2 cells over time, time-lapse imaging was performed to record the dynamics of Atx-1Q82 aggregation, at 1 day post transfection. The movies obtained from these time-lapse studies revealed that, adjacent aggregates in the nucleus of Pac2 cells sometimes fuse with each other to form larger aggregates (Fig.19), explaining the decrease in aggregate number over time.

These results obtained from zebrafish Pac2 cells show that the human pathogenic Atx1Q82, protein variant from aggregates in the nucleus of zebrafish cells. The aggregates growth results from two processes: individual aggregates grow larger by recruiting newly synthesize pathogenic protein but also, adjacent aggregates fuse with each other to increase aggregate size. These results are in good accordance to the observation in human cells that means Atx-1Q82 displays the same aggregation characteristics in zebrafish cells than in human cells.

3.2.2 Detection and dynamics analysis of Atx-1polyQ aggregate in vivo

In order to decipher the dynamics of Atx-1polyQ aggregation during SCA-1 pathogenesis in vivo, the aggregation behavior was addressed in a transient transgenic model of SCA-1 in zebrafish expressing Atx-1Q75 in cerebellar Purkinje neurons.

For this, a zebrafish Purkinje cell (PC) specific promoter was used to drive the expression of a transgene cassette containing a membrane localized Venus followed by a T2A sequence and the human pathogenic Atx-1Q75 variant fused to the Cyan fluorescent protein (CFP). A schematic drawing of the expression vector is shown in Fig.20.

The membrane localized fluorescent protein Venus serves for the observation of neuronal cell morphology, to monitor the neuronal degeneration. The T2A sequence results a cleavage of the peptide backbone during protein translation leading to equal amount of expression of memVenus and Atx-1Q75. The CFP fusion to the human Atx-1Q75, allowed the indirect observation of aggregation of human Atx-1Q75 which could be observed by confocal microscopy.

Fig. 20. Schematic drawing of zebrafish Purkinje cell promoter driving membrane localized Venus followed a T2A sequence and Atx-1Q75 fused to the CFP fluorescent protein encoding sequence.

This plasmid was injected into zebrafish wild type embryos at the one cell stage to express Atx-1Q75: CFP in zebrafish Purkinje cells. Atx1Q75-CFP expression initiated at 3 dpf. Due to this reason, the dynamics of Atx-1Q75 aggregation was investigated in zebrafish Purkinje cells starting from this time point.

After plasmid injection, the expressing embryos were embedded at 3, 4 and 5dpf in low melting agarose and imaged using a confocal microscope. Aggregate formation could be observed in the nucleus of zebrafish Purkinje cells at 3dpf (Fig.21 A). The average diameter changes of these aggregates were examined, and the percentile distribution of cells containing different sizes of aggregates was quantified. At 5 dpf, these aggregates were significantly larger indicating their progressive growth.

At 3dpf, the percentage of the Purkinje cells containing 1, 2 or 3 aggregates was 39%, 38% and 20%, respectively; the remaining of 4% cells contained more than 4 aggregates. At 4dpf, the percentage of cells containing 1, 2 or 3 aggregates were, 37%, 37% or 16% respectively,

and the remaining 10% cells contained more than 4 aggregates. At 5dpf, the percentage of cells containing 1, 2 or 3 aggregates were, 32%, 50% or 12% respectively, and the remaining 6% cells contained more than 4 aggregates (Fig.21 B). After an initial increase in aggregate number, a slight trend towards a decline in aggregate number can be deduced in zebrafish Purkinje cells, but not statistically significant.

The diameter of the aggregates at different time points were measured and the average diameter of Atx1Q82 aggregates in Purkinje cells at 3, 4 and 5 dpf was caculated respectively. The average diameter was increased from 1.0 μm at 3 dpf to 1.5 μm at 4 and 5 dpf (Fig.21 C). Based on these observations, it could be concluded that Atx-1Q75 forms nuclear aggregates in Purkinje neurons in vivo in a similar manner as in Pac2 cells but with slower progression.

Through time-lapse imaging, the same individual aggregates were traced overtime to investigate individual size alterations, for which the diameters of the aggregates were calculated. From the beginning of day 3 and the end of the image recording at 3.5 dpf, the average diameter of individual aggregates increased from 1.0 μm to 1.5 μm. This manner as in Pac2 cells, Atx-1polyQ aggregates grow by addition of newly synthesized protein (Fig.21 D).

In cultured Pac2 cells, the growth of Atx1Q82 came from two ways: the growth of individual aggregates and the fusion between aggregates. Thus are asked whether aggregates in Purkinje cells also grow by fusion? Movies obtained from time-lapse imaging of embryos injected with the Atx-1Q82 expression plasmid showed that, adjacent aggregates in Purkinje cells fused with each other to form bigger aggregates (Fig.21 E).

Based on all these results in zebrafish Purkinje cells, the protein Atx1Q82 aggregation in vivo follows similar dynamics as in cultured cells. The size of aggregates was increased from 3 to 5 dpf. Through time-lapse imaging, aggregates growth was shown to result from two processes: individual aggregates grow larger by recruiting newly synthesized protein and, nuclear aggregates fuse with each from time to time, resulting in few but large nuclear Atx-1 polyQ aggregates.

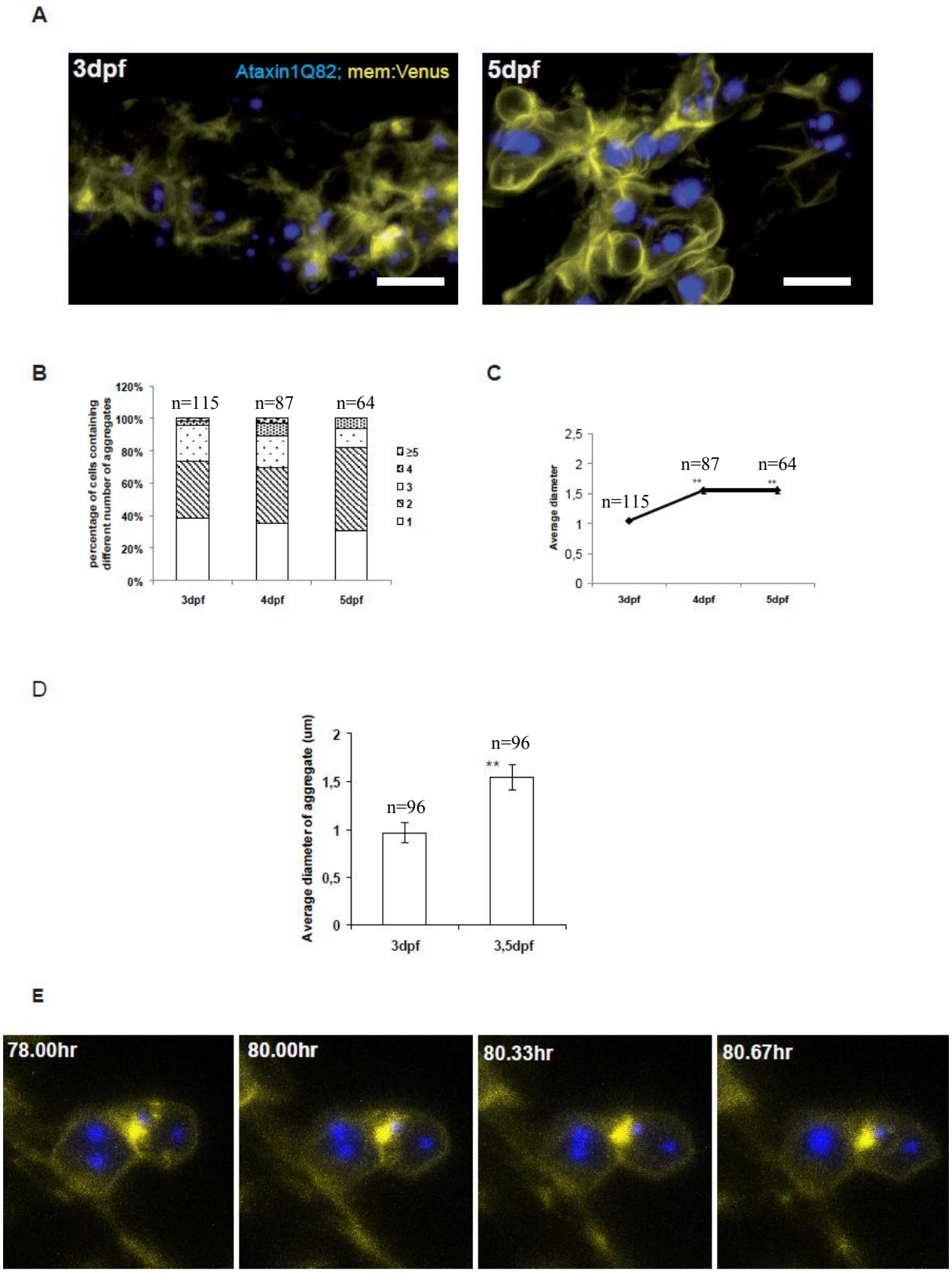

Fig. 21. Analysis of Atx-1Q82 aggregate growth in zebrafish Purkinje cells. A, Atx-1Q82 can form aggregates (red) in zebrafish Purkinje cells (fynVenus); B, the number of aggregates in zebrafish Purkinje cells decreases over time; C, the average diameter of aggregates in zebrafish Purkinje cells increases over time; D, single aggregate grow in zebrafish Purkinje cells by incorporating further newly synthesized Atx-1Q82 protein, as revealed by time lapse imaging. E, the fusion between Atx1Q75 aggregates (blue) in zebrafish Purkinje cells. Scale bars 5µm.

3.2.3 The fusion between Atx-1Q82 aggregates could be induced through Actin depolymerization by Latrunculin A

During the time-lapse imaging for investigating the aggregation in Pac2 cells, it was observed that, aggregates always kept their relative position to each other, even during the migration of the expressing cells (Fig.22). This suggests that aggregates cannot move freely and might be held in place by the nuclear matrix or other factors including nuclear Actin. Aggregate fusion though requires a change in aggregate position and may thus represent a regulated process.

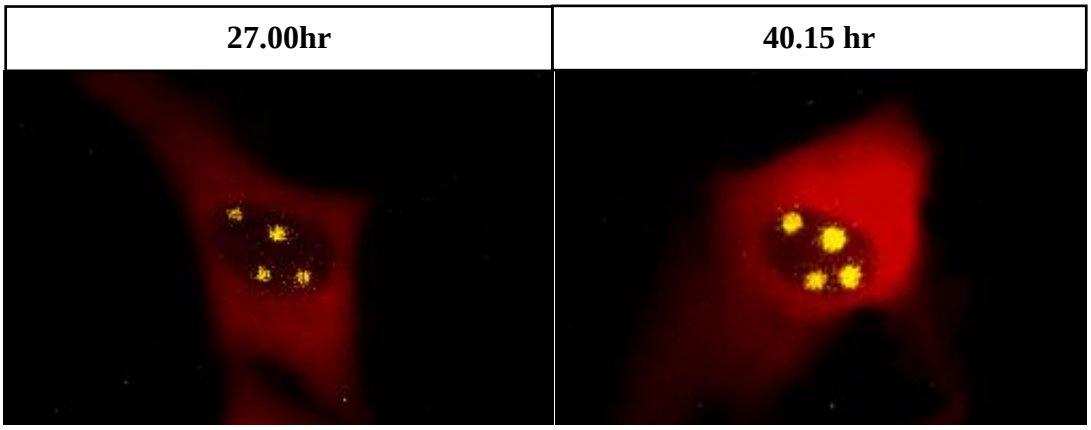

Fig. 22. Atx-1Q82 aggregates keep their relative position to each other in the nucleus of Pac2 cells, remaining stable during cell migration.

In order to address whether the behaviour of the aggregates could be changed via altering the Actin polymerization state, an Actin depolymerizing compound, Latrunculin A, was added to culltured Pac2 cells to destroy their filamentous Actin. Pac2 cells were transfected with expression vector containing human Atx-1Q82 fused to CFP, and the cytoplasmic localized tagRFP, for the observation of the cellular morphology. At 1day after transfection, the behavior of aggregates formed by Atx-1Q82 was recorded through time lapse live imaging, to ensure that no fusion was about to occur spontaneously. Subsequently, Latrunculin A was applied to the Pac2 cells at a final concentration of 1μM during the live imaging.

Rapid fusion between different aggregates were observed already after 12 min of the Latrunculin A exposure, while no fusion was observed in control, revealed with EtOH (Fig.23). This shows that, Actin depolymerization induced by Latrunculin A enhances the fusion between Atx-1Q82 aggregates and increase aggregation in cultured cells, suggesting an involvement of filamentous Actin either in the cytosol and/or in the nucleus of Atx1Q82 expressing cells regulating Atx1Q82 aggregate fusion events.

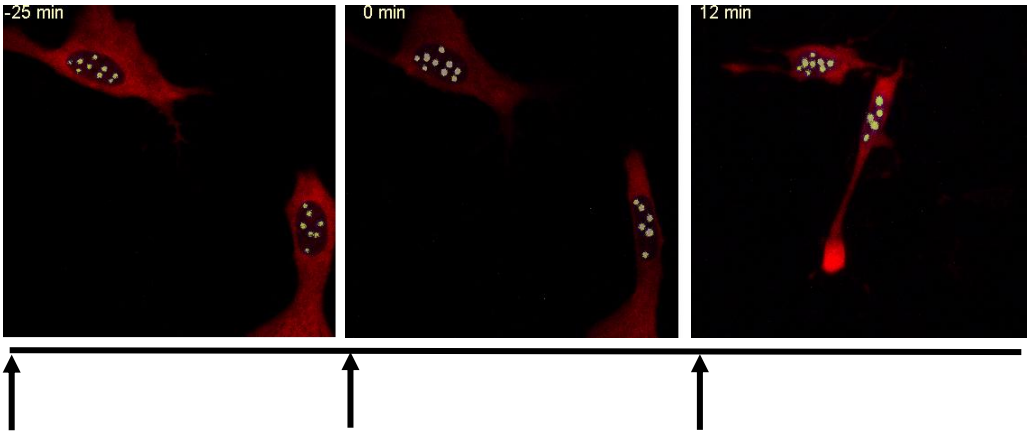

Fig. 23. Fusion between Atx-1Q82 aggregates could be enhanced via Actin depolymerization induced by Latrunculin A treatment, examined through time lapse imaging. Each recording was started 25 min before Latrunculin A application, the average time of Atx-1Q82 aggregate fusion was about 12 min after the Latrunculin A had been applied. n=6.

3.2.4 The interaction of Atx1Q83 aggregates and nuclear Actin

As Latrunculin A depolymerize the F-Actin in the cells, irrespective of its localization we aimed to resolve in which cellular component Actin (Spector et al., 1983) was involved in the Atx-1Q83 aggregation, Therefore, for this, expression plasmids Atx1Q83 was co-expressed with either nuclear or cytoplasmic Actin in Pac2 cells. Plasmids as shown in Fig.23A were constructed. The ubiquitous expression promoter CMV was used to drive expression of the human pathogenic protein Atx-1Q83 fused to the yellow fluorescent protein Venus, followed a T2A sequence and nuclear or cytoplasmic localized Actin fused to a Flag tag (Fig. 24A). Subsequently, the plasmids were transfected into Pac2 cells.

At 1 day after transfection, the number of Atx-1Q83 aggregates was determined. At 2 days after transfection, the morphology of the aggregates formed by Atx-1Q83 was recorded by using a confocal microscope.

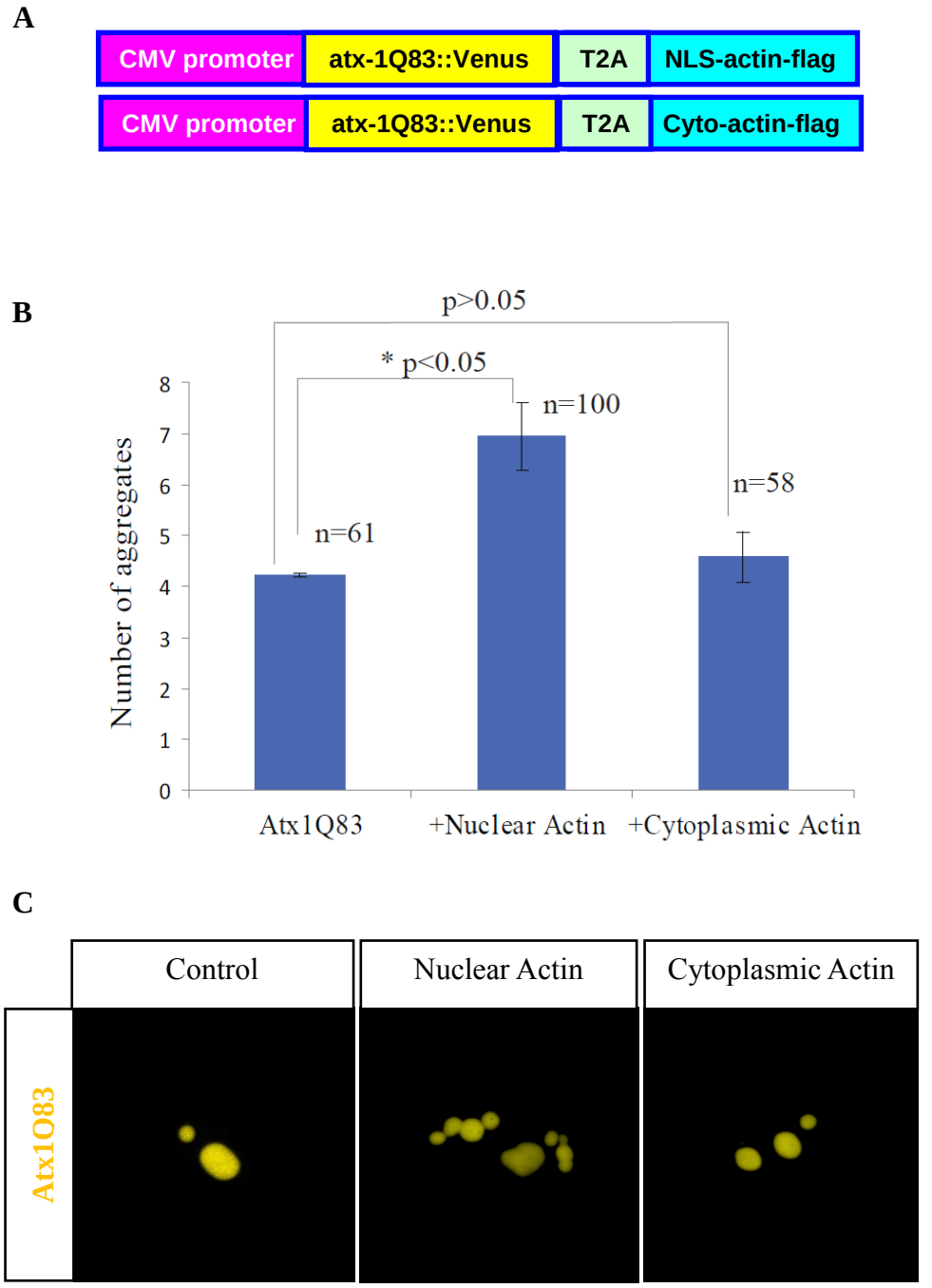

Fig. 24. Co-expression of nuclear Actin with Atx-1Q83 increased the number of aggregates and altered their morphology. A, diagram of the plasmids to co-express Atx-1Q83 fused to Venus and nuclear localized or cytoplasmic localized Actin. B, the average number of aggregates was significantly increased when nuclear-localized Actin was co-expressed with Atx-1Q83 in Pac2 cells, examined at 1day after transfection. No significant changes in number when Atx-1Q83 co-expressed with cytoplasmic Actin. *p<0.05 C, abnormal shape of Atx-1 aggregates can be observed upon co-expression of nuclear-localized Actin in Pac2 cells, while with co-expression of cytoplasmic Actin, the aggregates showed a normal globular morphology. Images were recorded at 2 days after transfection.

At 1 day after transfection, cells co-expressing the nuclear localized Actin together with Atx-1 Q83 fused to Venus showed significant increase in the number of aggregates from an average of 4.2 to 7.1. Overexpression of Atx-1Q83 fused to Venus with cytoplasmic localized Actin,

the aggregate number did not change significantly compared to Atx-1Q83 expression only (Fig.24 B).

At 2 days after transfection, the morphology of the aggregates was characterized by using a confocal microscope. With co-expression of nuclear Actin, the Atx-1Q83 aggregates showed an abnormal morphology. Aggregates looked as the fusion was paused as shown in Fig 23 C. In contrast, co-expression of Atx-1Q83 with cytoplasmic Actin resulted in aggregates with normal shape in the nucleus, similar to over expression of Atx-1Q83 alone (Fig.24 C).

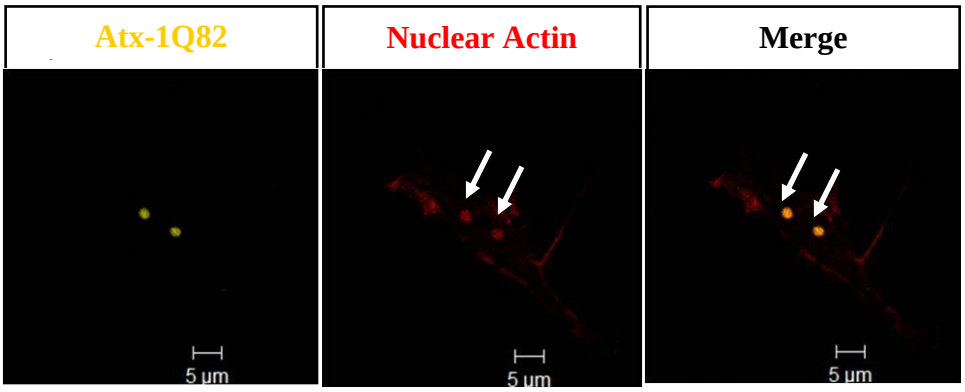

Fig. 25. Colocalization of nuclear Actin (Red) and Atx1Q82 aggregates (Yellow) in the nucleus of Pac2 cells. The localization of Atx-1Q83 aggregates and the nuclear Actin were examined when co-expressed nuclear localized Actin and Atx1Q83 fused to Venus in the nucleus of Pac2 cells at 1 day after transfection.

Next, the localization of Actin was investigated through immunostaining against the Flag tag fused to the Actin variant followed by confocal imaging. Nuclear Actin but not the cytoplasmic localized Actin induced co-localized with Atx-1Q83 aggregates in the nucleus in Pac2 cells (Fig. 25).

As only the nuclear variant was able to alter the morphology of Atx1Q82 aggregates and to increase aggregate numbers, and the observation that nuclear Actin colocalizing with the Atx-1Q83 aggregates in the nucleus, these findings allow to conclude that nuclear Actin is involved in regulating Atx1Q83 aggregate fusion events.

3.2.5 The involvement of Cofilin1 in Atx-1Q83 aggregation

For address the mechanism of Actin polymerization regulating in Atx-1Q83 aggregation, the localization of the Actin depolymerizing factor Cofilin1 was investigated in Atx-1Q83 expressing cells. First, Pac2 cells were transfected with the pCS-Atx-1Q82-RFP expressing plasmid. Subsequently, the Cofilin1 expression and localization was detected through

immunostaining at 1 day after transfection. This revealed that, Cofilin1 was localized in both the cytoplasm and the nucleus of Pac2 cells showing a strong colocalization in the nucleus with Atx-1Q83 aggregates (Fig.26). This suggests that Cofilin1 is involved in regulating Atx-1Q83 aggregation in Pac2 cells.

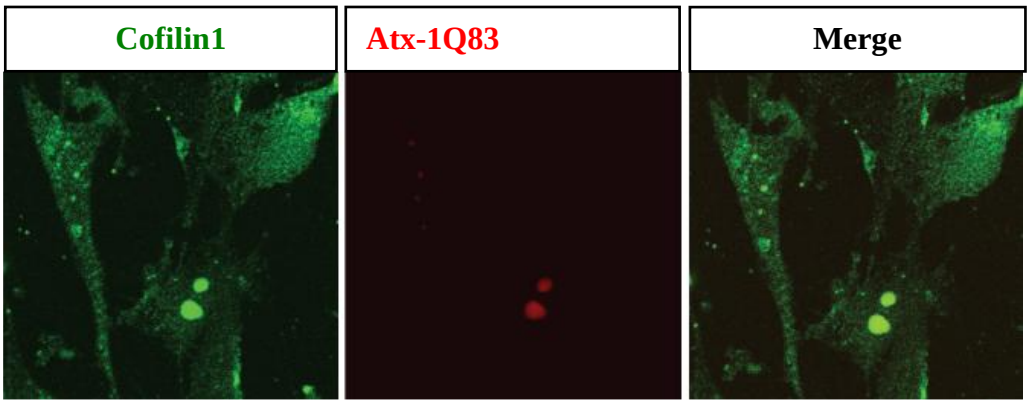

Fig. 26. Colocalization of Cofilin1 (Green) and Atx1Q82 aggregates (Red) in Pac2 cells. The aggregation of Atx-1Q83 fused to RFP and Cofilin1 expression and localization was detected through confocal microscope imaging at 1 day after transfection.

3.3 Summary

Firstly, the zebrafish homologue of SCA-3 disease causing gene *atx-3* was cloned through RT-PCR. The results of protein sequence comparison revealed that, Atx-3 is evolutionarily conserved between zebrafish and human. Subsequently, the zebrafish *atx-3* expression dynamics were clarified both in embryo and adult brain sections. In zebrafish embryo brain, *atx-3* was expressed in zebrafish embryos at 1 dpf and throughout development until 7 dpf. The spatial and temporal expression profiles of whole mount *atx-3 in situ* hybridized embryos reveal a ubiquitous *atx-3* expression during embryogenesis. In adult brain sections, *atx-3* is expressed more specifically, where it could be detected in the cerebellar Purkinje neurons. In addition, *atx-3* mRNA expression was found in cerebellar networks like the optic tectum, in dorsal areas of the hindbrain as well as in ventral diencephalic tissues. The nuclear accumulation behavior of zebrafish Atx-3 is similar like its human homologue upon oxidative stress. It was revealed that zebrafish Atx-3 has a tendency to form nuclear aggregates like its human counterpart. These findings show the conserved characteristics of zebrafish Atx-3, and suggest that it could be promising to model the human SCA-3 disease in zebrafish.

In addition, the aggregation ability of a HA tagged C-terminal Atx-3 polyQ fragment were confirmed in cell culture and in zebrafish brain via transient expression. Using the Gal4/UAS combinatorial genetics system, a stable SCA-3 disease model was generated in zebrafish via overexpression human pathogenic Atx-3 Q84 in cerebellar Purkinje cells. Atx-3 polyQ aggregation was mimicked in the zebrafish Purkinje neurons. Behavioral defects were also observed in zebrafish larvae. Larvae expressing the pathogenic variant of Atx-3 Q84 were swimming less and showed significantly reduced periods of long distance movements compared to Atx-3 wild type overexpressing specimens, suggesting locomotive difficulties in the SCA-3 model larvae. SCA-3 larvae showed irregular eye movements and impairment of respondse to the moving stripes continuously in an OKR test, thus displayed a phenotypical

characteristic for cerebellar dysfunction that are also observed in SCA-3 patients. This zebrafish SCA3 model could be used for decoding the mechanisms of SCA-3 pathogenesis and disease progression, and also provides the possibility for leading compounds screening in drug development.

In order to unravel the molecular mechanisms underlying polyQ protein aggregation and its links to disease pathogenesis, the dynamics of polyQ aggregation were analyzed for Spinocerebellar Ataxia type 1 (SCA-1), both in zebrafish fibroblast Pac2 cells and in a zebrafish SCA-1 model in cerebellar Purkinje cells. Time lapse microscopy could reveal the growth and dynamics of Atx-1 aggregates and was able to reveal fusion events of individual aggregates. It was proved that the growth of aggregates can occur in two ways: either from the direct recruitment of newly synthesized protein, or from fusion between two aggregates, both in vitro and in vivo.

Fusion between Atx-1polyQ aggregates could be enhanced via Actin depolymerization induced by Latrunculin A treatment, examined through time lapse imaging. Coexpression of nuclear Actin but not the cytoplasmic form with Atx-1polyQ increased the number of aggregates and altered their morphology. These findings allow to conclude that nuclear Actin is involved in regulating Atx-1polyQ aggregate fusion events. Furthermore, An Actin depolymerizing factor Cofilin1 was shown a strong colocalization in the nucleus with Atx-1 polyQ aggregates in Pac2 cells. This suggests that Cofilin1 is involved in regulating Atx-1 polyQ aggregation in Pac2 cells. These findings promise to unravel cell biological mechanisms that regulate aggregation behavior and thus cellular toxicity in SCA-1 degenerating neurons.

4 Discussion

4.1 Conservation of protein features across the Atx-3 family members

4.1.1 The conserved sequence of zebrafish Atx-3

The *atx-3* gene family is present in the genomes of different eukaryotic organisms, from invertebrates such as *C.elegans* (but not *Drosophila*) to higher vertebrates, for example human, mouse and zebrafish, etc. Here, in this study, the zebrafish *atx-3* cDNA was cloned and its amino acid sequence was compared to the zebrafish and human cDNA. Also the functional motifs and domains encoded by the *atx-3* cDNA of in zebrafish Atx-3 were predicted. The alignment between zebrafish and human Atx-3 revealed that the amino acid sequence of zebrafish Atx-3 is quite similar to its human homologue, with similar domain architectures, nuclear and cytoplasmic localization signal sequences and the post-translation modification sites. Based on the sequence prediction, zebrafish Atx-3 is possibly composed of a globular N-terminal catalytic Josephin domain, with deubiquitinating activity, followed by a flexible C-terminal tail containning 2 ubiquitin interaction motifs and polyglutamine sequence, but only 1 glutamine, much shorter glutamine repeats than human Atx-3. Mouse Atx-3 contains 6 glutamines, frog has 2 glutamines, which indicates that zebrafish Atx-3 is not an exception in the polyQ repeat length. Such short polyglutamine stretch in these vertebrates is much stable, compared to human wild type form. Therefore, the mutation with longer polyglutaime expansion and similar neurondegeneration disease were not observed among them. In addition, three serine residues present in the ubiquitin interaction motifs, a possible phosphorylation sites and a ubiquitinatable lysine residue, one nuclear localization signal and two nuclear export signals were predicted in the similar regions as in human Atx-3 (Thorsten et al., 2009). It might provide insights to introduce an artificial polyglutamine mutation into zebrafish Atx-3 using TALEN technology for mimicking the human SCA-3 disease in zebrafish.

The conservation of these sequences and domain structures between zebrafish and human Atx-3 suggests that the functional pathways in which Atx-3 participates are likely conserved among vertebrates. The Atx-3 proteins may have the same subcellular localization, cytoplasmic-nuclear shuttling behavior and deubiquitination activities and other related

pathways. Whether this prediction is true or not is necessary to be proved by functional investigations.

4.1.2 The conserved functional characteristics of zebrafish Atx-3

Wild type Atx-3 localizes primarily to the cytoplasm. In response to oxidative stress, one unique feature of human Atx-3 is its accumulation in the nucleus. Although the role of nuclear Atx-3 accumulation following upon oxidative stresses is unknown, one possibility is that Atx3 regulates transcription associated with cellular stress (Reina et al., 2010). After treatment with H_2O_2, which causes cellular oxidative stress, zebrafish Atx-3 behave similarly like its human counterpart, suggesting that the zebrafish Atx-3 may function in similar transcriptional regulation pathways, at least in response to oxidative stress.

Several investigations revealed that the nucleus is a primary site of pathogenesis in SCA-3, and that the nuclear localization of Atx-3 is required to induce the SCA-3characteristic symptoms in a mouse model, as preventing the nuclear localization of Atx-3 greatly reduced the behavioral disorders (Bichelmeier et al., 2007). This evidence stresses the importance of an observation that the nuclear accumulation of Atx-3 responding to oxidative stress is conserved throughout vertebrates. One possible mechanism of human neurodegenerative diseases is that, the increasing oxidative stress during aging could generate irreversible damage to normal neuronal function in the nervous system. The polyQ expanded Atx-3 performed aggregation in the nucleus and decreased the possible role in responding to oxidative stress, which maybe one possible pathogenetic mechanism in SCA-3.

The aggregation property of human Atx-3 is closely linked to the SCA-3 pathogenesis and disease progression. Even lacking a polyglutamine tract Atx-3 can undergo aggregation (Ellisdon and Bottomley et al., 2007). In this study, when human Atx-3 Q15 was expressed in Hela cells for 4 days, aggregates were formed in nucleus and cytoplasm by wild type human Atx-3. Like the human counterpart, zebrafish Atx-3 could also perform aggregation under the same expression condition. These findings reveal that, zebrafish Atx-3 is also an aggregation prone protein. Together with the other data obtained from human Atx-3, the aggregation properties of zebrafish Atx-3 may be enhanced by addition of a polyQ sequence.

4.1.3 The similar expression pattern of Atx-3 and its mRNA

It was revealed that, the zebrafish *atx-3* encoding mRNA was expressed ubiquitously in the embryonic brain. In adults specifically in cerebellar Purkinje cell layer and other brain regions

in adult brains, for example the telecephalon, hypothalamus and octarolateral nucleus, etc. These expression regions are also observed in mouse and human. These observations reveal that, zebrafish Atx-3 functions during embryonic development. Antibody staining against an Purkinje cell marker Zebrin II and combined with *atx-3* mRNA in situ hybridazation analysis showed that zebrafish *atx-3* is expressed in the adult cerebellar Purkinje cells, which supports a role for this gene product in maintaining Purkinje cell functions and this contribution of the cerebellum to locomotion control.

Conserved expression of *atx-3* among vertebrates suggests an involvement in similar cell type specific functions. These conserved features of Atx-3 in structure, expression and response to oxidative stress suggest that it could be promising to model the human SCA-3 disease in zebrafish, by overexpressing the polyQ expanded Atx-3 protein in zebrafish CNS.

4.2 Modeling of SCA-3 in zebrafish

4.2.1 Atx-3 aggregation and its neuronal toxicity

In this investigation, a transgenic SCA-3 disease model was generated in zebrafish, through overexpressing the human pathogenic Atx-3Q84 protein in zebrafish cerebellar Purkinje cells, which are vulnerable to polyQ-expanded Atx3-induced neurotoxicity in SCA-3 patients. The human wild type form Atx-3Q15 was used as a non-pathogenic control (Zoghbi and Orr, 2000). Zebrafish expressing an Atx-3Q84 variant specifically in cerebellar Purkinje cells developed several aggregation phenotypes and neurological disorders similar to SCA-3 patients. For example, intracellular aggregates containing pathogenic Atx-3Q84 were observed in cerebellar Purkinje cells. Behavioral tests indicated that Atx-3Q84 transgenic zebrafish exhibited swimming abilities and abnormal eye movement patterns when tracing to moving bars during optokinetic response test. Control transgenic zebrafish expressing the human wild type Atx-3Q15 variant did not exhibit any symptoms like protein aggregation, neither the motor dysfunction nor eye movement defects. These findings demonstrate that Atx3Q84 transgenic zebrafish generated here exhibit neurological phenotypes. These phenotypes are similar to observations of SCA-3 patients (Soong et al., 1997; Riess et al., 2008). These findings further suggest that the cellular pathology caused by polyQ expansion of Atx-3 in humans is conserved in zebrafish. This *in vivo* animal model could be used for exploring the pathogenic mechanisms of SCA-3, in which biosensors based a fluorescent protein are coexpressed in Purkinje cells by the help of non-invasive bio-imaging.

At present it is unclear how the presence of protein aggregates disturbs Purkinje cell functions. In addition, the possible causative link between aggregate formation and late-stage neurodegeneration remain to be decoded. Nevertheless, the fact that Atx-3Q84 aggregation was observed and that behavioral defects occurred with Purkinje cell specific expression of Atx-3Q84 suggests that Atx-3 aggregation plays a critical role in pathogenesis.

Through high resolution imaging, it is quite interesting to observe that, no apparent neurodegeneration of cerebellar Purkinje neurons in this transgenic zebrafish model could be found at 9dpf, although the respective zebrafish larvae apparently displayed several different behavioral defects. These behavioral defects are likely reflections of neuronal dysfunction occurring earlier than neuronal cell loss. For example, the integrity of synapses may be lost prior to cell death. And neurodegeneration may be a late pathological event in SCA-3 disease. The affected neurons may be able to temporarily bear with the presence of polyQ aggregates. These findings are consistent with data from other studies, which demonstrated that transgenic mice with polyQ expanded Atx-3 expression exhibited neurological symptoms but without a significant neuronal cell death in the cerebellum (Goti et al., 2004; Bichelmeier et al., 2007). A recent investigation completed in induced pluripotent stem cells from SCA-3 patients further strengthened this idea (Koch et al., 2011). These results indicated that, instead of neuronal degeneration, neuronal dysfunction induced by the mutant A**t**x-3Q84 impairs the motor control functions of the cerebellum and causing ataxia, and the neuronal dysfunction only later results in neuronal cell death as a late hallmark of SCA-3.

To reveal the altered functions of degenerating Purkinje neurons, behavioral assays were performed. Several behavioral defects were observed in Atx-3Q84 expressing larvae. One of the important questions is to address, how the Purkinje cell physiology is altered. In a mouse SCA-3 model, in which Atx-3 is overexpressed in Purkinje cells, Shakkottai et al (2011) reported early changes in cerebellar physiology accompanied with motor dysfunction. Preceding the onset of Purkinje cells loss, Purkinje neurons exhibit increased intrinsic excitability resulting in a depolarization block and a loss of the ability to sustain spontaneous repetitive firing. This is associated with altered kinetics of voltage-activated potassium currents. Electrophysiological recording could reveal whether the observed behavioral disorders in our zebrafish SCA-3 models may be due to similar physiological alterations like in this mouse model.

Purkinje cells are the only output neurons from the cerebellar cortex to inhibit neurons of the deep cerebellar nuclei. Purkinje cells play a critical role in motor coordination, based on the correct amount of inhibiting activities of deep cerebellar nuclei cells to produce an appropriate

output, and to inhibit of unwanted spontaneous activity of deep nuclei (Llinas 1981; Bengtsson et al., 2004). This inhibition is very important for the modulation of eye movements. It is possible that overexpression of polyQ expanded Atx-3 interferes with the normal Purkinje cell modulated inhibition, and produces an abnormal spontaneous repetitive firing, activity in deep nuclei. Thus the fine turning of eye movements in OKR tests is inhibited and only abnormal eye movements could be observed.

4.2.2 The effects of fusion partner: position and species

In this study, two different Atx-3 fusion constructs, a C-terminal CFP fusion and an N-terminal HA tag of the Atx-3 C-terminal fragment were tested regarding the aggregation ability of the polyQ protein. The aggregation ability was tested in cultured cells and zebrafish embryos via transient expression. When CFP was fused to the C-terminus of Atx-3, no aggregation was observed in cultured cells; in contrast, when an HA fusion was generated at the N-terminus of the Atx-3 fragment, apparent aggregates were observed in cultured Pac2 cells and in zebrafish brains. The difference in aggregation property may be due to the reason that, the fused protein or tag could exert disturbance on the aggregation property of Atx-3, and hereby possibly influence its neuronal toxicity, which needs to be investigated in the future. Considering that Atx-3 is composed of a globular Josephin domain followed by a free tail, where the polyQ stretch is located , a relative large sized protein like CFP fused to the short C-terminal fragment of Atx-3, might have stronger disturbance on the aggregation property of Atx-3, compared to the small HA tag. In addition, the HA tagged to the N-terminus of Atx-3 fragment might keep Atx-3 C-terminus in a free tail conformation, like its native state, which may help to maintain the native aggregation prone property in Atx-3.

4.2.3 The expression plasmids used to model SCA-3

4.2.3.1 Truncated form of Atx-3

In previous studies, both full length and truncated forms of Atx-3 were applied to generate SCA-3 disease models via overexpression in mouse, rat and fruit flies. The severity of behavioral symptoms differed from case to case. Based on the fact that, C-terminal fragment of Atx-3 and its aggregation products were observed in SCA-3 patients, it was hypothesized that the neuronal toxicity of Atx-3 come from its polyQ contained C-terminus. Therefore, in 1996, under the control mouse Purkinje cell specific promoter, Ikeda et al over expressed a

truncated C-terminal Atx-3 fragment, including the polyQ domain to mimic SCA-3 in mouse. An early onset and increased neurodegeneration were observed, compared to full-length Atx-3 overexpression mice (Ikeda et al., 1996). Besides mouse models of SCA-3, Warrick et al., generated a *Drosophila* model via expressing either the truncated or full length of Atx-3 in the CNS of *Drosophila*, in truncated Atx-3 group, severe eye degeneration was observed in the transgenic flies, strengthening the increased cellular toxicity of the truncated form of Atx-3. This also showed that the truncated C-terminal of polyQ expanded Atx-3 is sufficient to cause neurodegeneration and nuclear aggregates formation in animal models. Furthermore, these models exhibited several additional pathological aspects of SCA-3 in affected neurons, including transcriptional dysregulation, disturbance of calcium homeostasis and compromised protein quality control system, etc (Warrick et al., 1998 and 2005; McGurk et al., 2011).
Because the SCA-3 pathogenesis involves the proteolytic cleavage of Atx-3, and the cleavage products were widely discovered in human patient brains and animal models (Yoshizawa et al., 2000; Goti et al., 2004; Jung et al., 2009), the truncated form of Atx-3 was proposed and demonstrated to be sufficient to induce more severe SCA-3 pathogenesis in mouse. Although the expression of full-length Atx-3 in animal brains may better mimic human SCA-3 disease pathogenesis and progression, the truncated form could speed up disease progression. The truncated C-terminal of Atx-3 is able to induce an increasing neurotoxicity and cause an earlier onset of neurodegeneration, which is helpful to decode the general important disease characteristics and mechanisms in SCA-3. Thus, using the truncated form of Atx-3 may be a short cut for generating a novel zebrafish SCA-3 model.

4.2.3.1 Gal4/UAS system

In this zebrafish SCA-3 model, Gal4/UAS combinatorial genetics was used to drive the expression of pathogenic Atx-3Q84. With this expression system neuronal cell type specific expression could be obtained in the CNS of zebrafish. One of the important advantages of separating the pathogenic lines from its activating enhancer is the convenient maintenance of transgenic carriers without infertility. In addition, this Gal4/UAS system also allows for exploring the processes of neurondegeneration in different neuronal cell types give that suitable Gal4 driver lines are at hand. Many of such lines have been developed already within the zebrafish research community.

4.2.4 The advantages and disadvantages of this SCA-3 disease model in zebrafish

The zebrafish model of SCA-3 in this study displays some important features that mirror the human disease. These transgenic zebrafish with pathogenic Atx-3Q84 overexpression in cerebellar Purkinje cells showed: i) a loss in swimming ability and an oculo-motor defect with the failure of responding to the moving objects. These phenotypes are is consist with the quite common symptoms of this spinocerebellar ataxia; ii) aggregate formation in the expressing neurons, which is a hallmark of polyQ diseases; Further studies using this model may allow us to explore the mechanisms of SCA-3 disease pathogenesis and progression, the underlying links between cerebellar Purkinje cell neuronal dysfunction and pathological disorders.

Like in other disease models, it may be impossible to mimic all the disease symptoms and pathological phenotypes completely in one organism and neither in this SCA-3 zebrafish model. For example, the SCA-3 in human is a late onset disease. In most cases, the symptoms like failure in motor coordination appear after adulthood. In this zebrafish model, the neuronal pathological disorders were observed at 9 dpf in larvae, which are still in a young and developing age. Thus, the neuronal function and the cellular environment in the larvae may be quite different compared to adult fish. This might affect the accurate exploration of the pathogenic mechanisms and disease progression.

In addition, although zebrafish is quite conserved to human beings, it is not a mammalian, compared to rodents, are more genetically distant to humans, for a detailed and comprehensive exploration of the disease mechanisms, a zebrafish model is possibly relatively limited to be fully applied in such kind of investigations. Thus, for a comprehensive understanding of SCA-3, both the use of disease models in zebrafish and other animals are complementary in different study stages and purposes.

4.3 Analysis of Atx-1 polyQ aggregation dynamics

The aggregation of polyQ protein is a pathological hallmark in all polyQ diseases. Based on biophysical investigations, the polyQ protein aggregates are β-sheet rich structures. Even though polyQ disease mechanisms were widely investigated, how these aggregation products grow and behave in the disease affected neurons during pathogenesis is largely unknown. This is in particular interesting for Atx-1 aggregates as they are known for a different mobility compared to other polyQ aggregates (Chai et al., 2002). A clear description of the Atx-1 aggregation dynamics will be helpful to understand the mechanisms of disease progression. In addition, understandings of aggregate growth and the dynamics may suggest a promising strategy to interfere with disease progression.

4.3.1 Dynamics of Atx-1 aggregation in Pac2 cells

In this study, the dynamics of Atx-1 polyQ aggregation were first investigated in the nucleus of zebrafish fibroblast Pac2 cells. It was revealed that Atx-1Q82 fused to CFP could perform aggregation in zebrafish cells, like in cultured human cells. The number of aggregates decreased over time after transfection, while the size of individual aggregates grew larger. The growth of aggregates can occur in two ways: either from the direct recruitment of newly synthesized protein, or from fusion between two aggregates. The latter would cause the aggregate number to decrease in Pac2 cells. These findings are quite consistent with studies performed in human HEK 293 cells. Therefore, it could be concluded that, the behavior of Atx-1 polyQ aggregation in zebrafish fibroblasts is quite similar as in human cell lines. The similarities of aggregation dynamics between zebrafish and human cells show that aggregation of polyQ expanded Atx-1 is conserved, despite the lower environmental temperatures of zebrafish at 28 ℃ compared to 37℃ of human cells. Zebrafish fibroblast Pac2 cells thus provide a good tool to study the human pathogenic protein aggregation behaviors in vitro to later compare the data to in vivo fundings in live zebrafish. Because zebrafish larvae are accessible for bio-imaging, aggregation could be followed to study the human pathogenic Atx-1 protein aggregation in SCA-1 disease.

4.3.2 Dynamics of Atx-1 aggregation in zebrafish cerebellar Purkinje cells

One of the Atx-1 aggregation differences in Pac2 cells and zebrafish Purkinje cells is that, in Purkinje cells, the average aggregate number is lower than in the Pac2 cells. Based on our

quatification data, the aggregate growth in Purkinje cells mostly comes from the direct recruitment of the newly synthesized Atx-1 protein, and less offen, from the fusion between neighboring aggregates in the nucleus of Purkinje cells.

Through high resolution imaging, it is the first time that the dynamic behavior of Atx-1 aggregation was analyzed in disease affected neurons in an animal model. Neurodegeneration was not observed during the investigation period within 5 dpf, showing that aggregate occurs much earlier than neuronal death. This provides the opportunity to study the functions of mutated Atx-1 and related pathways during pathogenesis and disease progression.

4.3.3 The involvement of Actin in Atx-1 aggregation

As revealed in this study, when an Actin depolymerization agent Latrunculin A was applied to Atx-1 aggregate containing Pac2 cells, the fusion between individual aggregates was acutely induced. Coexpression of Actin with Atx-1 in the nucleus significantly increases the aggregate number in the nucleus of Pac2 cells. The colocalization of nuclear Actin with Atx-1 aggregates was also observed in Pac2 cells. This evidence strongly suggests an involvement of Actin in Atx-1 polyQ aggregation.

Several evidence also support links between Actin and its polymerization state and polyQ protein aggregation. Shao et al., (2008) showed that Htt or AR polyQ aggregation could be significantly decreased by overexpression of Profilin, an important promoter of Actin polymerization, or through inhibition of Profilin phosphorylation via genetical or pharmaceutical approaches. Furthermore, Actin binding by Profilin is required to inhibit the polyQ aggregation. Angeli et al., 2010 reported that the first 14 amino acid of Htt and the first 50 amino acid of AR receptor, mediate a direct binding to F-Actin. Deletion of these regions in Htt and AR receptor, the aggregation-prone property of these proteins was greatly reduced, as shown by the decreased aggregate number and increased SDS solubility of aggregates, the normal aggregate morphology and cellular distributions were also significantly affected. These findings together with the data obtained in this study; promise to provide further insights into the possible role of Actin related pathways in modulating polyQ protein aggregation.

In this study, Actin colocalization with Atx-1 polyQ aggregates was observed, which is suggesting an interaction between them.

During polyQ protein aggregation, many aberrant interactions between cellular proteins occur, which may be a cause of neuronal toxicity. One of the missions in this field is to explore such

molecules and the interaction domains in the polyQ proteins, which may provide possible insights to interfere with the regulation of polyQ aggregation.

One possible further work is to clarify the interaction domains in Atx-1 protein. The AXH domain in Atx-1 is reported to act in mediating the interaction with many other molecules, for example with the transcriptional repressors Gfi-1 and Capicua. Whether the AXH domain also mediates the interaction with F-Actin, needs to be further investigated. The aggregation and possible colocalization with F-Actin could be tested through coexpression of nuclear Actin with an Atx-1 polyQ variant after AXH domain deletion in Atx-1. For narrowing down the Actin interaction site of the AXH domain, co-immunoprecipitation with serial deletion and point mutations of AXH as well as with colocalization studies of fluorescent protein fusions of the different deletion variants could be performed.

From the abnormal morphology of aggregates when Actin is coexpressed in the nucleus, it appeared that as if aggregate movement was decreased, and thus the fusion of aggregates between each other was inhibited. This may be due to the possible interaction between nuclear Actin and Atx-1 aggregates, but whether such an interaction is direct remains unclear. It is unknown whether this possible interaction between F-Actin and Atx-1 aggregates could mitigate or increase the neuronal toxicity of the aggregation products. If so, the neuropathy of SCA-1 might be modulated through enhancing or reducing the interaction between F-Actin and Atx-1 polyQ aggregates. However the side effects of such modulation should be seriously considered.

4.3.4 Atx-1 may influence with Actin remodeling during neurodegeneration

In many neurodegenerative diseases, dendrite retraction is one of the early pathological features. In the case of SCA-1, the predominantly affected Purkinje neurons are lost due to a characteristic dying back degeneration that starts from the pruning of dendrite tips but soon after leads to the shrinkage of whole dendritic tree. The dendritic retraction of Purkinje neurons during degeneration in SCA-1 is likely through Actin remodeling (Watase et al., 2002; Duvick et al., 2010). Previous findings suggested the importance of the Actin modulators Profilin2 and Cofilin1 in Atx-1 polyQ-mediated dendrite retraction in polyQ diseases (Bauer et al., 2009; Burnett et al., 2008; Lee et al., 2011). Furthermore, a direct interaction between Atx-1 and Cofilin1 was revealed through yeast-two-hybrid (Lim et al., 2006), while Cofilin1 regulator 14-3-3ε has been shown to colocalize with and to regulate Cofilin1 during neurite extension (Yoon et al., 2011; Sudnitsyna et al., 2012). Interestingly, protein 14-3-3 could strongly bind to the polyQ expanded Atx-1, stimulated aggregation and aggravated

neurodegeneration (Chen et al. 2003; Lai et al., 2011). In neurons expressing pathogenic Atx-1 a diminished expression of Cofilin1 in neuronal dendrites has been observed (Lee et al., 2011). This suggest that Atx-1 represents a regulator of the Actin modulating factors misregulating their activity during the dying-back neurondegeneration in Purkinje cells. Here, a hypothetical model of Atx-1 polyQ induced neurodegeneration was proposed in Fig.4-1.

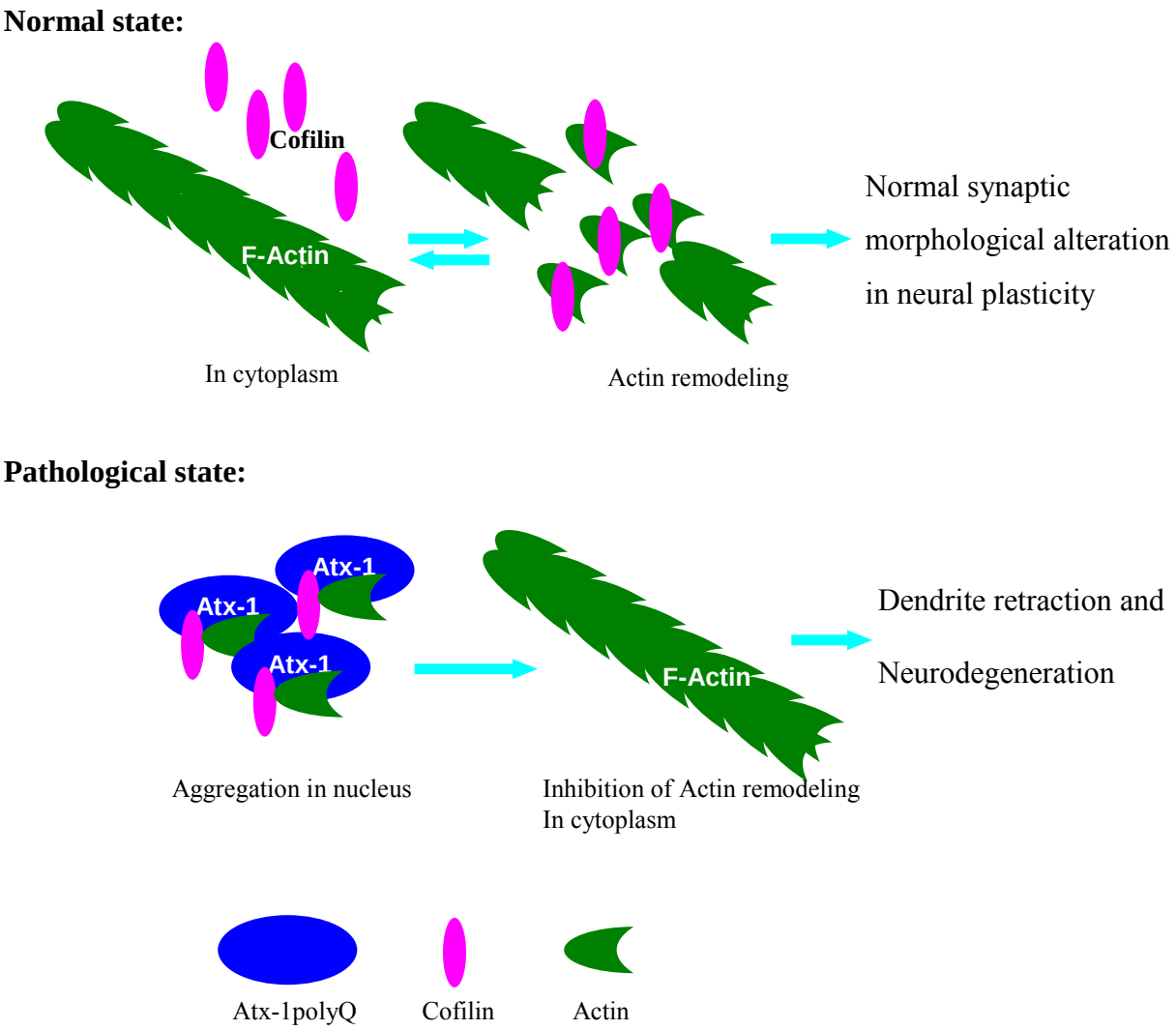

Fig. 4-1. A hypothetical model of Atx-1 polyQ acts as hub to modulate Actin remodeling and finally causes dendrite retraction and neurodegeneration. In Normal state, Cofilin can bind with F-actin in cytoplasm and causes Actin remodeling, thus involved in neuronal plasticity. In pathological stage, Cofilin and Actin might be aggregated with Atx-1 polyQ in nucleus. Thus, Actin remodeling could be inhibited due to the consumption of Cofilin or transcriptional dysregulation induced by the Atx-1 aggregation, therefore inducing dendrite retraction and neurodegeneration.

But how Cofilin1 and Profilin2 are involved in Atx-1 mediated neurodegeneration process relating to Actin remodeling remain unclear. To clarify the link between Atx-1 function, localization, Actin modulators and dendritic retraction would not only help to understand 14-

3-3, Profilin2 and Cofilin1 functions in dendrite retraction but also in the dying back degeneration of Purkinje cells during SCA-1 disease progression.
Furthermore, coexpression of Atx-1 polyQ variant with Profilin2 or Cofilin1 mutated variants in zebrafish Purkinje neurons could be performed, for analyzing the potential rescue of degeneration-mediated dendrite pruning and retraction. The findings could independently confirm a potential contribution of these factors to Actin cytoskeletal remodeling during neurondegeneration and further support the hypothesis that Atx-1 could act as a hub for Actin cytoskeleton remodeling.

Together, these findings show that zebrafish is well suited to model neurodegenerative diseases of the family of spinocerebellar ataxias providing the chance to use in vivo microscopy for addressing cell biological mechanisms of neuronal degeneration. While successful modeling was demonstrated for the case of SCA-3, cell biological analysis of Atx-1polyQ aggregation could reveal insights into so far unknown molecular mechanisms of aggregation. These zebrafish models could therefore help to further unravel molecular and cellular mechanisms of neurodegeneration directly in the living organism.

5. Appendix

5.1. Abbrevations

Atx, ataxin

AR, Androgen receptor

bp, base pair

BCIP, 5-bromo-4-chloro-3'- indolyphosphate p-toluidine

BSA, bovine serum albumin

CBP, CREB-binding protein

cDNA, complementary Deoxyribonucleic Acid

CFP, Cyan Fluorescent

CREB, cAMP-response-element binding protein

DAPI, 4', 6-diamidino-2-phenylindole

DIG, digoxin

DMSO, dimethylsulfoxid

DNA, Deoxyribonucleic Acid

DNAse, desoxyribonuclease

dNTP, deoxynucleotide triphosphate

DPBS, Dulbecco's Phosphate buffered saline

dpf, days post fertilization

E.coli, Escherichia coli

EtBr Ethidiumbromid

EtOH, ethanol

FRAP, Fluorescence Recovery after Photobleaching

GFP, green fluorescent protein

HD, Huntington’s Disease

h, hour

hpf, hours post fertilization

htt, huntington

kD, kilo dalton

µ, micro-

MeOH, methanol

min, minutes

mRNA, messenger RNA

MHB, Midbrain-Hindbrain Bundary

MJD, Machado-Joseph disease

mse, monomeric super enhanced

NBT, nitro-blue tetrazolium chloride

NES, Nuclear Export Signal

NLS, Nuclear Localization Signal

NGS, normal goat serum

PC, Purkinje Cell

PCR, Polymerase Chain Reaction

PBS, Phosphate Buffered Saline

polyQ, polyglutamine

RFP, Red Fluorescence Protein

RNA, RiboNucleic Acid

RNase, ribonuclease

rpm, rounds per minute

PFA, paraformaldehyde

PTW, PBS with Tween

PTU, phenylthiourea

RT-PCR, reverse-transcription polymerase chain reaction

SCA, Spinocerebellar ataxia

Tris, 2-Amino-2-hydroxymethyl-1,3-propandiol

U, Units

UAS, upstream activating sequence

UV, ultra violette

V, Volt

WIHC, Whole mount immunohistochemistry

WISH, Whole mount in situ hybridization

5.2 Publications in Preparation

1. **Changsheng Liu**, Kazuhiko Namikawa, Reinhard Koester.

   Characterization of the Zebrafish Homologue of Machedo-Joseph Disease Causing Gene ataxin3.

2. **Changsheng Liu**, Kazuhiko Namikawa, Reinhard Koester.

   Analysis of Cell Biological Mechanisms that Control Ataxin1 Aggregation In vivo.

5.3. Lebenslauf

Name: Changsheng Liu

Geburtstag: 28.05.1980

Geburtsort: Liaoning, China

AKADEMISCHER WERDEGANG

Mai/2009 bis Nov./2012

Promotion in der Zebrafisch Neuroimaging Gruppe von Dr. Reinhard Köster am Helmholtz Zentrum München (ab 05.2011 an der technischer Universität Btaunschweig) unter der Betreuung von Prof. Dr. Wolfgang Wurst

Titel: "*Genetic modeling of a neurodegenerative polyglutamine disorder in zebrafish and analysis of polyglutamine aggregate dynamics"*

Schwerpunkte:

- *In vivo confocal Bioimaging*
- Durchlicht und Epifluoreszenz Mikroskopie
- Zebrafisch Neurogenetik
- Zellkultur
- Molekularbiologie

Jul/2006

Master of Science in der Biologie an der landwirtschaftlichen Universität Shenyang, China.
Titel der Masterarbeit: "*Neuronal mitochondrial toxicity of malondialdehyde: inhibitory effects on respiratory function and enzyme activities in rat brain mitochondria"*

Schwerpunkte:

- Proteinbiochemie
- Immunhistochemie
- *confocal Bioimaging*

Sep/2003 bis Jul/2006

Lehramtsstudium in Biochemie und Molekularbiologie an der landwirtschaftlichen Universität Shenyang (Oct/2004 - Apr/2006, Gaststudent in Institut für Ernährungswissenschaft, "*Chinese Academy of Science"*)

Jul/2003

Bachelor in Agronomie an der landwirtschaftlichen Universität Shenyang,China
Hauptfach: Agronomie

Sep/1999 bis Jul/2003

Lehramtsstudium in Agronomie an der landwirtschaftlichen Universität Shenyang

SCHULAUSBILDUNG

Sep/1996 bis Juni/1999

"No.1 High School Dengta, China"

.

6. Reference

Aislinn J. Williams and Henry L. Paulson (2007) Polyglutamine neurodegeneration: protein misfolding revisited. *Trends in Neurosciences* 31 521-528

Albrecht M., M. Golatta, U. Wullner, T. Lengauer. (2004) Structural and functional analysis of ataxin-2 and ataxin-3. Eur. J. Biochem., 271, 3155-3170

Alves S., E. Regulier, I. Nascimento-Ferreira, R. Hassig, N. Dufour, A. Koeppen, A.L. Carvalho, S. Simoes, M.C. de Lima, E. Brouillet, V.C. Gould, N. Deglon, L.P. de Almeida (2008) Striatal and nigral pathology in a lentiviral rat model of Machado–Joseph disease. Hum. Mol. Genet., 17, 2071-2083

Amsterdam Adam, Shawn Burgess, Gregory Golling, Wenbiao Chen, Zhaoxia Sun, Karen Townsend, Sarah Farrington, Maryann Haldi, and Nancy Hopkins**.** (1999) A large-scale insertional mutagenesis screen in zebrafish. Genes & Dev. 13: 2713-2724

Angeli S, Shao J, Diamond MI (2010) F-Actin Binding Regions on the Androgen Receptor and Huntingtin Increase Aggregation and Alter Aggregate Characteristics. PLoS one 5(2): e9053.

Antony, P.M.A., Mäntele, S., Mollenkopf, P., Boy, J, Kehlenbach, R.H., Riess, O, Schmidt, T. (2009) Identification and functional dissection of localization signals within ataxin-3. Neurobiology of Disease. Vol 36 (2), , 280-292

Bauer PO, Wong HK, Oyama F, Goswami A, Okuno M, Kino Y, Miyazaki H, Nukina N. (2009) Inhibition of Rho kinases enhances the degradation of mutant huntingtin. J Biol Chem.; 284(19):13153-64

Bengtsson, F. P. Svensson and G. Hesslow (2004) Feedback control of Purkinje cell activity by the cerebello-olivary pathway, European Journal of Neuroscience Vol. 20, 2999-3005

Berke S.J., F.A. Schmied, E.R. Brunt, L.M. Ellerby, H.L. Paulson. (2004) Caspase-mediated proteolysis of the polyglutamine disease protein ataxin-3. J. Neurochem. 89, 908-918

Bevivino A.E., P.J. Loll. (2001)An expanded glutamine repeat destabilizes native ataxin-3 structure and mediates formation of parallel beta -fibrils. Proc. Natl. Acad. Sci. U.S.A., 98, 11955-11960

Bichelmeier U, Schmidt T, Hübener J, Boy J, Rüttiger L, Häbig K, Poths S, Bonin M, Knipper M, Schmidt WJ, Wilbertz J, Wolburg H, Laccone F, Riess O. (2007) Nuclear localization of ataxin-3 is required for the manifestation of symptoms in SCA3: in vivo evidence. J Neurosci. 27(28):7418-28.

Boy J, Schmidt T, Schumann U, Grasshoff U, Unser S, Holzmann C, Schmitt I, Karl T, Laccone F, Wolburg H, Ibrahim S, Riess O. (2010)A transgenic mouse model of spinocerebellar ataxia type 3 resembling late disease onset and gender-specific instability of CAG repeats. Neurobiol Dis. 37(2):284-93.

Breuer P., A. Haacke, B.O. Evert, U. Wullner. (2010). Nuclear aggregation of polyglutamine-expanded ataxin-3: fragments escape the cytoplasmic quality control. J. Biol. Chem., 285 6532-6537

Burnett B., F. Li, R.N. Pittman. (2003)The polyglutamine neurodegenerative protein ataxin-3 binds polyubiquitylated proteins and has ubiquitin protease activity. Hum. Mol. Genet., 12, 3195-3205

Burnett BG, Andrews J, Ranganathan S, Fischbeck KH, Di Prospero NA. (2008) Expression of expanded polyglutamine targets profilin for degradation and alters actin dynamics. Neurobiol Dis. 30(3):365-74.

Cemal C.K., C.J. Carroll, L. Lawrence, M.B. Lowrie, P. Ruddle, S. Al-Mahdawi, R.H. King, M.A. Pook, C. Huxley, S. Chamberlain. (2002), YAC transgenic mice carrying pathological alleles of the MJD1 locus exhibit a mild and slowly progressive cerebellar deficit. Hum. Mol. Genet., 11 1075-1094

Cesira de Chiara, Rajesh P. Menon, Molly Strom, Toby J. Gibson, Annalisa Pastore. (2009). Phosphorylation of S776 and 14-3-3 Binding Modulate Ataxin-1 Interaction with Splicing Factors. PLoS ONE 4(12): e8372. doi:10.1371/journal.pone.0008372

Chai Y., S.L. Koppenhafer, S.J. Shoesmith, M.K. Perez, H.L. Paulson. (1999), Evidence for proteasome involvement in polyglutamine disease: localization to nuclear inclusions in SCA3/MJD and suppression of polyglutamine aggregation in vitro. Hum. Mol. Genet., 8 673-682

Chai Y., S.L. Koppenhafer, N.M. Bonini, H.L. Paulson. (1999)Analysis of the role of heat shock protein (Hsp) molecular chaperones in polyglutamine disease. J. Neurosci., 19, 10338-10347

Chai Y., S.S. Berke, R.E. Cohen, H.L. Paulson. (2004), Poly-ubiquitin binding by the polyglutamine disease protein ataxin-3 links its normal function to protein surveillance pathways. J. Biol. Chem., 279 3605-3611

Chai Y., J. Shao, V.M. Miller, A. Williams, H.L. Paulson. (2002) Live-cell imaging reveals divergent intracellular dynamics of polyglutamine disease proteins and supports a sequestration model of pathogenesis. Proc. Natl. Acad. Sci. U.S.A., 99, 9310-9315

Chen N, Furuya S, Doi H, Hashimoto Y, Kudo Y, Higashi H. (2003) Ganglioside/calmodulin kinase II signal inducing cdc42-mediated neuronal actin reorganization. Neuroscience.;120(1):163-76.

Chen S., V. Berthelier, J.B. Hamilton, B. O'Nuallain, R. Wetzel. (2002)Amyloid-like features of polyglutamine aggregates and their assembly kinetics. Biochemistry, 41, 7391-7399

Chiara Pozzi, Marco Valtorta, Gabriella Tedeschi, Elena Galbusera, Valentina Pastori, Alessandra Bigi, Simona Nonnis, Eleonora Grassi, and Paola Fusi, (2008) Study of subcellular localization and proteolysis of ataxin-3 *Neurobiology of Disease* 30 190-200

Chiara de C, Menon RP, Dal Piaz F, Calder L, Pastore A. (2005) Polyglutamine is not all: the functional role of the AXH domain in the ataxin-1 protein. J Mol Biol. 354(4):883-93

Chou An-Hsun, Tu-Hsueh Yeh, Pin Ouyang, Ying-Ling Chen, Si-Ying Chen, Hung-Li Wang. (2008) Polyglutamine-expanded ataxin-3 causes cerebellar dysfunction of SCA3 transgenic mice by inducing transcriptional dysregulation. Neurobiology of Disease. Vol31(1), , 89-101

Chou, A.-H, Chen, S.-Y., Yeh, T.-H., Weng, Y.-H., Wang, H.-L. (2011) HDAC inhibitor sodium butyrate reverses transcriptional downregulation and ameliorates ataxic symptoms in a transgenic mouse model of SCA3. Neurobiology of Disease Vol 41, Issue 2, 481-488

Chow M.K., H.L. Paulson, S.P. Bottomley. (2004) Destabilization of a non-pathological variant of ataxin-3 results in fibrillogenesis via a partially folded intermediate: a model for misfolding in polyglutamine disease. J. Mol. Biol., 335 333-341

Chow M.K., J.P. Mackay, J.C. Whisstock, M.J. Scanlon, S.P. Bottomley. (2004) Structural and functional analysis of the Josephin domain of the polyglutamine protein ataxin-3. Biochem. Biophys. Res. Commun. 322 387-394

Chow M.K., A.M. Ellisdon, L.D. Cabrita, S.P. Bottomley. (2004) Polyglutamine expansion in ataxin-3 does not affect protein stability: implications for misfolding and disease. J. Biol.Chem., 27947643-47651

Christopher A. Ross, Michelle A. Poirier, Erich E. Wanker, and Mario Amzel. (2003) Polyglutamine fibrillogenesis: The pathway unfolds. Proc Natl Acad Sci U S A. 7; 100(1): 1-3.

Christopher J. Cummings, Yaling Sun, Puneet Opal, Barbara Antalffy, Ruben Mestril, Harry T. Orr, Wolfgang H. Dillmann and Huda Y. Zoghbi.(2001) Over-expression of inducible HSP70 chaperone suppresses neuropathology and improves motor function in SCA1 mice . Human Molecular Genetics. Vol 10, Issue 14,1511-1518

Conceição Bettencourt and Manuela Lima. (2011) Machado-Joseph Disease: from first descriptions to new perspectives. Orphanet Journal of Rare Diseases, 6:35

Cooper JK, Schilling G, Peters MF, Herring WJ, Sharp AH, Kaminsky Z, Masone J, Khan FA, Delanoy M, Borchelt DR, Dawson VL, Dawson TM, Ross CA. (1998) Truncated N-terminal fragments of huntingtin with expanded glutamine repeats form nuclear and cytoplasmic aggregates in cell culture. Hum Mol Genet. May; 7(5):783-90.

Costa M.C., J. Gomes-da-Silva, C.J. Miranda, J. Sequeiros, M.M. Santos, P. Maciel. (2004) Genomic structure, promoter activity, and developmental expression of the mouse homologue of the Machado–Joseph disease (MJD) gene. Genomics, 84, 361-373

Coutinho P., C. Andrade (1978) Autosomal dominant system degeneration in Portuguese families of the Azores Islands. A new genetic disorder involving cerebellar, pyramidal, extrapyramidal and spinal cord motor functions. Neurology, 28, 703-709

Cui L, Jeong H, Borovecki F, Parkhurst CN, Tanese N, Krainc D. (2006) Transcriptional repression of PGC-1α by mutant huntingtin leads to mitochondrial dysfunction and neurondegeneration. Cell 127: 59-69.

David C. Rubinsztein. (2006) The roles of intracellular protein-degradation pathways in neurodegeneration Nature 443, 780-786

Davies S.W, M Turmaine, B.A Cozens, M DiFiglia, A.H Sharp, C.A Ross, E Scherzinger, E.E Wanker, L Mangiarini, G.P Bates. (1997) Formation of neuronal intranuclear inclusions underlies the neurological dysfunction in mice transgenic for the HD mutation. Cell, 90 537-548

Distel Martin, Wullimannand Mario F. Köster Reinhard, (2009) Optimized Gal4 genetics for permanent gene expression mapping in zebrafish, Proc Natl Acad Sci U S A. 11;106(32):13365-70

DiFiglia M, E Sapp, K.O Chase, S.W Davies, G.P Bates, J.P Vonsattel, N Aronin. (1997) Aggregation of huntingtin in neuronal intranuclear inclusions and dystrophic neurites in brain. Science, 277 1990-1993

Doi H, Koyano S, Suzuki Y, Nukina N, Kuroiwa Y. (2010) The RNA-binding protein FUS/TLS is a common aggregate-interacting protein in polyglutamine diseases. Neurosci Res. 66(1):131-3.

Donaldson K.M., W. Li, K.A. Ching, S. Batalov, C.C. Tsai, C.A. Joazeiro. (2003) Ubiquitin-mediated sequestration of normal cellular proteins into polyglutamine aggregates. Proc. Natl. Acad. Sci. U.S.A., 100 8892-8897

Doss-Pepe E.W., E.S. Stenroos, W.G. Johnson, K. Madura. (2003) Ataxin-3 interactions with rad23 and valosin-containing protein and its associations with ubiquitin chains and the proteasome are consistent with a role in ubiquitin-mediated proteolysis. Mol. Cell. Biol. 23, 6469-6483

Dürr A, Stevanin G, Cancel G, Duyckaerts C, Abbas N, Didierjean O, Chneiweiss H, Benomar A, Lyon-Caen O, Julien J, Serdaru M, Penet C, Agid Y, Brice A. (1996) Spinocerebellar ataxia 3 and Machado-Joseph disease: clinical, molecular, and neuropathological features. Ann Neurol.; 39(4):490-9.

Durr A., G. Stevanin, G. Cancel, C. Duyckaerts, N. Abbas, O. Didierjean, H. Chneiweiss, A. Benomar, O. Lyon-Caen, J. Julien, M. Serdaru, C. Penet, Y. Agid, A. Brice. (1996) Spinocerebellar ataxia 3 and Machado–Joseph disease: clinical, molecular, and neuropathological features. Ann. Neurol., 39 490-499

Duvick L, Barnes J, Ebner B, Agrawal S, Andresen M, Lim J, Giesler GJ, Zoghbi HY, Orr HT. (2010) SCA1-like disease in mice expressing wild-type ataxin-1 with a serine to aspartic acid replacement at residue 776. Neuron.67(6):929-35.

Ellisdon A.M., M.C. Pearce, S.P. Bottomley. (2007) Mechanisms of ataxin-3 misfolding and fibril formation: kinetic analysis of a disease-associated polyglutamine protein. J. Mol. Biol. 368 595-605

Ellisdon A.M., B. Thomas, S.P. Bottomley. (2006) The two-stage pathway of ataxin-3 fibrillogenesis involves a polyglutamine-independent step. J. Biol. Chem., 281 16888-16896

Evert B.O., J. Araujo, A.M. Vieira-Saecker, R.A. de Vos, S. Harendza, T. Klockgether, U. Wullner. (2006) Ataxin-3 represses transcription via chromatin binding, interaction with histone deacetylase 3, and histone deacetylation. J. Neurosci., 26, 11474-11486

Evert B.O., I.R. Vogt, A.M. Vieira-Saecker, L. Ozimek, R.A. de Vos, E.R. Brunt, T. Klockgether, U. Wullner. (2003) Gene expression profiling in ataxin-3 expressing cell lines reveals distinct effects of normal and mutant ataxin-3. J. Neuropathol. Exp. Neurol., 62, 1006-1018

Ferrigno P., P.A. Silver. (2000) Polyglutamine expansions: proteolysis, chaperones, and the dangers of promiscuity. Neuron, 26, 9-12

Gales L., L. Cortes, C. Almeida, C.V. Melo, M.C. Costa, P. Maciel, D.T. Clarke, A.M. Damas, S. Macedo-Ribeiro. (2005) Towards a structural understanding of the fibrillization pathway in Machado–Joseph's disease: trapping early oligomers of non-expanded ataxin-3. J. Mol. Biol., 353642-654

Gatchel J.R., H.Y. Zoghbi (2005) Diseases of unstable repeat expansion: mechanisms and common principles Nat. Rev. Genet., 6 743-755

Gervais, F.G., Singaraja, R., Xanthoudakis, S., Gutekunst, C.A., Leavitt, B.R., Metzler, M., Hackam, A.S., Tam, J., Vaillancourt, J.P., Houtzager, V. Rasper DM, Roy S, Hayden MR, Nicholson DW. (2002) Recruitment and activation of caspase-8 by the Huntingtininteracting protein Hip-1 and a novel partner Hippi. Nat. Cell Biol., 4, 95–105.

Graham FL, Smiley J, Russell WC, Nairn R. (1977) Characteristics of a human cell line transformed by DNA from human adenovirus type 5. J Gen Virol. 36(1):59-74.

Goti D, Katzen SM, Mez J, Kurtis N, Kiluk J, Ben-Haı¨em L (2004) A mutant ataxin-3 putative-cleavage fragment in brain of Machado-Joseph disease patients and transgenic mice is cytotoxic above a critical concentration. *J* Neurosci 24:10266-10279

Goto J., M. Watanabe, Y. Ichikawa, S.B. Yee, N. Ihara, K. Endo, S. Igarashi, Y. Takiyama, C. Gaspar, P. Maciel, S. Tsuji, G.A. Rouleau, I. Kanazawa. (1997) Machado–Joseph disease gene products carrying different carboxyl termini. Neurosci. Res., 28, 373-377

Gunawardena S., L.S. Her, R.G. Brusch, R.A. Laymon, I.R. Niesman, B. Gordesky-Gold, L. Sintasath, N.M. Bonini, L.S. Goldstein. (2003) Disruption of axonal transport by loss of huntingtin or expression of pathogenic polyQ proteins in *Drosophila.* Neuron, 40, 25-40

Haacke A., Broadley S.A., R. Boteva, N. Tzvetkov, F.U. Hartl, P. Breuer. (2006) Proteolytic cleavage of polyglutamine-expanded ataxin-3 is critical for aggregation and sequestration of non-expanded ataxin-3. Hum. Mol. Genet. 15 555-568

Haacke A., F.U. Hartl, P. Breuer. (2007) Calpain inhibition is sufficient to suppress aggregation of polyglutamine-expanded ataxin-3. J. Biol. Chem., 282, 18851-18856

Hanako Ikeda, Masahiro Yamaguchi, Satoshi Sugai, Yoshiya Aza, Shuh Narumiya and Akira Kakizuka, (1996) Expanded polyglutamine in the Machado-Joseph disease protein induces cell death in vitro and in vivo. Nat Genetics 13,196-202

Harris G.M., K. Dodelzon, L. Gong, P. Gonzalez-Alegre, H.L. Paulson. (2010) Splice isoforms of the polyglutamine disease protein ataxin-3 exhibit similar enzymatic yet different aggregation properties. PLoS One, 5 p. e13695

Ichikawa Y., J. Goto, M. Hattori, A. Toyoda, K. Ishii, S.Y. Jeong, H. Hashida, N. Masuda, K. Ogata, F. Kasai, M. Hirai, P. Maciel, G.A. Rouleau, Y. Sakaki, I. Kanazawa. (2001) The genomic structure and expression of MJD, the Machado–Joseph disease gene. J. Hum. Genet. 46 413-422

Jana N.R., N. Nukina. (2004) Misfolding promotes the ubiquitination of polyglutamine-expanded ataxin-3, the defective gene product in SCA3/MJD. Neurotox. Res. 6, pp. 523-533

Lim Anghoo, Juan Crespo-Barreto, Paymaan Jafar-Nejad, Aaron B. Bowman, Ronald Richman, David E. Hill, Harry T. Orr & Huda Y. Zoghbi, (2008) Opposing effects of polyglutamine expansion on native protein complexes contribute to SCA1 Nature 452 713-719

Joana Branco, Ismael Al-Ramahi, Lubna Ukani, Alma M. Pe´rez, Pedro Fernandez-Funez, Diego Rinco´n-Limas1 and Juan Botas (2008) Comparative analysis of genetic modifiers in Drosophila points to common and distinct mechanisms of pathogenesis among polyglutamine diseases Human Molecular Genetics, Vol. 17. No. 3 376-390.

John M. Warrick, Henry L. Paulson, Gladys L. Gray-Board, Quang T. Bui, Kenneth H. Fischbeck, Randall N. Pittman, and Nancy M. Bonini. (1998) Expanded Polyglutamine Protein Forms Nuclear Inclusions and Causes Neural Degeneration in *Drosophila.* Cell, 93, 939-949

Jung J., K. Xu, D. Lessing, N.M. Bonini. Preventing ataxin-3 protein cleavage mitigates degeneration in a *Drosophila* model of SCA3. Hum. Mol. Genet., 18 (2009), 4843-4852

Kanda T., E. Isozaki, S. Kato, H. Tanabe, M. Oda. (1989) Type III Machado–Joseph disease in a Japanese family: a clinicopathological study with special reference to the peripheral nervous system. Clin. Neuropathol. 8 134-141

Kitamura A, Kubota H, Pack CG, Matsumoto G, Hirayama S, Takahashi Y, Kimura H, Kinjo M, Morimoto RI, Nagata K (2006) Cytosolic chaperonin prevents polyglutamine toxicity with altering the aggregation state. Nat. Cell Biol. 8, 1163-1170.

Krol HA, Krawczyk PM, Bosch KS, Aten JA, Hol EM, Reits EA (2008) Polyglutamine Expansion Accelerates the Dynamics of Ataxin-1 and Does Not Result in Aggregate Formation. *PLoS One* 3(1): e1503

Lai S, O'Callaghan B, Zoghbi HY, Orr HT. (2011) 14-3-3 Binding to ataxin-1(ATXN1) regulates its dephosphorylation at Ser-776 and transport to the nucleus. J Biol Chem. 286(40):34606-16.

Lajoie Patrick, Erik Lee Snapp (2010) Formation and Toxicity of Soluble Polyglutamine Oligomers in Living Cells PLoS ONE 5(12): e15245. doi:10.1371/journal.pone.0015245

Lee SB, Bagley JA, Lee HY, Jan LY, Jan YN. (2011) Pathogenic polyglutamine proteins cause dendrite defects associated with specific actin cytoskeletal alterations in Drosophila. Proc Natl Acad Sci U S A. 108(40):16795-800

Li F., T. Macfarlan, R.N. Pittman, D. Chakravarti. (2002) Ataxin-3 is a histone-binding protein with two independent transcriptional corepressor activities. J. Biol. Chem., 277,

45004-45012

Lim J, Hao T, Shaw C, Patel AJ, Szabó G, Rual JF, Fisk CJ, Li N, Smolyar A, Hill DE, Barabási AL, Vidal M, Zoghbi HY. (2006) A protein-protein interaction network for human inherited ataxias and disorders of Purkinje cell degeneration. Cell.125(4):801-14.

Llinas R. **(**1981) Electrophysiology of cerebellar networks. In: Handbook of Physiology. The Nervous System. Motor Control, Am. Physiol. Soc., , sect. 1, vol. II, p. 831-976.

Kimmel CB, Ballard WW, Kimmel SR, Ullmann B, Schilling TF (1995) Stages of embryonic development of the zebrafish. Dev Dyn 203: 253–310.

Koch P, Breuer P, Peitz M, Jungverdorben J, Kesavan J, Poppe D, Doerr J, Ladewig J, Mertens J, Tüting T, Hoffmann P, Klockgether T, Evert BO, Wüllner U, Brüstle O. (2011) Excitation-induced ataxin-3 aggregation in neurons from patients with Machado-Joseph disease. Nature. 480(7378):543-6.

Macedo-Ribeiro S, Cortes L, Maciel P, Carvalho AL (2009) Nucleocytoplasmic Shuttling Activity of Ataxin-3. PLoS ONE 4(6): e5834.

Maciel P., M.C. Costa, A. Ferro, M. Rousseau, C.S. Santos, C. Gaspar, J. Barros, G.A. Rouleau, P. Coutinho, J. Sequeiros (2001) Improvement in the molecular diagnosis of Machado–Joseph disease. Arch. Neurol., 58, 1821-1827

Martinez-Vicente M, Talloczy Z, Wong E, Tang G,Koga H, Kaushik, S, de Vries, R, Arias E, Harris S, Suzer D, Cuervo AM. (2010) Cargo recognition failure is responsible for inefficient autophagy in Huntington´s disease Nat Neurosci 13(5): 567-576

Masino L., G. Nicastro, L. Calder, M.A.P. Vendruscolo. (2011) Functional interactions as a survival strategy against abnormal aggregation. FASEB J., 25, 45-54

Masino L., G. Nicastro, R.P. Menon, F. Dal Piaz, L. Calder, A. Pastore. (2004), Characterization of the structure and the amyloidogenic properties of the Josephin domain of the polyglutamine-containing protein ataxin-3. J. Mol. Biol., 344 1021-1035

Masino L., V. Musi, R.P. Menon, P. Fusi, G. Kelly, T.A. Frenkiel, Y. Trottier, A. Pastore. (2003), Domain architecture of the polyglutamine protein ataxin-3: a globular domain followed by a flexible tail. FEBS Lett., 549 21-25

Matos CA, de Macedo-Ribeiro S, Carvalho AL. (2011) Polyglutamine diseases: the special case of ataxin-3 and Machado-Joseph disease. Prog Neurobiol. 95(1):26-48.

McCampbell A., J.P. Taylor, A.A. Taye, J. Robitschek, M. Li, J. Walcott, D. Merry, Y. Chai, H. Paulson, G. Sobue, K.H. Fischbeck. (2000) CREB-binding protein sequestration by expanded polyglutamine. Hum. Mol. Genet., 9 2197-2202

McGurk Leeanne and Bonini Nancy M., **(**2012) Protein interacting with C kinase (PICK1) is a suppressor of spinocerebellar ataxia 3-associated neurodegeneration in Drosophila Hum Mol Genet.; 21(1): 76-84.

Miller VM, Nelson RF, Gouvion CM, Williams A, Rodriguez-Lebron E, Harper SQ, Davidson BL, Rebagliati MR, Paulson HL. (2005) CHIP suppresses polyglutamine aggregation and toxicity in vitro and in vivo. J Neurosci.25(40):9152-61.

Muchowski P.J., J.L. Wacker. (2005) Modulation of neurodegeneration by molecular chaperones. Nat. Rev. Neurosci., 6, 11-22

Muchowski P.J., G. Schaffar, A. Sittler, E.E. Wanker, M.K. Hayer-Hartl, F.U. Hartl. (2000) Hsp70 and hsp40 chaperones can inhibit self-assembly of polyglutamine proteins into amyloid-like fibrils. Proc. Natl. Acad. Sci. U.S.A., 97, 7841-7846

Muñoz E, Rey M.J, Milà M, Cardozo A, Ribalta T, Tolosa E, Ferrer I, (2002) Intranuclear inclusions, neuronal loss and CAG mosaicism in two patients with Machado–Joseph disease. Journal of the Neurological Sciences, Vol 200, (1-2):19-25

Nagai Y., T. Inui, H.A. Popiel, N. Fujikake, K. Hasegawa, Y. Urade, Y. Goto, H. Naiki, T. Toda. (2007) A toxic monomeric conformer of the polyglutamine protein. Nat. Struct. Mol. Biol., 14 332-340

Nicastro G., R.P. Menon, L. Masino, P.P. Knowles, N.Q. McDonald, A. Pastore. (2005) The solution structure of the Josephin domain of ataxin-3: structural determinants for molecular recognition. Proc. Natl. Acad. Sci. U.S.A., 102, 10493-10498

Palla` s M, Casadesu´ s G, Smith MA, Coto-Montes A, Pelegri C, Vilaplana J, Camins A (2009) Resveratrol and neurodegenerative diseases: activation of SIRT1 as the potential pathway towards neuroprotection. Curr. Neurovasc. Res. 6, 70-81.

Parker JA, Arango M, Abderrahmane S, Lambert E, Tourette C, Catoire H, Ne´ ri C (2005) Resveratrol rescues mutant polyglutamine cytotoxicity in nematode and mammalian neurons. Nat. Genet. 37, 349-350

Paulson, H.L., Perez, M.K., Trottier, Y., Trojanowski, J.Q., Subramony, S.H., Das, S.S., Vig, P., Mandel, J.L., Fischbeck, K.H. and Pittman, R.N. (1997) Intranuclear inclusions of expanded polyglutamine protein in spinocerebellar ataxia type 3. *Neuron*, 19, 333-344.

Paulson H.L., S.S. Das, P.B. Crino, M.K. Perez, S.C. Patel, D. Gotsdiner, K.H. Fischbeck, R.N. Pittman. (1997) Machado–Joseph disease gene product is a cytoplasmic protein widely expressed in brain. Ann. Neurol., 41, 453-462

Peter O. Bauer, Hon Kit Wong, Fumitaka Oyama, Anand Goswami, Misako Okuno, Yoshihiro Kino, Haruko Miyazaki, and Nobuyuki Nukina. (2009) Inhibition of Rho Kinases Enhances the Degradation of Mutant Huntingtin J Biol Chem. 284(19): 13153-13164.

Provost E, Rhee J, Leach SD (2007) Viral 2A peptides allow expression of multiple proteins from a single ORF in transgenic zebrafish embryos. Genesis 45: 625-629.

Puck TT, Marcus PI, and Cieciura SJ (1956) Clonal growth of mammalian cells in vitro: growth characteristics of colonies from single HeLa cells with and without a "feeder" layer Journal of Experimental Medicine, 103 (2), 273-284

Reina CP, Zhong X, Pittman RN. (2010) Proteotoxic stress increases nuclear localization of ataxin-3. Hum Mol Genet. 19(2):235-49.

Rich Tina, Archana Varadaraj (2007) Ataxin-1 Fusion Partners Alter PolyQ Lethality and Aggregation. PLoS ONE 2 (10): e1014.

Riess O., U. Rüb, A. Pastore, P. Bauer, L. Schöls (2008) SCA3: neurological features, pathogenesis and animal models. Cerebellum, 7 (2) 125-137

Rodrigues A.J., G. Coppola, C. Santos, C. Costa Mdo, M. Ailion, J. Sequeiros, D.H. Geschwind, P. Maciel. (2007) Functional genomics and biochemical characterization of the *C. elegans* orthologue of the Machado–Joseph disease protein ataxin-3. FASEB J., 21, 1126-1136

Romanul FC, Fowler HL, Radvany J, Feldman RG, Feingold M. (1977) Azorean disease of the nervous system. N Engl J Med. 296(26):1505-8.

Rosenberg R.N. (1992) Machado–Joseph disease: an autosomal dominant motor system degeneration. Mov. Disord. 7 , 193-203

Rüb U, Brunt ER, Deller T. (2008) New insights into the pathoanatomy of spinocerebellar ataxia type 3 (Machado-Joseph disease). Curr Opin Neurol. (2):111-6.

Rupp, R.A.W., Snider, L., and Weintraub, H. (1994). *Xenopus* embryos regulate the nuclear localization of XMyoD. Genes and Development 8: 1311-1323.

Sambrook AF. (2001) Molecular Cloning: Cold Spring Harbor.

Schmidt T., G.B. Landwehrmeyer, I. Schmitt, Y. Trottier, G. Auburger, F. Laccone, T. Klockgether, M. Volpel, J.T. Epplen, L. Schols, O. Riess. (1998), An isoform of ataxin-3 accumulates in the nucleus of neuronal cells in affected brain regions of SCA3 patients. Brain Pathol. 8 669-679

Schmidt T., K.S. Lindenberg, A. Krebs, L. Schols, F. Laccone, J. Herms, M. Rechsteiner, O. Riess, G.B. (2002) Landwehrmeyer. Protein surveillance machinery in brains with

spinocerebellar ataxia type 3: redistribution and differential recruitment of 26S proteasome subunits and chaperones to neuronal intranuclear inclusions. Ann. Neurol., 51 302-310

Scherzinger E, R Lurz, M Turmaine, L Mangiarini, B Holenbach, R Hasenbank, G.P Bates, S.W Davies, H Lehrach, E.E Wanker. (1997) Huntingtin-encoded polyglutamine expansions form amyloid-like protein aggregates in vitro and in vivo. Cell, 90 549-558

Schöls L, Bauer P, Schmidt T, Schulte T, Riess O. (2004) Autosomal dominant cerebellar ataxias: clinical features, genetics, and pathogenesis. Lancet Neurol. 3(5):291-304.

Seidel K., W.F. den Dunnen, C. Schultz, H. Paulson, S. Frank, R.A. de Vos, E.R. Brunt, T. Deller, H.H. Kampinga, U. Rub. (2010) Axonal inclusions in spinocerebellar ataxia type 3., Acta Neuropathol., 120 449-460.

Senghass Niklas and Koester Reihard. (2009) Culturing and Transfecting Zebrafish PAC2 Fibroblast Cells Cold Spring Harb Protoc; 4(6):725-731

Shao Jieya, and Marc I. Diamond, (2007) Polyglutamine diseases: emerging concepts in pathogenesis and therapy. Human Molecular Genetics, Vol. 16, Review Issue 2 R115-R123

Shao Jieya, William J. Welch, Nicholas A. DiProspero, and Marc I. Diamond (2008) Phosphorylation of Profilin by ROCK1 Regulates Polyglutamine Aggregation molecular and cellular biology, 28(17):5196-208

Silva-Fernandes A, Costa Mdo C, Duarte-Silva S, Oliveira P, Botelho CM, Martins L, Mariz JA, Ferreira T, Ribeiro F, Correia-Neves M, Costa C, Maciel P. (2010) Motor uncoordination and neuropathology in a transgenic mouse model of Machado-Joseph disease lacking intranuclear inclusions and ataxin-3 cleavage products. Neurobiol Dis. 40(1):163-76.

Shimizu H., M. Yamada, Y. Toyoshima, T. Ikeuchi, O. Onodera, H. Takahashi. (2010) Involvement of Onuf's nucleus in Machado–Joseph disease: a morphometric and immunohistochemical study. Acta Neuropathol., 120 pp. 439-448

Sudarsky L., P. Coutinho. (1995) Machado–Joseph disease. Clin. Neurosci. 3 pp. 17-22

Sudnitsyna MV, Seit-Nebi AS, Gusev NB. (2012) Cofilin weakly interacts with 14-3-3 and therefore can only indirectly participate in regulation of cell motility by small heat shock protein HspB6 (Hsp20). Arch Biochem Biophys.; 521(1-2):62-70.

Soong B., C. Cheng, R. Liu, D. Shan. (1997) Machado–Joseph disease: clinical, molecular, and metabolic characterization in Chinese kindreds. Ann. Neurol., 41pp. 446-452

Spector I, Shochet NR, Kashman Y, Groweiss A. (1983) Latrunculins: novel marine toxins that disrupt microfilament organization in cultured cells. Science. 219 (4584):493-495.

Stenoien David L., Mielke Marilyn, Mancini Michael A. (2002) Intranuclear ataxin1 inclusions contain both fast- and slow-exchanging components. Nature Cell Biology 4, 806-810

Tanaka M., I. Morishima, T. Akagi, T. Hashikawa, N. Nukina. (2001) Intra- and intermolecular beta-pleated sheet formation in glutamine-repeat inserted myoglobin as a model for polyglutamine diseases. J. Biol. Chem., 276 pp. 45470-45475

Tam S, Geller R, Spiess C, Frydman J (2006) The chaperonin TRiC controls polyglutamine aggregation and toxicity through subunit-specific interactions. Nat. Cell Biol. 8, 1155-1162.

Tarlac V., E. Storey (2003) Role of proteolysis in polyglutamine disorders. J. Neurosci. Res., 74 pp. 406-416

Toshiaki Takahashi1, Shinya Kikuchi, Shinichi Katada, Yoshitaka Nagai, Masatoyo Nishizawa and Osamu Onodera. (2008) Soluble polyglutamine oligomers formed prior to inclusion body formation are cytotoxic. Human Molecular Genetics, Vol. 17, No. 3 345–356

Trottier Y., G. Cancel, I. An-Gourfinkel, Y. Lutz, C. Weber, A. Brice, E. Hirsch, J.L. Mandel. (1998) Heterogeneous intracellular localization and expression of ataxin-3., Neurobiol. Dis., 5 pp. 335-347

Van Alfen N, Sinke RJ, Zwarts MJ, Gabreëls-Festen A, Praamstra P, Kremer BP, Horstink MW. (2001) Intermediate CAG repeat lengths (53, 54) for MJD/SCA3 are associated with an abnormal phenotype. Ann Neurol. Jun; 49(6):805-7.

Vale J., P. Bugalho, I. Silveira, J. Sequeiros, J. Guimarães, P. Coutinho (2010) Autosomal dominant cerebellar ataxia: frequency analysis and clinical characterization of 45 families from Portugal. European Journal of Neurology Vol17, Issue 1, pages 124-128,

Veronica F. Colomer Gould, Daniel Goti, Donna Pearce, Guillermo A. Gonzalez, Hong Gao, Mario Bermudez de Leon, Nancy A. Jenkins, Neal G. Copeland, Christopher A. Ross, and Dale R. BrownA (2007) Mutant ataxin-3 fragment results from processing at a site N-terminal to amino acid 190 in brain of Machado–Joseph disease-like transgenic mice Neurobiology of Disease, 27 362-369

Veronica F. Colomer Gould. (2012) Mouse Models of Spinocerebellar Ataxia Type 3 (Machado-Joseph Disease) Neurotherapeutics 9:285-296

Wang Qiuyan, Lianyun Li, and Yihong Ye, (2006) Regulation of retrotranslocation by p97-associated deubiquitinating enzyme ataxin-3, J Cell Biol. 174(7): 963–971.

Warrick J. M, Henry L Paulson, Gladys L Gray-Board, Quang T Bui, Kenneth H Fischbeck, Randall N Pittman, Nancy M Bonini. (1998) Expanded Polyglutamine Protein Forms

Nuclear Inclusions and Causes Neural Degeneration in *Drosophila*. Cell Vol 93(6), , 939-949

Warrick J.M., H.Y. Chan, G.L. Gray-Board, Y. Chai, H.L. Paulson, N.M. Bonini. (1999) Suppression of polyglutamine-mediated neurodegeneration in *Drosophila* by the molecular chaperone HSP70. Nat. Genet., 23 pp. 425-428

Warrick John M., Lance M. Morabito, Julide Bilen, Beth Gordesky-Gold, Lynn Z. Faust, Henry L. Paulson, Nancy M. Bonini. (2005) Ataxin-3 Suppresses Polyglutamine Neurodegeneration in *Drosophila* by a Ubiquitin-Associated Mechanism. Molecular cell Vol 18, Issue 1, 1, Pages 37-48

Watase K, Weeber EJ, Xu B, Antalffy B, Yuva-Paylor L, Hashimoto K, Kano M, Atkinson R, Sun Y, Armstrong DL, Sweatt JD, Orr HT, Paylor R, Zoghbi HY. (2002) A long CAG repeat in the mouse Sca1 locus replicates SCA1 features and reveals the impact of protein solubility on selective neurodegeneration. Neuron. 13; 34(6):905-19

William M. Landau, Robert E. Schmidt, Ronald C. McGlennen, Stephen G. Reich, (2000) Hereditary Spastic Paraplegia and Hereditary AtaxiaPart 2: A Family Demonstrating Various Phenotypic Manifestations with the SCA3 Genotype. Archives of Neurology, , 57(5):733-739

Woods BT, Schaumburg HH. (1972) Nigro-spino-dentatal degeneration with nuclear ophthalmoplegia. A unique and partially treatable clinico-pathological entity. J Neurol Sci.17(2):149-66

Yoon BC, Zivraj KH, Strochlic L, Holt CE. (2012) 14-3-3 proteins regulate retinal axon growth by modulating ADF/cofilin activity. Dev Neurobiol. 72(4):600-14

Yoshizawa T., Y. Yamagishi, N. Koseki, J. Goto, H. Yoshida, F. Shibasaki, S. Shoji, I. Kanazawa (2000) Cell cycle arrest enhances the in vitro cellular toxicity of the truncated Machado–Joseph disease gene product with an expanded polyglutamine stretch. Hum. Mol. Genet., 9, 69-78

Zeron, M.M., Hansson, O., Chen, N., Wellington, C.L., Leavitt, B.R., Brundin, P., Hayden, M.R. and Raymond, L.A. (2002) Increased sensitivity to N-methyl-D-aspartate receptor-mediated excitotoxicity in a mouse model of Huntington's disease. Neuron, 33, 849–860.

Eidesstattliche Erklärung

Ich erkläre hiermit an Eides statt, dass ich die vorliegende Arbeit selbständig ohne unzulässige fremde Hilfe angefertigt habe. Die verwendeten Literaturquellen sind im Literaturverzeichnis vollständig zitiert.

Braunschweig, 17.09.2012

(Changsheng Liu)